Elucidation of Cyclophilin Inhibition through Free Energy Perturbation Simulations and the Development of Custom Ionic Liquid Force Fields

by

Somisetti Venkata Sambasivarao

A dissertation submitted to the Graduate Faculty of
Auburn University
in partial fulfillment of the
requirements for the Degree of
Doctor of Philosophy

Auburn, Alabama
August 06, 2011

Keywords: Ionic Liquid, Cyclophilin, Force Field,
Docking, Free Energy Perturbation, QM/MM

Approved by

Orlando Acevedo, Co-Chair, Assistant Professor of Chemistry and Biochemistry
J. V. Ortiz, Co-Chair, Professor of Chemistry and Biochemistry
Michael McKee, Professor of Chemistry and Biochemistry
Michael Squillacote, Associate Professor of Chemistry and Biochemistry

Abstract

Cyclophilins (Cyp) are a family of cellular enzymes possessing peptidyl-prolyl isomerase activity which catalyze the *cis-trans* interconversion of proline-containing peptide bonds. The two most abundant family members, CypA and CypB, have been identified as valid drug targets for a wide range of diseases including HCV, HIV, and multiple cancers. However, the development of small-molecule inhibitors that possess nM potency and high specificity for a particular Cyp is difficult given the complete conservation of all active site residues between the enzymes. Monte Carlo statistical sampling coupled to free energy perturbation theory (MC/FEP) calculations have been carried out to elucidate the origin of the experimentally observed nM inhibition of CypA by acylurea-based derivatives and the >200-fold in vitro selectivity between CypA and CypB from aryl 1-indanylketone-based μM inhibitors. The computed free-energies of binding were in close accord with those derived from experiment. Binding affinity values for the inhibitors were determined to be dependent upon the stabilization strength of the nonbonded interactions provided towards two catalytic residues: Arg55 and Asn102 in CypA and the analogous Arg63 and Asn110 residues in CypB; fine-tuning of the hydrophobic interactions allowed for enhanced potency among derivatives. The aryl 1-indanylketones are predicted to differentiate between the cyclophilins by using distinct binding motifs that exploit subtle differences in the active site arrangements. Ideas for the development of new selective compounds with the potential for advancement to low-nanomolar inhibition are presented.

OPLS-AA force field parameters have been developed and validated for use in the simulation of 68 unique combinations of room temperature ionic liquids featuring 1-alkyl-3-methylimidazolium [RMIM] (R = Me, Et, Bu, Hex, Oct), N-alkylpyridinium [RPyr], and choline cations, along with Cl^-, PF_6^-, BF_4^-, NO_3^-, $AlCl_4^-$, $Al_2Cl_7^-$, TfO^-, saccharinate, and acesulfamate anions. The new parameters were fit to conformational profiles from gas-phase ab initio calculations at the LMP2/cc-pVTZ(-f)//HF/6-31G(d) theory level and compared to experimental condensed-phase structural and thermodynamic data. Monte Carlo simulations of the ionic liquids gave relative deviations from experimental densities of ca. 1-3% at 25 °C for most combinations and also yielded close agreement over a temperature range of 5 to 90 °C. Predicted heats of vaporization compared well with available experimental data and estimates. Transferability of the new parameters to multiple alkyl side chain lengths for [RMIM] and [RPyr] was determined to give excellent agreement with charges and torsion potentials developed specific to desired alkyl lengths in 35 separate ionic liquid simulations. As further validation of the newly developed parameters, the Kemp elimination reaction of benzisoxazole via piperidine in 1-butyl-3-methylimidazolium hexafluorophosphate [BMIM][PF_6], and β-elimination of 1,1,1-tribromo-2,2-bis(phenyl-substituted)ethanes in 1-butyl-3-methylimidazolium hexafluorophosphate [BMIM][PF6], and 1-butyl-3-methylimidazolium tetrafluoroborate [BMIM][BF_4] with piperidine and pyrrolidine as amines were computed using mixed quantum and molecular mechanics (QM/MM) simulations and found to give close agreement with the experimental free energy of activation for the kemp elimination and overestimated free energies of activation with the experiment for the β-elimination.

Acknowledgments

"Truly said success depends in a large measure upon individual initiative, exertion and hard work, but it won't be an exaggeration to say that nothing can ever be achieved without the guidance, support and care of those in who you place your trust."

Emotions flush my face when I express my profound sense of gratitude to my esteemed guide Dr. Orlando Acevedo, Professor of Dept. of Chemistry and Biochemistry, who has involved right from the inception of ideas to the finalization of the work. He has been a continuous source of information, without his guidance scholarly suggestions an urge to bring out the best would not have been possible. I hope I can propagate his scientific and professional fervors to the best of my abilities.

I am thankful to Dr. J. V. Ortiz, Professor and Head, Dept. of Chemistry and Biochemistry, Auburn University, Dr. Michael Squillacote, Professor of Chemistry and Biochemistry, Auburn University, and Dr. Michael McKee, Professor of Chemistry and Biochemistry, Auburn University for their invaluable help and advice throughout my tenure in the department.

I am thankful to The President, Auburn University, Auburn, for providing adequate facilities.

Words are inadequate to express my sincere thanks to Billy, Caley, Kira, Jonah, Divya Prakash, Lee and Symon, Graduate students, for their kind co-operation and guidance during my course of study.

I would like to express my thanks to Librarian, Auburn University, for providing library facilities, and Dr. David Young for providing supercomputing facilities at Alabama Super Computing Center.

I am extremely grateful thanks to Dr. Patrick Flaherty, Dept. of Pharmacy**,** Duquesne University, and Dr. Zandrea Ambrose, School of Medicine, University of Pittsburgh for their help and kind co-operation.

I wish my sincere thanks to Dr. Rajesh Amin, School of Pharmacy, Auburn University, Janardhanan Krishnamurthy for their co-operation and valuable suggestion.

I am thankful to Chemical Computing Group, for providing MOE software.

My heartfelt thanks to Na Song, Catherine, Bhavin, Payal, Ram Mohan, Vijay, Rajesh, Hari, sunil, Suman, Monimoy, Sri, Raj, Vasavi, Sateesh, Divya, Smith, Chun Chun, Nootham, Chandu, Hanu, Vansee, Aadesh, Razia, Carol, Lynn for their innovative help at right time to complete my course successfully.

Last but not least it's my privilege to say thanks to my family for their continuous encouragement and moral support throughout my life.

Somisetti Venkata Sambasivarao

Table of Contents

List of Tables

Chapter III

Chapter IV

Chapter V

List of Figures

Chapter I

Chapter II

Chapter III

List of Abbreviations

QM/MM	Quantum and molecular mechanics
FEP	Free energy perturbation
MC	Monte Carlo

Chapter I. Introduction

I.I. Cyclophilins

Cyclophilins (Cyp) belong to a class of cellular enzymes possessing peptidyl-prolyl isomerase (PPIase) activity which catalyze the *cis-trans* interconversion of the imide bond in proline residues.[1-4] This isomerization has been identified as the rate-limiting step in protein folding.[5,6] Eight human Cyps with molecular masses ranging from 18 to 150 kDa[6] and an additional 12 multidomain Cyps (masses up to 352 kDa) have been reported to utilize a highly conserved active site making specific inhibition of a particular family member difficult.[7] Of specific interest to this research are human CypA and CypB[8] as both cyclophilins have been identified as valid drug targets for hepatitis C virus (HCV) treatment.[9-14] CypA and CypB are found to interact with the HCV RNA-dependent RNA polymerase NS5B, essential in HCV replication.[15] HCV is a key player in the development of major liver diseases including liver cirrhosis and hepatocellular carcinoma, and accounts for a significant proportion of hepatitis cases worldwide with most infections becoming chronic, i.e., approximately 60% of patients develop liver disease.[16] Unfortunately, the difficulty in treating HCV is attributable to limited therapy options and a substantial risk of premature discontinuation of medication due to side effects.[17]

Cyclosporin A (CsA), a global cyclophilin inhibitor, has been identified to substantially inhibit intracellular HCV replication[1,11,12,18] and additional inhibitors derived from natural products and peptide analogs have also been reported, e.g., FK506,[19] rapamycin,[20] sanglifehrin A,[21] and Debio-025.[9] New compounds are urgently needed that selectively bind with cyclophilins in order to reduce side effects; however, controversy surrounds which cyclophilin, CypA or CypB, plays the largest role in HCV replication and hence which one should be targeted for treatment. For example, Watashi et al. recently reported that downregulation of CypB reduced HCV RNA titer, but knockdown of CypA or CypC did not.[10] Conversely, Yang et al. reported that silencing of CypB or CypC expression had no significant effect on replication, but HCV showed a dependency for CypA.[13] Nakagawa et al. determined that knockdown of CypA, CypB, and CypC suppressed HCV replication significantly.[12] It is clear that a detailed atomic-level understanding of the selective inhibition of cyclophilins is needed to both treat hepatitis C and to elucidate the role that the enzymes play in HCV replication. In addition, compounds displaying selective inhibition of CypA,[22] CypB,[23] CypC,[4,24] or CypD[25] could be extended to treatments of other diseases beyond HCV, including HIV,[26] multiple cancers,[27] e.g., breast,[28] pancreatic,[29] and non-small cell lung cancers,[30] and inflammatory diseases,[31] such as rheumatoid arthritis.[32]

Early insights into the catalytic mechanism of CypA with HIV-1 CA protein is given by Howard et al.[33] Their crystallographic studies revealed that tight binding of the proline side chain of substrate and main chain oxygen atom require that conformational changes resulting from isomerization occur by rotation of groups N-terminal to isomeric proline. They differ from Eissenmesser et al[34] NMR studies of chemical shift and relaxation rate changes with and without the modeled tetrapeptide substrate, Suc-Ala-Phe-Pro-Phe-NA, where Suc is succinyl and NA is

p-nitroanilide with CypA concluded that catalysis is achieved by rotation of C-terminal residues of the substrate while the N-terminal remains stationary and catalytic pathway involve cis conformation. Zaho[35] and Vajdos[36] found that catalysis occurs closely with the trans CypA-CA derived hexapeptide complexes. Howard et al[33] noted that trans-Gly/Ala-Pro peptides of the CA substrate are planar, not strongly twisted (the average ω-angle is 0.2^{o} away from a planar 180^{o}) in CypA-CA crystal complexs. But, all the cis conformations show some twist toward the transition state by ~10^{o}. Hur et al[37] carried out a molecular dynamics study of four tetrapeptides with CypA suggested that both cis and trans conformations of the peptides bind with the CypA twisted ~20^{o} from planar. All these results support the idea that CypA-CA catalysis involves proline isomerization by transition state stabilization of substrate rather than selectively binding of conformations. Another molecular dynamics studies of Hamelberg and McCammon[2] on hexapeptide (Ace-His-Ala-Gly-Pro-Ile-Ala-Nme) substrate with CypA suggested that the transition state interacts more favorably with CypA than the cis isomer, which in turn more favorably interacts than the trans isomer. The transition state stabilization in the binding site of CypA is due to favorable hydrophobic and long-lasting strong hydrogen bonding interactions.

All the X-ray crystal structures of CypA with cyclosporine, cyclosporine analogues and various peptides give pharmacophore model for potential Cyp inhibitors. The important pharmacophore (Figure 1)[38] consists of a hydrophobic region that binds to proline residue of the substrate, and a group of hydrogen bonding acceptor and donor atoms.

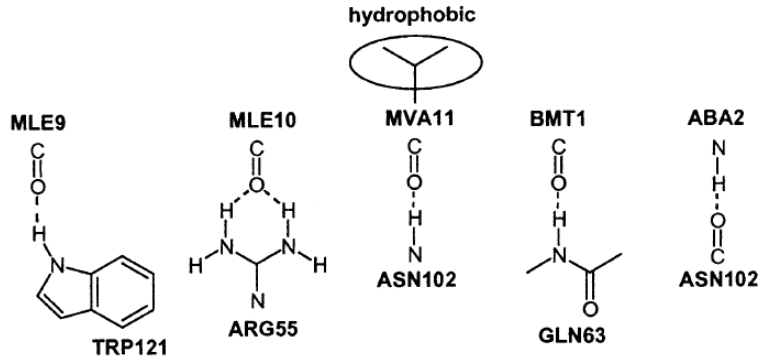

Figure 1: Pharmacophore from the cyclosporine-Cyp complex.

Non-peptidic compounds (Figure 2) reported for Cyp inhibition are symmetrical 1,3-Phenyl/Cyclohexyl Bis-ureas,[38] substituted thio-ureas(Ar1-NH-CS-NH-Ar2),[39] acylurea,[40] and aryl 1-indanylketone-[41] compounds.

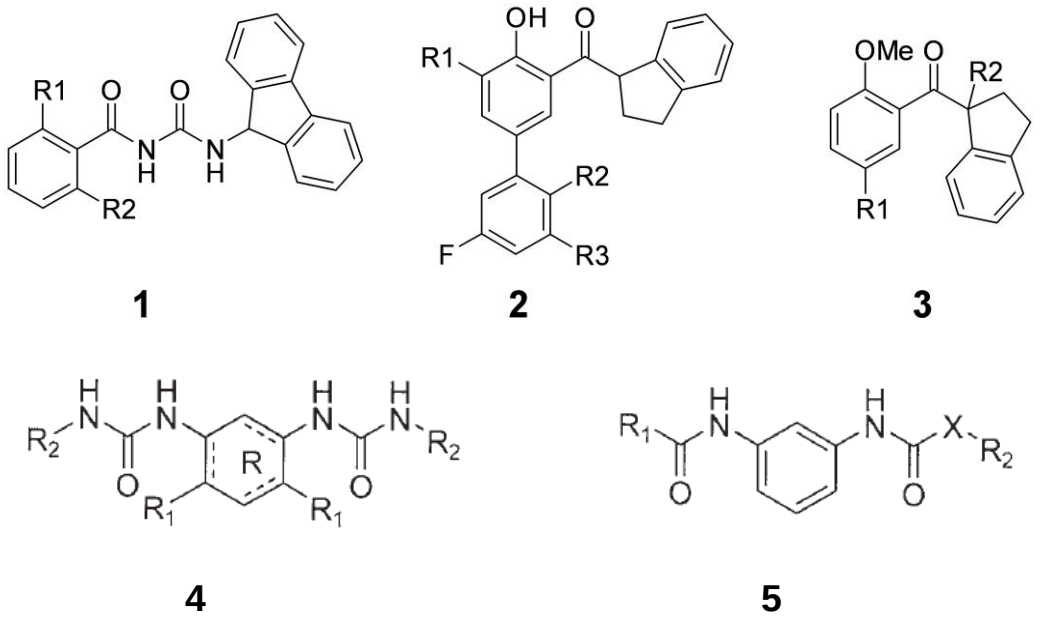

Figure 2. Chemical structures of acylurea-based (**1**), aryl 1-indanylketone-based (**2** and **3**) and 1,3-aryl Bis-urea (**4** and **5**) based cyclophilin inhibitors.

I.II. Ionic Liquids

Ionic liquids are a unique class of solvent, generally defined as a material containing only ionic species with a melting point below 100 °C.[1,2] They have growing interest in the scientific community during the past decade.[2] These "designer" solvents are typically composed of a low symmetry organic cation, such as the well-recognized 1-alkyl-3-methylimidazolium [RMIM] and N-alkylpyridinium [RPyr], tetra-alkyl phosphonium, N-methyl-N-alkyl-morpholinium, N-methyl-N-alkyl-pyrrolidinium cation classes, and a weakly coordinating inorganic or organic anion with a diffuse negative charge like hexafluorophosphate [PF_6] or tetrafluoroborate [BF_4].[3] Ion components can be fine-tuned through different functional groups to enhance the degree of localized structuring in the liquid phase, which distinguishes ionic liquids from molecular solvents and solutions containing dissociated ions.[4] This distinctive structural behavior[5] in conjunction with their attractive properties, e.g. low viscosities, negligible vapor pressure, and excellent thermal and chemical stabilities, has led to numerous advances in electrochemistry,[6] separation science,[7] catalysis,[8-10] organic synthesis,[11] materials,[12] and applications with lanthanides and actinides.[13]

Ionic liquids are often touted as green alternatives to volatile organic solvents. However, their potential impact on the environment is strongly dictated by ionic liquid selection.[9,14,15] For example, toxicity testing of 1-butyl-3-methylimidazolium [BMIM] and N-1-butylpyridinium [BPyr] on *Daphnia magna*, a common fresh water crustacean and aquatic food-chain base, found the cations to be half as toxic as toluene (EC_{50} of ca. 20 mg/L) and increasing the alkyl chain length to dodecyl increased the ecotoxicity by a factor of 2500 (EC_{50} of 4 μg/L).[15] In addition, combinations of [BMIM] with [BF_4] or [PF_6] anions have been determined to possess a negligible biodegradability,[16] allowing for their persistence in the environment for a considerable

length of time. More environmentally-friendly ionic liquids have recently been explored based on the choline cation [Chol],[17] a food-grade additive, and imidazolium derivatives designed for biodegradability[18] in combination with anions based on amino acids,[19] saccharinate [Sacc],[17] and acesulfamate [Ace],[17,20] ([Sacc] and [Ace] are used as artificial sweeteners).

Molecular modeling studies using dynamic simulations is a very powerful tool to study the condensed phase environment and structure; however many simulation studies reported on ionic liquids have focused on a local-scale environment around given a cation-anion combination. Some research groups including Padua, Lopes, Maginn, Acevedo and Borodin have contributed in designing ionic liquid force fields for variety of compounds, while other groups have reported monte carlo/molecular dynamics simulations for a few ionic liquids only.[21-24] Ionic liquid ions of interest are shown in Figure 3.

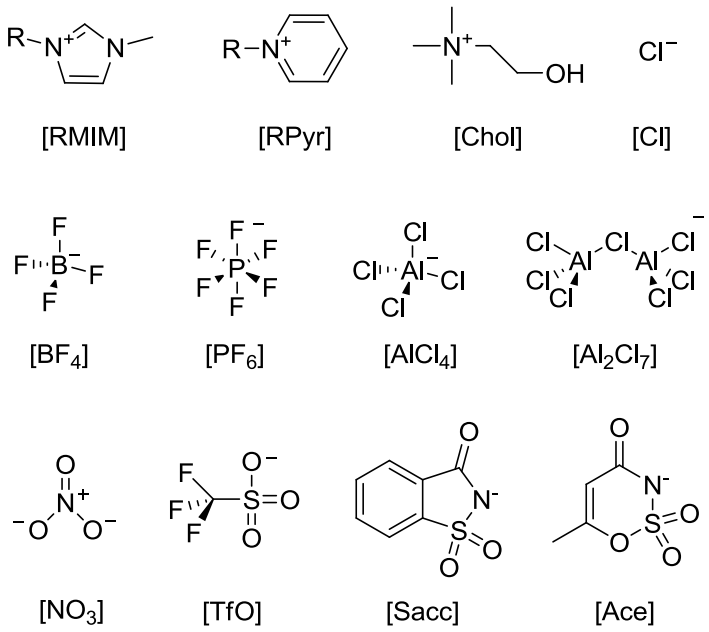

Figure 3. Ionic liquid forming ions. R = M (methyl), E (ethyl), B (butyl), H (hexyl), and O (octyl).

I.III. Elimination Reactions

Despite being one of the most studied reactions in organic chemistry, controversial experimental results have been reported regarding the position and the nature of the borderline between stepwise elimination via carbanionic intermediate E1cB mechanism and concerted one-step E2 elimination mechanism in the base catalyzed β-elimination reactions (Figure 4).[1] In some cases, the β-substituent is responsible for changing the mechanism from concerted E2 to stepwise E1cB.[2] A kinetic deuterium isotope exchange study was performed to distinguish between E2 and E1cB mechanisms.[1.l] The base catalyzed elimination reaction of 1-(2-chloro-2-propyl)indene in methanol favored E2 mechanism with the transition state having a large hydrogen transfer and extensive cleavage of the bond towards to chlorine.[1.l] The reported data was inconclusive with regards to the true mechanism, E1cB or E2, for the elimination of (2-arylethyl)quinuclidinium ions.[1.j] Experimental results of elimination of 4-nitrophenyl N-methylsulfamate with a series of bases have shown the mechanism to occur via a E2 route with some degree of carbanionic E1cB-like character.[3] A kinetic study of methoxide prompted suggested that 1,1,1,-trichloro-2,2-bis(phenyl-substituted)ethanes favored E1cB mechanism,[4] while the same elimination reaction turns to E2 mechanism in ionic liquids.[5]

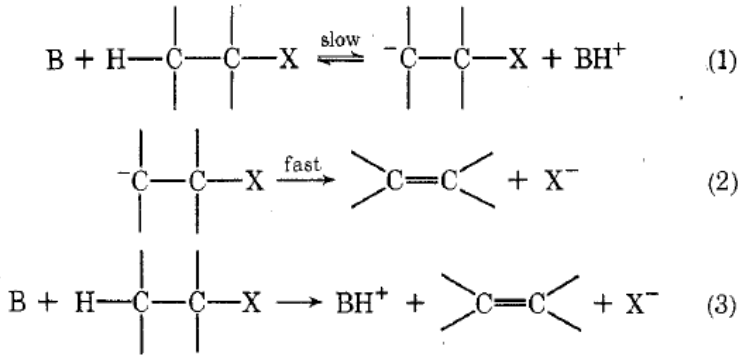

Figure 4. Base catalyzed E1cB mechanism (1 and 2), E2 mechanism (3) in substituted ethanes.

The base catalyzed E2 elimination of benzisoxazole to *o*-cyanophenolate is called Kemp[6] elimination, in which both C-H and N-O bonds are cleaved in large extent (Figure 5). This reaction has been studied extensively in water using hydroxide or trimethylamine as bases,[7] in the presence of cationic vesicles,[8] catalyzed enzymes and antibodies,[9] and cyclodextrins.[10]

The reactions studied in this work are (1) The Kemp elimination[6] (Figure 5) ring opening of benzisoxazole in 1-butyl-3-methylimidazolium hexafluorophosphate [BMIM][PF6] using piperidine as the base, and (2) β-elimination of 1,1,1-tribromo-2,2-bis(phenyl-substituted)ethanes[5] (Figure 6) in 1-butyl-3-methylimidazolium hexafluorophosphate [BMIM][PF6], 1-butyl-3-methylimidazolium tetrafluoroborate [BMIM][BF_4] with piperidine and pyrrolidine as amines, computed using mixed quantum and molecular mechanics (QM/MM) simulations to elucidate the origin of the ionic liquid properties upon the rates and mechanisms of the reactions.

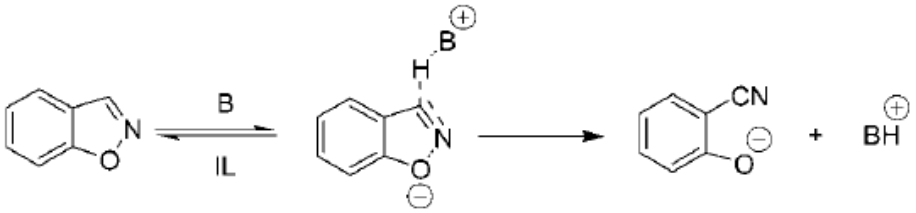

1 2

Figure 5. Schematic representation of Kemp elimination; benzisoxazole (1), o-cyanophenolate (2), piperidine (B), [BMIM][PF_6] (IL).

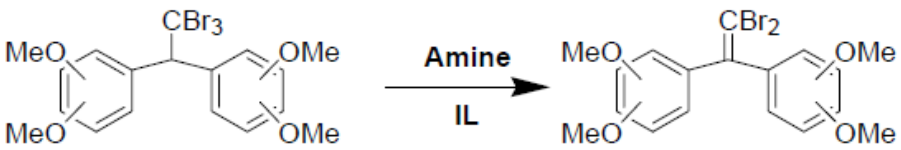

Figure 6. β-elimination of 1,1,1-tribromo-2,2-bis(phenyl-substituted)ethane into corresponding ethene; piperidine and pyrrolidine (Amine), [BMIM][PF_6] and [BMIM][BF_4] (IL).

References

I.I. Cyclophilins

(1) Handschumacher, R. E.; Harding, M. W.; Rice, J.; Drugge, R. J.; Speicher, D. W. *Science* **1984**, *226*, 544-547.

(2) Hamelberg, D.; McCammon, J. A. *J. Am. Chem. Soc.* **2009**, *131*, 147-152.

(3) (a) Fraser, J. S.; Clarkson, M. W.; Degnan, S. C.; Erion, R.; Kern, D.; Alber, T. *Nature* **2009**, *462*, 669-674; (b) Ke, H.; Zhao, Y.; Luo, F.; Weissman, I.; Friedman, J. *Proc. Natl. Acad. Sci. USA* **1993**, *90*, 11850-11854.

(4) Schneider, H.; Charara, N.; Schmitz, R.; Wehrli, S.; Mikol, V.; Zurini, M. G. M.; Quesniaux, V. F. J.; Movva, N. R. *Biochemistry* **1994**, *33*, 8218-8224.

(5) Schreiber, S. L. *Science* **1991**, *251*, 283-287.

(6) Göthel, S. F.; Marahiel, M. A. *Cell. Mol. Life Sci.* **1999**, *55*, 423-436.

(7) Fischer, G.; Aumüller, T. *Rev. Physiol. Biochem. Pharmacol.* **2003**, *148*, 105-150.

(8) Dornan, J.; Taylor, P.; Walkinshaw, M. D. *Curr. Top. Med. Chem.* **2003**, *3*, 1392-1409.

(9) Flisiak, R.; Horban, A.; Gallay, P.; Bobardt, M.; Selvarajah, S.; Wiercinska-Drapalo, A.; Siwak, E.; Cielniak, I.; Higersberger, J.; Kierkus, J.; Aeschlimann, C.; Grosgurin, P.; Nicolas-Métral, V.; Dumont, J.-M.; Porchet, H.; Crabbé, R.; Scalfaro, P. *Hepatology* **2008**, *47*, 817-826.

(10) Watashi, K.; Ishii, N.; Hijikata, M.; Inoue, D.; Murata, T.; Miyanari, Y.; Shimotohno, K. *Mol. Cell* **2005**, *19*, 111-122.

(11) Watashi, K.; Hijikata, M.; Hosaka, M.; Yamaji, M.; Shimotohno, K. *Hepatology* **2003**, *38*, 1282-1288.

(12) Nakagawa, M.; Sakamoto, N.; Tanabe, Y.; Koyama, T.; Itsui, Y.; Takeda, Y.; Chen, C. H.; Kakinuma, S.; Oooka, S.; Maekawa, S.; Enomoto, N.; Watanabe, M. *Gastroenterology* **2005**, *129*, 1031-1041.

(13) Yang, F.; Robotham, J. M.; Nelson, H. B.; Irsigler, A.; Kenworthy, R.; Tang, H. *J. Virol.* **2008**, *82*, 5269-5278.

(14) (a) Watashi, K.; Ishii, N.; Hijikata, M.; Inoue, D.; Murata, T.; Miyanari, Y.; Shimotohno, K. *Hepatology* **2005**, *42*, 1455-1458; (b) Jarvis, L. M. The Waiting Game. *C&EN* **2010**, *88*, 12-17; (c) Tang, H. *Viruses* **2010**, *2*, 1621-1634.

(15) Lohmann, V.; Korner, F.; Herian, U.; Bartenschlager, R. *J. Virol.* **1997**, *71*, 8416-8428.

(16) (a) Tang, H.; Grise, H. *Clin. Science* **2009**, *117*, 49-65; (b) Cuthbert, J. A. *Clin. Microbiol. Rev.* **1994**, *7*, 505-532; (c) Liang, T. J.; Jeffers, L. J.; Reddy, K. R.; Medina, M. D.; Parker, I. T.; Cheinquer, H.; Idrovo, V.; Rabassa, A.; Schiff, E. R. *Hepatology* **1993**, *18*, 1326-1333.

(17) Martinot-Peignoux, M.; Boyer, N.; Pouteau, M.; Castelnau, C.; Giuily, N.; Duchatelle, V.; Aupérin, A.; Degott, C.; Benhamou, J.-P.; Erlinger, S.; Marcellin, P. *J. Hepatol.* **1998**, *29*, 214-223.

(18) (a) Nakagawa, M.; Sakamoto, N.; Enomoto, N.; Tanabe, Y.; Kanazawa, N.; Koyama, T.; Kurosaki, M.; Maekawa, S.; Yamashiro, T.; Chen, C.-H.; Itsui, Y.; Kakinuma, S.; Watanabe, M. *Biochem. Biophys. Res. Commun.* **2004**, *313*, 42-47; (b) Kofron, J. L.; Kuzmic, P.; Kishore, V.; Colon-Bonilla, E.; Rich, D. H. *Biochemistry* **1991**, *30*, 6127-6134; (c) Inoue, K.; Sekiyama, K.; Yamada, M.; Watanabe, T.; Yasuda, H.; Yoshiba, M. *J. Gastroenterol.* **2003**, *38*, 567-572; (d) Inoue, K.; Yoshiba, M. *Transplant. Proc.* **2003**, *37*, 1233-1234.

(19) Siekierka, J. J.; Hung, S. H. Y.; Poe, M.; Lin, C. S.; Sigal, N. H. *Nature* **1989**, *341*, 755-757.

(20) Calne, R. Y.; Lim, S.; Samaan, A.; Collier, D. S. J.; Pollard, S. G.; White, D. J. G.; Thiru, S. *Lancet* **1989**, *334*, 227.

(21) Sedrani, R.; Kallen, J.; Cabrejas, L. M. M.; Papageorgiou, C. D.; Senia, F.; Rohrbach, S.; Wagner, D.; Thai, B.; Eme, A.-M. J.; France, J.; Oberer, L.; Rihs, G.; Zenke, G.; Wagner, J. *J. Am. Chem. Soc.* **2003**, *125*, 3849-3859.

(22) (a) Kallen, J.; Spitzfaden, C.; Zurini, M. G. M.; Wider, G.; Widmer, H.; Wuthrich, K.; Walkinshaw, M. D. *Nature* **1991**, *353*, 276-279; (b) Ke, H. M.; Zydowsky, L. D.; Liu, J.; Walsh, *Proc. Nat. Acad. Sci. USA* **1991**, *88*, 9483-9487.

(23) Price, E. R.; Zydowsky, L. D.; Jin, M. J.; Baker, C. H.; McKeon, F. D.; Walsh, C. T. *Proc. Nat. Acad. Sci. USA* **1991**, *88*, 1903-1907.

(24) Friedman, J.; Weissman, I. *Cell* **1991**, *66*, 799-806.

(25) Kajitani, K.; Fujihashi, M.; Kobayashi, Y.; Shimizu, S.; Tsujimoto, Y.; Miki, K. *Proteins* **2008**, *70*, 1635-1639.

(26) Luban, J.; Bossolt, K. L.; Franke, E. K.; Kalpana, G. V.; Goff, S. P. *Cell* **1993**, *73*, 1067-1078.

(27) Yao, Q.; Li, M.; Yang, H.; Chai, H.; Fisher, W.; Chen, C. *World J. Surg.* **2005**, *29*, 276-280.

(28) (a) Zheng, J.; Koblinski, J. E.; Dutson, L. V.; Feeney, Y. B.; Clevenger, C. V. P*Cancer Res.* **2008**, *68*, 7769-7778; (b) Fang, F.; Flegler, A. J.; Du, P.; Lin, S.; Clevenger, C. V. *Am. J. Pathol.* **2009**, *174*, 297-308.

(29) Shen, J.; Person, M. D.; Zhu, J.; Abbruzzese, J. L.; Li, D. *Cancer Res.* **2004**, *64*, 9018-9026.

(30) Howard, B. A.; Zheng, Z.; Campa, M. J.; Wang, M. Z.; Sharma, A.; Haura, E.; Herndon II, J. E.; Fitzgerald, M. C.; Bepler, G.; Patz Jr, E. F. *Lung Cancer* **2004**, *46*, 313-323.

(31) Arora, K.; Gwinn, W. M.; Bower, M. A.; Watson, A.; Okwumabua, I.; MacDonald, H. R.; Bukrinsky, M. I.; Constant, S. L. *J. Immunol.* **2005**, *175*, 517-522.

(32) Billich, A.; Winkler, G.; Aschauer, H.; Rot, A.; Peichl, P. *J. Exp. Med.* **1997**, *185*, 975-980.

(33) Howard, B. R.; Vajdos, F. F.; Sundquist, W I.; Hill, C. P. *Nature Str. Biotech.* ***2003,*** *10(6),475-481*.

(34) Eissenmesser, E. Z.; Bosco, D. A.; Akke, M.; Kern, D. *Science* ***2002****,295, 1520-1523.*

(35) Zhao, Y.; Chen, Y.; Schutkowski, M.; Fischer, G.; Ke, H. *Structure*, ***1997,*** 5, 139-146.

(36) Vajdos, F. F.; Yoo, S.; Houseweart, M.; Sundquist, W. I.; Hill, C. P. *Protein Sci.* **1997**, *6(11)*, 2297-307.

(37) Hur, S.; Bruice, T. C. *J. Am. Chem. Soc.* **2002,** *124*, 7303-7313.

(38) Wu, Yong-Qian.; Belyakov, S.; Choi, C.; Limburg, D.; Thomas IV, B. E.; Vaal, M.; Wei, L.; Wilkinson, D. E.; Holmes, A.; Fuller, M.; McCormick , J.; Connolly, M.; Moeller, T.; Steiner, J.; Hamilton, G. S.. J. Med. Chem, 2003, 46(7), 1112-1115.

(39) Li, J.; Tan, Z.; Tang, S.; Hewlett, I.; Pang, R.; He, M.; He, S.; Tian, B .; Chen, K.; Yang, M. *Bioorg & Med chem*, **2009**, *17*, 3177-3188.

(40) Ni, S.; Yuan, Y.; Huang, J.; Mao, X.; Lv, M.; Zhu, J.; Shen, X.; Pei, J.; Lai, L.; Jiang, H.; Li, J. *J. Med. Chem.* **2009**, *52*, 5295-5298.

(41) Daum, S.; Schumann, M.; Mathea, S.; Aumller, T.; Balsley, M. A.; Constant, S. L.; Lacroix, B. F. d.; Kruska, F.; Braun, M. *Biochemistry* **2009**, *48*, 6268-6277.

I.II. Ionic Liquids

(1) Weingaertner, H. *Angew. Chem. Int. Ed.* **2008,** *47*, 654-670.

(2) (a) Forsyth, S. A.; Pringle, J. M.; MacFarlane, D. R. *Aust. J. Chem.* **2004,** *57*, 113-119; (b) Welton, T. *Chem. Rev.* **1999,** *99*, 2071-2083; (c) Seddon, K. R. *J. Chem. Tech. Biotechnol.* **1997,** *68*, 351-356; (d) Smiglak, M.; Metlen, A.; Rogers, R. D. *Acc. Chem. Res*. **2007**, *40*, 1182-1192.

(3) Bonhote, P.; Dias, A.-P.; Papageorgiou, N.; Kalyanasundaram, K.; Gratzel, M. *Inorg. Chem.* **1996,** *35*, 1168-1178.

(4) (a) Iwata, K.; Okajima, H.; Saha, S.; Hamaguchi, H. *Acc. Chem. Res.* **2007,** *40*, 1174-1181; (b) Castner, E. W.; Wishart, J. F.; Shirota, H. *Acc. Chem. Res.* **2007,** *40*, 1217-1227.

(5) (a) Hardacre, C.; Holbrey, J. D.; Nieuwenhuyzen, M.; Youngs, T. G. A. *Acc. Chem. Res.* **2007,** *40*, 1146-1155; (b) Hardacre, C.; Holbrey, J. D.; McMath, S. E. J. *J. Chem. Phys.* **2003,** *118*, 273-278.

(6) (a) MacFarlane, D. R.; Forsyth, M.; Howlett, P. C.; Pringle, J. M.; Sun, J.; Annat, G.; Neil, W.; Izgorodina, E. I. *Acc. Chem. Res.* **2007,** *40*, 1165-1173; (b) Tsuda, T.; Hussey, C. L. *Electrochem. Soc. Interface* **2007,** *16*, 42-49; (c) Silvester, D. S.; Compton, R. G. *Z. Phys. Chem.* **2006,** *220*, 1247-1274.

(7) (a) Han, X.; Armstrong, D. W. *Acc. Chem. Res.* **2007,** *40*, 1079-1086; (b) Visser, A. E.; Swatloski, R. P.; Reichert, W. M.; Jr., J. H. D.; Rogers, R. D.; Mayton, R.; Sheff, S.; Wierzbicki, A. *Chem. Commun.* **2001**, 135-136; (c) Huddleston, J. G.; Rogers, R. D. *Chem. Commun.* **1998**, 1765-1766.

(8) Pârvulescu, V. I.; Hardacre, C. *Chem. Rev.* **2007,** *107*, 2615-2665.

(9) van Rantwijk, F.; Sheldon, R. A. *Chem. Rev.* **2007,** *107*, 2757-2785.

(10) (a) Welton, T. *Coord. Chem. Rev.* **2004,** *248*, 2459-2477; (b) Wasserscheid, P.; Keim, W. *Angew. Chem. Int. Ed.* **2000,** *39*, 3772-3789.

(11) (a) Sheldon, R. *Chem. Commun.* **2001**, 2399 - 2407; (b) Haumann, M.; Riisager, A. *Chem. Rev.* **2008,** *108*, 1474-1497; (c) Zhang, Z. C. *Advances in Catalysis* **2006,** *49*, 153-237.

(12) (a) Smiglak, M.; Metlen, A.; Rogers, R. D. *Acc. Chem. Res.* **2007,** *40*, 1182-1192; (b) Lodge, T. P. *Science* **2008,** *321*, 50-51.

(13) Binnemans, K. *Chem. Rev.* **2007,** *107*, 2592-2614.

(14) (a) Ranke, J.; Stolte, S.; Störmann, R.; Arning, J.; Jastorff, B. *Chem. Rev.* **2007,** *107*, 2183-2206; (b) Docherty, K. M.; Kulpa Jr., C. F. *Green Chem.* **2005,** *7*, 185-189; (c) Stolte, S.; Arning, J.; Bottin-Weber, U.; Matzke, M.; Stock, F.; Thiele, K.; Uerdingen, M.; Welz-Biermann, U.; Jastorff, B.; Ranke, J. *Green Chem.* **2006,** *8*, 621-629.

(15) Wells, A. S.; Coombe, V. T. *Org. Process Res. Dev.* **2006,** *10*, 794-798.

(16) Gathergood, N.; Garcia, M. T.; Scammels, P. J. *Green Chem.* **2004,** *6*, 166-175.

(17) Nockemann, P.; Thijs, B.; Driesen, K.; Janssen, C. R.; Van Hecke, K.; Van Meervelt, L.; Kossmann, S.; Kirchner, B.; Binnemans, K. *J. Phys. Chem. B* **2007,** *111*, 5254-5263.

(18) Gathergood, N.; Scammels, P. J.; Garcia, M. T. *Green Chem.* **2006,** *8*, 156-160.

(19) Fukumotu, K.; Yoshizawa, M.; Ohno, H. *J. Am. Chem. Soc.* **2005,** *127*, 2398-2399.

(20) Pernak, J.; Stefaniak, F.; Wglewski, J. *Eur. J. Org. Chem.* **2005**, 650-652.

(21) (a) Lynden-Bell, R. M.; Del Pópolo, M. G.; Youngs, T. G. A.; Kohanoff, J.; Hanke, C. G.; Harper, J. B.; Pinilla, C. C. *Acc. Chem. Res.* **2007,** *2007*, 1138-1145; (b) Pádua, A. A. H.; Costa Gomes, M. F.; Canongia Lopes, J. N. A. *Acc. Chem. Res.* **2007,** *40*, 1087-1096; (c) Wang, Y.; Jiang, W.; Yan, T.; Voth, G. A. *Acc. Chem. Res.* **2007,** *40*, 1193-1199; (d) Cadena, C.; Zhao, Q.; Snurr, R. Q.; Maginn, E. J. *J. Phys. Chem. B* **2006,** *110*, 2821-2832; (e) Hunt, P. A. *Mol. Simul.*

2006, *31*, 1-10; (f) Canongia Lopes, J. N.; Padua, A. H. *J. Phys. Chem. B* **2004,** *108*, 16893-16898; (g) Liu, Z.; Huang, S.; Wang, W. *J. Phys. Chem. B* **2004,** *108*, 12978-12989; (h) Morrow, T. I.; Maginn, E. J. *Fluid Phase Equilibria* **2004,** *217*, 97-104; (i) de Andrade, J.; Böes, E. S.; Stassen, H. *J. Phys. Chem. B* **2002,** *106*, 3546-3548; (j) Borodin, O. *J. Phys. Chem. B.* **2009**, *113*, 11463-11478; (k) Hanke, C. G.; Price, S. L.; Lynden-Bell, R. M. *Mol. Phys.* **2001**, *99*, 801; (l) de Andrade, J.; Boes, E. S.; Stassen, H. *J. Phys. Chem. B* **2002**, *106*, 3546; (m) Margulis, C. J.; Stern, H. A.; Berne, B. J. *J. Phys. Chem. B* **2002**, *106*, 12017; (n) Morrow, T. I.; Maginn, E. J. *J. Phys. Chem. B* **2002**, *106*, 12807; (o) del Po´polo, M. G.; Voth, G. A. *J. Phys. Chem. B* **2004**, *108*, 1704; (m) Sambasivarao,S. V.; Acevedo, O. *J. Chem. Theory. Comput*., **2009**, *5(4)*, 1038-1050.

(22) Canongia Lopes, J. N.; Padua, A. A. H. *J. Phys. Chem. B* **2006,** *110*, 19586-19592.

(23) Canongia Lopes, J. N.; Deschamps, J.; Padua, A. H. *J. Phys. Chem. B* **2004,** *108*, 2038-2047.

(24) de Andrade, J.; Böes, E. S.; Stassen, H. *J. Phys. Chem. B* **2002,** *106*, 13344-13351.

I.III. Elimination Reactions

(1) (a) Hine, J.; Ramsay, O. B. *J. Am. Chem. Soc*. **1962**, *84*, 973; (b) Bordwell, F. G. *Acc. Chem. Res*. **1970**, *3*, 281; (c) Bordwell, F. G. Acc. Chem. Res. **1972**, *5*, 374; (d) More O'Ferrall, R. A.; Warren, P. J. J. *J.Chem. Soc., Chem. Commun.* **1975**, 483; (e) Saunders, W. H., Jr. *Acc. Chem. Res*. **1976**, *9*, 19; (f) More O'Ferrall, R. A. In *Structure and Dynamics in Chemistry*; Proceedings from Symposium held at Uppsala, 1977; Ahlberg, P., Sundelo¨f, L.-O., Eds.; Acta Universitatis Upsaliensis, Symposia Universitatis Uppsaliensis, Annum Quingentesimum Celebratis 12, Almqvist and Wiksell International, Stockholm; p 209; (g) Marshall, D. R.;

Thomas, P. J. M.; Stirling, C. J. *J. Chem. Soc., Perkin Trans. 2* **1977**, 1914; (h) Cavestri, R. C.; Fedor, L. R. *J. Am. Chem.Soc.* **1970**, *92*, 4610; (i) Fedor, L. R.; Glave, W. R. *J. Am. Chem. Soc.* **1971**, *93*, 985; (j) Gandler, J. R.; Jencks, W. P. *J. Am. Chem. Soc.* **1982**, *104*, 1937-1951; (k) Thibblin, A. *J. Am. Chem. Soc.* **1988**, *110*, 4582; (l) Jia, Z.S.; Rudzinski, J.; Paneth, P.; Thibbin. A. *J. Org. Chem.* **2002**, *67*, 177-181.

(2) (a) Saunders, W. H.; Cockerill, A. F. *Mechanisms of elimination Reactions*. Wiely: New York, 1973; Chapt. 2 280-293; (b) MacLennan, D. J.; Wong, R. J. *J. Chem. Soc., Perkin Trans. 2* **1974,** 1373-1377; (c) Gandler, J. R.; Storer, J. W.; Ohlberg, D. A. A. *J. Am. Chem. Soc.* **1990,** *112*, 7756-7762.

(3) Spillane, W.; McGrath, P.; Brack, C.; O'Byrne, A. *J. Org. Chem.* **2001**, *66*, 6313-6316.

(4) (a) Fontana, G.; Frenna, V.; Gruttaadauria, M.; Natoli, M. C.; Noto, R. *J. Phys. Org. Chem*, **1998**, *11*, 54-58; (b) Fontana, G.; Frenna, V.; Lamartina, L.; Natoli, M. C.; Noto, R. *J. Phys. Org. Chem*, **2002**, *15*, 108-114.

(5) D'Anna, F.; Frenna, V.; Pace, V.; Noto, R. *Tetrahedron* **2006**, *62*, 1690–1698;

(6) D'Anna, F.; La Marca, S.; Noto, R. Kemp Elimination: A Probe Reaction To Study Ionic Liquids Properties. *J. Org. Chem*., **2008**, 73, 3397– 3403.

(7) (a) Casey, M. L.; Kemp, D. S.; Paul, K. G.; Cox, D. D. *J. Org. Chem.***1973**, *38*, 2294–2301; (b) Kemp, D. S.; Cox, D. D.; Paul, K. G. *J. Am. Chem.Soc.* **1975**, *97*, 7312–7318.

(8) (a) Peréz-Juste, J.; Hollfelder, F. *Org. Lett.* **2000**, *2*, 127–130; (b) Klijn, J. E.; Engberts, J. B. F. N. *J. Am. Chem. Soc.* **2003**, *125*, 1825–1833; (c) Klijn, J. E.; Engberts, J. B. F. N. *Org. Biomol. Chem.* **2004**, *2*, 1789–1799.

(9) (a) Thorn, K. K. S. N.; Hilvert, D. *J. Am. Chem. Soc.* **1996**, *118*, 8184–8185; (b) Hollfelder, F.; Kirby, A. J.; Tawfik, D. S. *J. Am. Chem. Soc.* **1997**, *119*, 9578–9579; (h) Hollfelder, F.;

Kirby, A. J.; Tawfik, D. S.; Kikuchi, K.; Hilvert, D. *J. Am. Chem. Soc.* **2000**, *122*, 1022–1029; (c) Hotta, K.; Kikuchi, K.; Hilvert, D. *Hel*V. *Chim. Acta* **2000**, *83*, 2183–2191; (d) Hollfelder, F.; Kirby, A. J.; Tawfik, D. S. *J. Org. Chem.* **2000**, *66*, 5866–5874; (e) Lemma-Gray, P. *Biotechnol. Bioeng.* **2001**, *74*, 524–527; (f) Hu, Y.; Houk, K. N.; Kikuchi, K.; Hotta, K.; Hilvert, D. *J. Am. Chem. Soc.* **2004**, *126*, 8197–8205; (g) Seebeck, F. P.; Hilvert, D. *J. Am. Chem. Soc.* **2005**, *127*, 1307–1312; (h) Acevedo, O. *J. Phys. Chem. B* **2009,** *113*, 15372–15381.

(10) McCraken, P. G.; Ferguson, C. G.; Vizitiu, D.; Walkinshaw, C. S.; Wang, Y.; Thatcher, G. R. J. *J. Chem. Soc., Perkin Trans. 2* **1999**, *911*, 912.

Chapter II. Computational Methods

II.I. Cyclophilins inhibition: Free energy perturbation calculations

The accurate prediction of protein-ligand binding affinities is one of the great challenges in computational modeling ligand design.[1] Among all the available methods, theoretically most accurate and time consuming, free energy perturbation (FEP) in conjunction with Monte Carlo statistical mechanics (MC) or molecular dynamics simulations is able to predict binding energies most accurately.[1,2] Conjunction of FEP with MC generates an ensemble of thermodynamically accessible conformations of the ligand and calculate averages of the binding affinities.[3] The free energy changes can be computed with the use of classical force fields with extensive sampling, FEP and thermodynamic integration (TI) calculations.[2] The results of the prediction methods depend on the three dimensional structure of biomolecule in complexed with ligand. A docking methodology is used to construct the protein-ligand complexes for binding free energy calculations.[4] Relative binding affinities are obtained, but for lead optimization, it is sufficient to study the effects of change by functional substituents.[2] Although FEP/TI calculations are most rigorous, the accuracy of the results is affected by polarization effects, quality of force fields, and inadequate sampling.[2]

De Novo Design of ligands: BOMB is used for growing molecules by adding various substituents to an isolated core/lead, or that is placed in a binding site of a protein.[5] A library of ca. 700 possible substituents are included in BOMB. For typical setup in BOMB, the user should specify the core, the topology, and the substituents. The hydrogens in the core structure are replaced by the user specified substituents. For the growing molecule, a thorough conformational search and dihedral optimization are performed in the binding site using OPLS-AA force field for the protein and OPLS/CM1A for the analogue molecule.[6] A docking-like scoring function is used to evaluate and predict activity for the lowest-energy conformer.

The free energy perturbation (FEP) technique serves as the foundation for computing protein-ligand binding affinities in this work. FEP uses the Zwanzig[7] expression (eq 1) to relate the free energy difference between an initial (0) and final (1) state of a system. The difference in free energies of binding for the ligands X and Y then comes from eq 2. For relative free energies of binding, single-topology perturbations[1] are made to convert one ligand to another using the thermodynamic cycle shown in Figure 1. Two series of mutations are performed to convert X to Y unbound in water and complexed to the protein which yield ΔG_F and ΔG_C.[1,2]

$$\Delta G(X \rightarrow Y) = -k_B T \ln \langle \exp [-(E_Y - E_X)/k_B T] \rangle_X \quad (1)$$

$$\Delta\Delta G_{bind} = \Delta G_X - \Delta G_Y = \Delta G_F - \Delta G_C \quad (2)$$

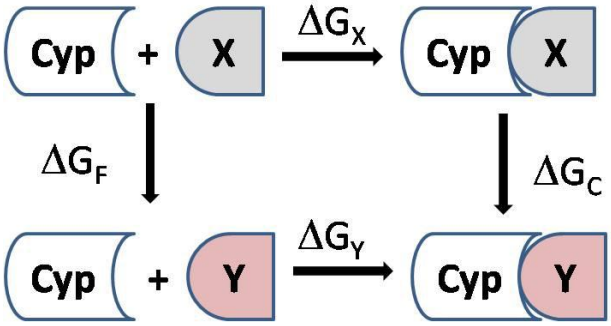

Figure 1. Thermodynamic cycle for relative free energies of binding. Cyp is the cyclophilin receptor and X and Y are different ligands.

The ligand mutations of compounds **1**-**3** used double-wide sampling with 14 FEP windows; a similar methodology was recently reported.[2,8] A window refers to a Monte Carlo (MC) simulation at one point along the mutation coordinate λ, which interconverts two ligands as λ goes from 0 to 1. Double-wide implies that two free energy changes are computed at each window, corresponding to a forward and backwards increment. The spacing between the windows, Δλ, is primarily 0.1 with the exception of λ = 0 – 0.2 and 0.8 – 1 where the spacing is 0.05, which addresses the fact that the free energy often changes most rapidly in these regions.

Preparation of Protein-Ligand Complexes for simulations: Initial Cartesian coordinates for the protein-ligand structures were generated with the molecule growing program BOMB starting from the PDB files 1awq[9] for CypA and 1cyn[10] for CypB; the existing complexed ligands were removed and replaced by cores such as formaldehyde to grow the desired analogues in the binding site. The present models include one active site, the inserted ligand, and all crystal structure residues. Terminal residues were capped with acetyl or N-methylamine groups. The system was then subjected to conjugate-gradient energy minimization in order to relax the contacts between protein residues and the ligand. The total charge of the

system was set to zero by adjusting the protonation states of a few residues furthest away from the center of the system. The entire system was solvated with 25-Å caps containing 1250 and 2000 TIP4P water molecules[11] for the protein complexes and unbound ligands, respectively; a half-harmonic potential with a force constant of 1.5 kcal mol^{-1} A^{-2} was applied to water molecules at a distance greater than 25 Å. The MC/FEP calculations were executed with MCPRO.[12] The energetics of the systems were classically described with the OPLS-AA force field for the protein and OPLS/CM1A for the ligands.[13] For the MC simulations, all degrees of freedom were sampled for the ligands, while TIP4P water molecules only translated and rotated; bond angles and dihedral angles for protein side chains were also sampled, while the backbone was kept fixed after the conjugate-gradient relaxation. Each mutation window for the unbound ligands in water consisted minimally of 20 million (M) configurations of MC equilibration followed by 40M configurations of averaging. For the bound calculations, the equilibration period is minimally 5 M configurations of solvent only moves, followed by 10 M configurations of full equilibration, followed by 20 M configurations of averaging. All MC simulations were carried out at 25 °C. A recent QM/MM study of catalytic antibody 4B2 by Acevedo used a similar computational setup and produced close agreement with experimental rate data.[14]

In some cases, AUTODOCK 4.2[15] was used to dock the full inhibitors (not cores) into the crystal structures for verification of the binding conformations predicted by BOMB. AutoDockTools (ADT) was used to prepare, run, and analyze the docking simulations. The rigid roots of each ligand were defined automatically, and the amide bonds were made non-rotatable. Polar hydrogens were added, and Gasteiger charges were assigned; non-polar hydrogens were subsequently merged. A grid was centered on the catalytic active site region and included all amino acid residues within a box size set at x = y = z = 40 Å. AutoGrid 4 was used to produce

grid maps with the spacing between the grid points of 0.375 Å. The Lamarckian Genetic Algorithm (LGA) was chosen to search for the best conformers. During the docking process, 50-100 conformers were considered for each compound. The population size was set to 150 and the individuals were initialized randomly. The maximum number of energy evaluations was set up to 2500000; default docking parameters were primarily used, for example: maximum number of generations to 27000, maximum number of top individuals that automatically survived set to 1, mutation rate of 0.02, crossover rate of 0.8, step sizes were 2 Å for translations, 50° for quaternions, and 50° for torsions, and a cluster tolerance of 2 Å was employed.

II.II. Force Fields or Potential Energy functions

Quantum mechanical (QM) calculations are suitable for studies of smaller, chemical systems of about 150 atoms or less in the gas phase; however, development is underway to treat larger systems.[1] Biochemical systems involve macromolecules and proteins in a condensed phase environment containing 20,000 or more atoms. The dynamics and mobility of biological molecules require a large number of conformations in energy calculations.[2] Thus, for the systems containing 10^N atoms, an energy function is required which allows 10^{N+1} or more calculations.

Potential energy functions can fulfill the computational demands required in the elucidation of larger molecules or biological systems. Force fields contain mathematical equations to describe the physical interactions which dictate the structure and dynamic properties of large macromolecular systems. Force fields use an atomistic approach to calculate the energy of the system, rather than an electronic approach in quantum mechanical calculations; allow computational demands required to perform sufficient number of energy calculations on larger systems. To attain the required chemical accuracy, the parameters in the mathematical models

should be properly optimized. Initially, potential energy functions applied to small organic molecules and recently to biological systems.[2]

A force field or potential energy function is a mathematical equation that calculates the potential energy of a chemical system as a function of its structure. The mathematical equation contains terms which describe the various physical interactions of the structure and properties of a chemical or biological system. The basic form of force field contains both bonded and non-bonded terms. Bonded terms are linked by covalent bonds and the non-bonded terms describe the electrostatic and van der Waals (VDW) forces. The total potential energy of a chemical system E_{total} can be represented by equation 3.

$$E_{total} = E_{bonds} + E_{angles} + E_{torsion} + E_{nonbond} \quad (3)$$

The total energy of the systems are evaluated as a sum of individual energies for the harmonic bond stretching and angle bending terms, a Fourier series for torsional energetics, and Coulomb and 12-6 Lennard-Jones terms for the nonbonded interactions, see equations 4-7. The parameters are the force constants k, the r_o and θ_o reference values for bond length and angle, the Fourier coefficients V referred to the height of the barrier to the rotation, the partial atomic charges, q, and the Lennard-Jones radii σ, and well-depths ε indicate the magnitude of the favorable London's dispersion interactions between the two atoms.

$$E_{bonds} = \sum_i k_{b,i}(r_i - r_{o,i})^2 \quad (4)$$

$$E_{angles} = \sum_i k_{b,i}(\theta_i - \theta_{o,i})^2 \quad (5)$$

$$E_{torsion} = \sum_i [\tfrac{1}{2}V_{1,i}(1+\cos\phi_i) + \tfrac{1}{2}V_{2,i}(1+\cos 2\phi_i) + \tfrac{1}{2}V_{3,i}(1+\cos 3\phi_i) + \tfrac{1}{2}V_{4,i}(1+\cos 4\phi_i)] \quad (6)$$

$$E_{nonbond} = \sum_i \sum_{j>i} \{\frac{q_i q_j e^2}{r_{ij}} + 4\varepsilon_{ij}[(\frac{\sigma_{ij}}{r_{ij}})^{12} - (\frac{\sigma_{ij}}{r_{ij}})^6]\} \quad (7)$$

The geometric combining rules regularly used for the Lennard-Jones coefficients are employed: $\sigma_{ij} = (\sigma_{ii}\sigma_{jj})^{1/2}$ and $\varepsilon_{ij} = (\varepsilon_{ii}\varepsilon_{jj})^{1/2}$.[28] Nonbonded interactions are evaluated intermolecularly and for intramolecular atom pairs separated by three or more bonds. $1/r^{12}$ and $1/r^{6}$ represent the exchange repulsive and attractive terms between atoms, 12-6 is purely for rapid calculations. In order to use identical parameters for both intra- and intermolecular interactions, the 1,4-intramolecular interactions are reduced by a factor of 2.[3]

The size of the condensed phase and biological systems are always a limiting factor in computational simulations. Extended-atom/united atom models versus all-atom models are a useful tool to represent the minimum size of the system. In extended-atom model, all hydrogens are not explicitly represented and treated as part of a nonhydrogen atom to which bonded covalently. But polar hydrogens, which are responsible for hydrogen bonding, should be treated explicitly. The use of extended-atom models is decreasing with ever increasing computer resources; however, these models are useful for the systems having large conformational space.[4]

The parameterization of the force field is follows: (1) charges to each atom and equilibrium geometries obtained through ab initio calculations. (2) Adjust force constants to fit the vibrational frequency data (3) Determine torsion parameters by fitting torsion energy profiles. (4) The VDW parameters are refined to validate QM training set and obtain new set of parameters. (5) Repeat 2, 3, 4 steps until a small deviation is observed between two sets of parameters. (6) Validate the force field through liquids simulations using Monte Carlo (MC) in the NPT or Molecular dynamics (MD) in NVE conditions, and compare to experimental densities and heats of vaporization.[5]

Currently, the most widely used potential energy functions for organic, biological and condensed phase systems are OPLS-AA,[3] CHARMM,[6] and AMBER[7] and follows the above

mentioned format with minor variations in the VDW parameters. The method to determine atomic charges in OPLS[3] is through ab intio electro static potential (ESP) fit/ an empirical way. In CHARMM,[6] charges will fit interaction between probe water and model molecules, and its force field contains improper Urey-Bradly term to treat 1,3 atoms. A restraint electrostatic potential (RSEP) fit method is used in AMBER.[8] OPLS-AA and AMBER force fields are generally transferable. Other force fields of interest are MM4 and MMFF4.[9]

OPLS-AA Force Field Parameters for Ionic Liquids: To achieve compatibility with OPLS-AA, all present parameters were developed for ionic liquid simulations in a similar fashion to recent parameterization efforts by Jorgensen and coworkers.[10-12] Whenever appropriate, published potentials were retained without change. This includes assigning all standard bond stretching and angle bending force constants from OPLS-AA, which may also include some entries from the AMBER-AA force field.[7] All Lennard-Jones parameters also came from the OPLS-AA parameter set except when explicitly stated. The present work then focused on the development of Fourier coefficients, partial charges, and equilibrium geometries, and the validation of multiple ionic liquid combinations.

Ab Initio Calculations. All individual ions, i.e. [RMIM] (R=Me, Et, Bu), [RPyr] (R=Me, Et, Bu), and [Chol] cations with [Cl], [PF_6], [BF_4], [NO_3], [$AlCl_4$], [Al_2Cl_7], [TfO], [Sacc], and [Ace] anions (see Chapter I, Figure 3), were optimized using the Jaguar program[13] at the Hartree-Fock (HF) theory level using the 6-31G(d) basis set with subsequent single-point energy calculations using the local Møller-Plesset second-order perturbation (LMP2)[14] method and the correlation-consistent polarized valence cc-pVTZ(-f) basis set.[15] This LMP2/cc-pVTZ(-f)//HF/6-31G(d) method is the current practice for OPLS-AA parameterization.[12] Vibrational analytical frequency calculations at the HF/6-31G(d) were carried out to confirm all minima as

stationary points. The ab initio derived ion geometries were used for the equilibrium bond and angle, r_o and θ_o, reference values in the force field and given in the Supporting Information. Partial charges were computed by fitting the molecular electrostatic potential (ESP) at the atomic centers. For a better description of the charge density, LMP2 dipole moments were also computed along with a coupled perturbed Hartree-Fock (CPHF) term. Charges were symmetrized for similar atoms and used for the Coulombic nonbonded force field partial charges. Torsional energies were fit to reproduce computed LMP2/cc-pVTZ(-f)//HF/6-31G(d) energy scans. Calculations at this level have been reported to yield highly accurate conformational energies with average errors of ca. 0.25 kcal/mol for reported test sets and 0.6 kcal/mol for perfluorolalkanes.[12] Greater detail on the torsional scans and assignment of partial charges are given in Chapter 4.

Ionic Liquid Simulations. The Metropolis Monte Carlo (MC) simulations were performed with the BOSS 4.6 program.[16] All cations were fully flexible; all bond stretching, angle bending, and torsional motions were sampled. Anions were simulated as rigid molecules and as a result no additional intramolecular anion parameterization was necessary. The use of rigid anions in OPLS-AA has been shown to provide an accurate representation of ionic liquid physical properties,[17] including use as a reaction medium for a computed QM/MM Diels-Alder reaction study.[18] Periodic boundary conditions have been applied to boxes containing 190 ion pairs with long range interactions handled with Ewald summations. In short, Ewald summations calculate the exact electrostatic energy of an infinite lattice of identical copies of the simulation cell. This suppresses artifacts resulting from the simple cutoff of the long-range electrostatic interactions prevalent in the ionic liquid. The liquid phase simulations were carried out by placing the 380 ions at random positions in the simulation box (see Figure 2) and a temperature

value of 1000 °C was initially applied for 10 million configurations in the NVT ensemble to encourage a thorough mixing. The simulations were then equilibrated at 25 °C for 100-200 million MC steps in the NPT ensemble. The heating/NVT and equilibration/NPT simulations on each ionic liquid system were repeated sequentially an average of 4-6 times until the energy and volume of the system no longer decreased. A pressure of 1 atm was used in all cases. The computed densities, heats of vaporization, energy distributions, and conformational properties were very well converged with MC simulations of this length.

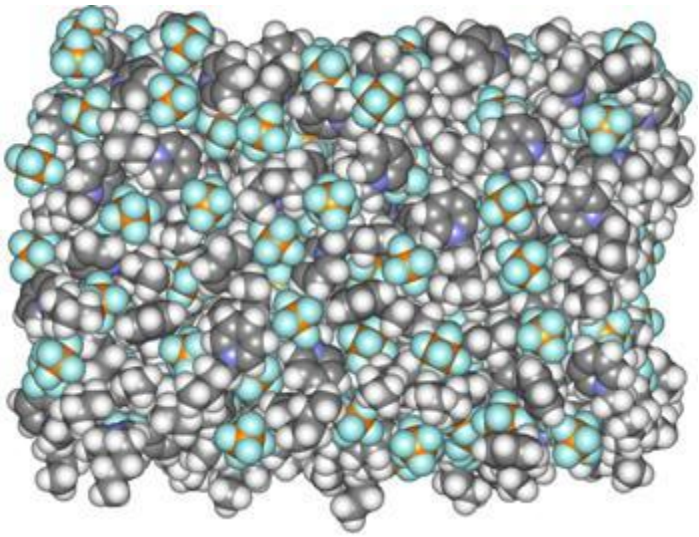

Figure 2. Illustration of an equilibrated [BPyr][PF_6] ionic liquid simulation box.

In order to compute the heats of vaporization, ΔH_{vap}, MC simulations needed to be performed on the gas-phase ion pair of the corresponding ionic liquid due to the flexibility of the cations. Experimental evidence suggests that ionic liquids go into the vapor phase in ion pairs.[19] Gas-phase simulations consisted of 1 million configurations of equilibration, followed by 2 million configurations of averaging. For the liquids, the systems were periodic and tetragonal with *c/a* = 1.5; as an example, *a* is ca. 34.3 and 35.5 Å for [BMIM][BF_4] and [BMIM][PF_6] (box sizes for all ionic liquids are given in the Supporting Information of this thesis).

Solvent-solvent intermolecular cutoff distances of 12 Å were employed for the tail carbon atom of each side chain (methyl and alkyl), a midpoint carbon on the alkyl chain, and the ring carbon between both nitrogens for imidazolium. Cutoff atoms were also based on alkyl side chain length for N-pyridinium using the carbon at the end of the alkyl chain, a mid-point carbon on the side-chain, the nitrogen atom, and the carbon ring atom *para* to the nitrogen. For choline, atoms O and N, along with two Cs bonded to N (methyl and on the chain) were used for cutoffs. Center atoms, e.g. B in BF_4^- and P in PF_6^-, were used for the anions. If any distance is within the cutoff, the entire solvent-solvent interaction was included. Adjustments to the allowed ranges for rotations, translations, and dihedral angle movements led to overall acceptance rates of about 40-50% for new configurations. The ranges for bond stretching and angle bending were set automatically by the BOSS program on the basis of force constants and temperature. All MC calculations were run on a Linux cluster at Auburn University and all ab initio calculations were performed on computers located at the Alabama Supercomputer Center.

II.III. Elimination Reactions

Potentials of Mean force: The free energy changes along the surface of the chosen coordinate is known as potential of mean force (PMF).[1] The free energy changes as a function of inter or intra molecular coordinate, e.g., an interatomic distance between two molecules or the torsion angle of a bond within a molecule. If a reaction is carried out in a solvent, the PMF includes solvent effects along with the interaction between two particles. The point of highest energy on the free energy surface obtained through PMF calculations is the transition state for the process, and rate constants activation energies are derived from it.[1]

The simple form of the PMF is the free energy change over the distance (r) between two particles is changed. The PMF can be calculated from the radial distribution function (RDF) using the eq 8.

$$A(r) = -k_B T \ln g(r) + \text{constant} \quad (8)$$

Monte Carlo or molecular dynamics simulations alone do not sufficiently sample regions where RDF differs more from the average value. Application of Umbrella sampling avoids this problem; it overcomes the sampling problem by including the weighting function potential. The unfavorable states are sampled sufficiently with umbrella sampling, so this method can be used with MC or MD simulations. PMF can also be calculated using the FEP method with MC or MD simulations.[2]

Combined Quantum and Molecular Mechanics Approaches:

Organic and enzymatic reactions in solution can be performed using a quantum mechanics and molecular mechanics methodology.[1] The reacting system is described by QM methods, and the remainder of the system is represented by MM force field. These methods can perform bond-making and bond breaking processes in reactions, and it can be applied to systems to larger than QM alone or that lack MM force field parameters.[1] The total energy E_{TOT} of the system can be calculated using the eq 9.

$$E_{TOT} = E_{QM} + E_{MM} + E_{QM/MM} \quad (9)$$

Where E_{QM} is the energy of the system treated with quantum mechanics (semi-empirical, ab initio, density functional theory or valence bond), and E_{MM} is the energy of the system treated purely with molecular mechanics. $E_{QM/MM}$ is the energy of the junction between the QM and MM

parts of the system. The potential energy of the regions between QM and MM is given by Coulombic and Lennord-Jones interactions (eq 10)

$$E_{\text{nonbond}} = \sum_{i} \sum_{j>i} \left\{ \frac{q_i q_j e^2}{r_{ij}} + 4\varepsilon_{ij} \left[\left(\frac{\sigma_{ij}}{r_{ij}} \right)^{12} - \left(\frac{\sigma_{ij}}{r_{ij}} \right)^{6} \right] \right\} \qquad (10)$$

The σ and ε parameters are taken from MM force field along with atomic charge q_i assigned for MM atoms. Computation of atomic charges for QM atoms is an important issue, so suitable charge model with appropriate scaling factors is required.

The important way to handle QM/MM region is to avoid half-filled orbitals in QM region, which would arise on simply truncation of connection bonds. This problem can be eliminated by implementing the hybrid sp^2 orbital containing one electron along the QM/MM region,[1.b] use of link atoms (typically hdrogens, sometimes halogens or methyl groups) to ensure valency is maintained[3] or treated with simple valence bond like potential model.[4]

References

II.I. Cyclophilins inhibition: Free energy perturbation calculations

(1) (a) Straatsma, T. P.; McCammon, J. A. Computational Alchemy. *Ann. Rev. Phys. Chem.* **1992**, *43*, 407-435; (b) Jorgensen, W. L.; Thomas, L. L. Perspective on Free-Energy Perturbation Calculations for Chemical Equilibria. *J. Chem. Theory Comput.* **2008**, *4*, 869-876.

(2) Jorgensen, W. L. *Acc. Chem. Res.* **2009**, *42*, 724-733.

(3) Nervall, M.; Hanspers, P.; Carlsson, J.; Aqvist, J. *J. Med. Chem*. **2008**, *51*, 2657-2667.

(4) Taylor, R. D.; Jewsbury, P. J.; Essex, J. W. *J. Comput. Aided Mol. Des*. **2002**, *16*, 151-166.

(5) Barreiro, G.; Kim, J. T.; Guimaraes, C. R. W.; Bailey, C. M.; Domaoal, R. A.; Wang, L.; Anderson, K. S.; Jorgensen, W. L. *J. Med. Chem.* 2007, *50*, 5324–5329.

(6) Jorgensen, W. L.; Tirado-Rives, J. *Proc. Natl. Acad. Sci. U.S.A.* 2005, *102*, 6665–6670.

(7) Zwanzig, R. W. *J. Chem. Phys*. **1954**, *22*, 1420-1426.

(8) Zeevaart, J. G.; Wang, L.; Thakur, V. V.; Leung, C. S.; Tirado-Rives, J.; Bailey, C. M.; Domaoal, R. A.; Anderson, K. S.; Jorgensen, W. L. *J. Am. Chem. Soc.* **2008**, *130*, 9492-9499.

(9) Vajdos, F. F.; Yoo, S.; Houseweart, M.; Sundquist, W. I.; Hill, C. P. *Prot. Sci.* **1997**, *6*, 2297-2307.

(10) Mikol, V.; Kallen, J.; Walkinshaw, M. D. *Proc. Natl. Acad. Sci. USA* **1994**, *91*, 5183-5186.

(11) Jorgensen, W. L.; Chandrasekhar, J.; Madura, J. D.; Impey, W.; Klein, M. L. *J. Chem. Phys.* **1983**, *79*, 926-935.

(12) Jorgensen, W. L.; Tirado-Rives, J. *J. Comput. Chem.* **2005**, *26*, 1689-1700.

(13) Jorgensen, W. L.; Tirado-Rives, J. *Proc. Nat. Acad. Sci. USA* **2005**, *102*, 6665-6670.

(14) Acevedo, O. *J. Phys. Chem. B* **2009**, *113*, 15372-15381.

(15) Morris, G. M.; Huey, R.; Lindstrom, W.; Sanner, M. F.; Belew, R. K.; Goodsell, D. S.; Olson, A. J. *J. Comput. Chem.* **2009**, *30*, 2785-2791.

II.II. Force Fileds of Potential energy functions

(1) York, D. M.; Lee, T. S.; Yang, W.; *J. Am. Chem. Soc.* **1996**, *118*, 10940-10941.

(2) (a) Brooks III, C. L.; Karplus, M.; Pittitt, B. M. Proteins, A Theoretical Perspective: Dynamica, Structure, and Thermodynamics, Vol 71. New York: Wiley, 1988; (b) McCammon, J. A.; Harvey, S. C. Dynamics of Proteins and Nucleic Acids. New York: Cambridge Unit Press, 1987; (c) Burkert, U.; Allinger, N. L. Molecular Mechanics. Washington, DC: American Chemical Society, 1992.

(3) Jorgensen, W. L.; Maxwell, D. S.; Tirado-Rives, J. *J. Am. Chem. Soc.* **1996,** *118*, 11225-11236.

(4) Lazaridis, T.; Karpplus, M. *Science*, **1997**, *278*, 1928-1931.

(5) Jorgensen, W. L.; Tirado-Rives J. *PNAS*. **2005**, *102*(*19*), 6665-6670.

(6) (a) Brooks, B. R.; Bruccoleri, R. E.; Olafson, B. D.; States, D. J.; Swaminathan, S.; Karplus, M. *J. Comput. Chem.* **1983**, *4*, 187-217; (b) MacKerell, A. D. Jr. Protein force fields. In: Pvr Schleyer, Schleyer, Allinger, N. L.; Clark, T.; Gasteiger, J.; Kollaman, P. A.; Schreiner P. R.; eds. The Encyclopedia of Computational Chemistry, Vol 3 . Chichester, UK, Wiley 1998, 2191-2200. (c) MacKrell A.D.; Jr.; Bashford, D.; Bellott, M.; Dunbrack, R. L.; Evanseck, J .D.; Field, M. J.; Fischer, S.; Guo, H.; Ha, S.; et al. *J. Phys. Chem. B.* **1998**, *102*, 3586.

(7) Cornell, W. D.; Cieplak, P.; Bayly, C. I.; Gouls, I. R.; Merz, K. M.; Ferguson, D. M.; Spellmeyer, D. C.; Fox, T.; Caldwell, J. W.; Kollaman, P. A. *J. Am. Chem. Soc.* **1995**, *117*, 5179-5197.

(8) Bayly, C. I.; Cieplak, P.; Cornell, W. D. Kollaman, P. A. *J. Phys. Chem.* **1993**, *97*, 10269.

(9) Allinger, N. L.; Chen, K.; Li, J. H. *J. Comput. Chem.* **1996**, *17*, 642-668. (b) Halgren, T. A. *J. Comput. Chem.* **1996**, *17*, 490-519.

(10) (a) Jensen, K. P.; Jorgensen, W. L. *J. Chem. Theory Comput.* **2006,** *2*, 1499-1509; (b) Price, M. L. P.; Ostrovsky, D.; Jorgensen, W. L. *J. Comput. Chem.* **2001,** *22*, 1340-1352; (c) Rizzo, R. C.; Jorgensen, W. L. *J. Am. Chem. Soc.* **1999,** *121*, 4827-4836; (d) Jorgensen, W. L.; McDonald, N. A. *J. Phys. Chem. B* **1998,** *102*, 8049-8059.

(11) Jorgensen, W. L.; Tirado-Rives, J. *Proc. Nat. Acad. Sci. USA* **2005,** *102*, 6665-6670.

(12) (a) Kaminski, G. A.; Friesner, R. A.; Tirado-Rives, J.; Jorgensen, W. L. *J. Phys. Chem. B* **2001,** *105*, 6474-6487; (b) Watkins, E. K.; Jorgensen, W. L. *J. Phys. Chem. A* **2001,** *105*, 4118-4125.

(13) Jaguar, version 6.0, Schrödinger, LLC, New York, NY, 2005.

(14) (a) Saebo, S.; Pulay, P. *Ann. Rev. Phys. Chem.* **1993,** *44*, 213-236; (b) Saebo, S.; Tong, W.; Pulay, P. *J. Chem. Phys.* **1993,** *98*, 2170-2175.

(15) Dunning Jr., T. H. *J. Chem. Phys.* **1989,** *90*, 1007-1023.

(16) Jorgensen, W. L.; Tirado-Rives, J. *J. Comput. Chem.* **2005,** *26*, 1689-1700.

(17) Canongia Lopes, J. N.; Deschamps, J.; Padua, A. H. *J. Phys. Chem. B* **2004,** *108*, 2038-2047.

(18) Acevedo, O.; Jorgensen, W. L.; Evanseck, J. D. *J. Chem. Theory Comput.* **2007,** *3*, 132-138.

(19) Armstrong, J. P.; Hurst, C.; Jones, R. G.; Licence, P.; Lovelock, K. R. J.; Satterley, C. J.; Villar-Garcia, I. J. *Phys. Chem. Chem. Phys.* **2007,** *9*, 982-990.

II.III. Elimination Reactions: PMF, QM/MM

(1) (a) Warshel, A.; Karplus, M. *J. Am. Chem.Soc.* **1972**, *94*, 5612–5625; (b) Warshel, A.; Levitt, M. *J. Mol. Biol.* **1976**, *103*, 227–249; (c) Warshel, A. *Acc. Chem. Res.* **2002**, *35*, 385–395; (d) Kamerlin, S. C. L.; Haranczyk, M.; Warshel, A. *J. Phys. Chem.B* **2009**, *113*, 1253–1272; (e) Senn, H. M.; Thiel, W. *Angew. Chem.,Int. Ed.* **2009**, *48*, 1198–1229; (f) Gao, J.; Ma, S.; Major, D. T.; Nam, K.; Pu, J.; Truhlar, D. G. *Chem. Rev.* **2006**, *106*, 3188–3209; (g) Vreven, T.; Morokuma, K. *Ann. Rep.Comput. Chem.* **2006**, *2*, 35–51; (h) Acevedo, O.; Jorgensen, W. L. *Ann. Rep. Comput. Chem.* **2006**, *2*, 263–278; (i) Jorgensen, W. L. *Acc. Chem. Res.* **1989**, *22*, 184–189. (j) Kollman, P. A. *Chem.Rev.* **1993**, *93*, 2395–2417; (k) Jorgensen, W. L.; Blake, J. F.;

Lim, D.; Severance, D. L. *J. Chem. Soc., Faraday Trans.* **1994**, *90*, 1727–1732; (l) Acevedo, O.; Jorgensen, W. L. *Acc. Chem. Res.* **2010**, *43*, 142-151; (m) Leech, A. R. Molecular Modelimg: principles and applications, 2nd ed. Chapter 11, 563.

(2) (a) Jorgensen, W. L.; Buckner, J. K. *J. Phys. Chem.* **1987**, *91*, 6083-6085; (b) Acevedo, O.; Jorgensen, W. L.; Evanseck, J. D. *J. Chem. Theory Comput.* **2007**, *3*, 132-138; (c) Acevedo, O.; Jorgensen, W. L. *J. Am. Chem. Soc.* **2005**, *127*, 8829-8834.

(3) Singh, U. and Kollman, P. *J. Comput. Chem.* **1986**, *7*, 718-730.

(4) (a) Aqvist, J.; Warshal, A. Chem. Rev, 1993, 93, 2523-2544; (b) Warshal, A. Computer Modeling of chemical Reactions in Enzymes and Solutions. **1991**, New York, John Wiley & Sons.

Chapter III. Computational insight into small molecule inhibition of cyclophilins

In the current study, Monte Carlo statistical mechanics simulations utilizing free energy perturbation theory (MC/FEP) have been used to calculate the relative free-energies of binding, $\Delta\Delta G_{bind}$, for multiple potent small molecule inhibitors of CypA and CypB (Figure 1). Atomic-level computer models of the proteins were constructed from high-resolution crystal structures and the resultant MC/FEP calculations have yielded good agreement with recently reported experimental IC_{50} (*in vitro*) values for substituted acylurea-based compounds (**1**) in CypA[1] and K_i (inhibitory constant) values for multiple variations of aryl 1-indanylketone-based compounds (**2** and **3**) in CypA and CypB.[2] Insight is provided into the origin of the nanomolar inhibitory potency of compound **1** and the observed binding specificity between CypA and CypB by compounds **2** and **3**. The reasons behind the selectivity have been difficult to rationalize from an experimental perspective given the complete conservation of all active site residues between the

*Reprinted in part from *J. Chem. Inf. Model.*, **2011**, 51, 475-482.

cyclophilins. An enhanced understanding of the intermolecular interactions occurring in the multiple protein-ligand complexes is given and could aid in the creation of antiviral therapeutics based on small organic inhibitors that display desirable pharmacokinetic and physicochemical characteristics.

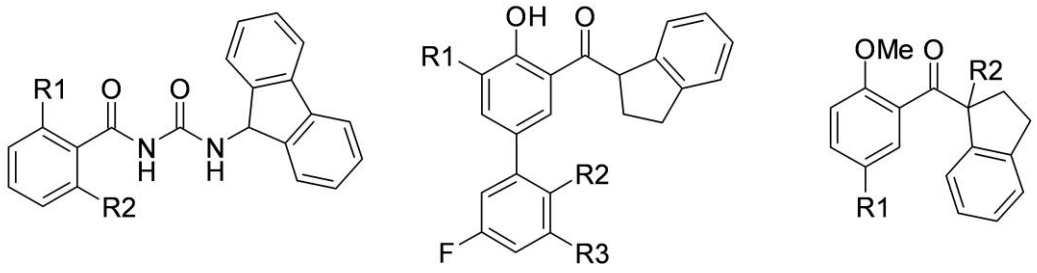

Figure 1. Chemical structures of acylurea-based (**1**), and aryl 1-indanylketone-based (**2** and **3**) based cyclophilin inhibitors.

Acylurea-based compounds. Configurationally-averaged MC/FEP calculations have been carried out by smoothly mutating the acylurea-based scaffold reported by Ni et al.[1] (**1**) to 10 different compounds, **1a-1j**, featuring variations of R_1 and R_2 (see Figure 1 and Table 1). Table 1 provides the computed $\Delta\Delta G_{bind}$ values with the correct binding affinity trend predicted when compared to the IC_{50} enzyme inhibition assay results. Uncertainties in the $\Delta\Delta G_{bind}$ have been calculated by propagating the standard deviation (σ_i) on the individual ΔG_i values for each $\Delta\lambda$ window. Some deviations from experiment were found, for example, **1j** ($R_1 = R_2 = H$) was predicted to have a $\Delta\Delta G_{bind}$ value similar to that of **1f** ($R_1 = R_2 = F$) despite showing no activity in the IC_{50} assay. Ni et al. also predicted **1j** to be active with a computed K_d value of 316 nM using their LigBuilder 2.0 program;[1] the results may suggest a breakdown of the scoring functions or force field. Interestingly, a buried water molecule is located in the hydrophobic sub-pocket where the phenyl ring of **1j** resides that is not found in **1f** (see Supporting Information

Figure S1); annihilation of buried waters in enzymes using a double-decoupling method has been shown to improve FEP accuracy in recent work.[3] Figure 2 provides images constructed from the last configuration of an MC/FEP calculation for the most potent inhibitor **1a** (R_1 = Cl and R_2 = F) bound to CypA; a hydrophobicity surface is given in Figure 2A ranging from blue for the most polar residues to white to orange-red for the most hydrophobic region (image made using Chimera[4]). The binding mode of compound **1** as predicted by BOMB is consistent with previous motifs generated from AUTODOCK 3 and LigBuilder 2.0, where an rmsd of ca. 1.5 Å was found between the methods.[1] The tandem amide forms multiple tight hydrogen bond interactions with the Arg55, Gln63, and Asn102 residues located in the "saddle" region of the active site while the planar fluorene rings and 2,6-disubstituted phenyl moiety of the inhibitors insert favorably into two adjacent hydrophobic sub-binding pockets.

Table 1. MC/FEP Results for the Mutation of Acylurea-based Inhibitors (**1**).[a]

compd	R_1	R_2	$\Delta\Delta G_{bind}$ (calc)	$\Delta\Delta G_{bind}$ (exptl)[b]	IC_{50}, (nM)[c]
1a	Cl	F	-1.48 ± 0.07	-3.05	1.52 ± 0.10
1a	F	Cl	8.38 ± 0.26		
1b	Cl	Cl	-1.37 ± 0.10	-2.74	2.59 ± 0.20
1c	CN	H	-0.21 ± 0.16	-0.78	71.2 ± 0.30
1c	H	CN	-1.67 ± 0.19		
1d	Cl	H	-0.68 ± 0.09	-0.56	103 ± 5
1d	H	Cl	1.44 ± 0.10		
1e	F	H	-0.13 ± 0.07	-0.30	159 ± 7
1e	H	F	0.51 ± 0.07		
1f	F	F	0	0	263 ± 24
1g	NO_2	H	0.54 ± 0.30	0.51	620 ± 32
1g	H	NO_2	2.62 ± 0.36		
1h	OH	H	1.67 ± 0.13	> 2.15	> 10,000
1h	H	OH	1.56 ± 0.14		
1i	NH_2	H	0.05 ± 0.20	> 2.15	> 10,000
1i	H	NH_2	0.07 ± 0.22		
1j	H	H	0.27 ± 0.09	inactive	inactive

[a]Positive $\Delta\Delta G_{bind}$ value (kcal/mol) means R_1=R_2=F (**1f**) was preferred and negative means new mutation is preferred. [b]Calculated from $\Delta\Delta G_{bind}$ = RT ln [IC_{50}(**1***x*)/IC_{50}(**1f**)] at 298 K. [c]Experimental IC_{50} values from ref. 1.

The large differences in the binding affinities of **1** derivatives have been attributed to the groups present on the 2,6-disubstituted phenyl ring, i.e., R_1 or R_2, where the potency is generally improved by the addition of greasy substituents and electron-withdrawing groups.[1] In the present calculations R_1 and R_2 are not equivalent as they do not interconvert during the MC simulation requiring separate simulations for each "conformer." If only one equivalent position is energetically preferred, then a penalty of RT ln 2 (0.6 kcal/mol) can be expected for loss of one rotameric state upon binding.[5] For example, simulations found that a Cl at the R_1 position of **1a**, which points into a hydrophobic pocket, improved the binding affinity relative to **1f** with a computed $\Delta\Delta G_{bind}$ of -1.48 kcal/mol compared to 8.38 kcal/mol when the Cl points out to the

bulk phase water, i.e., the R_2 position. While **1a** provided the most extreme preference for the R_1 position, hydrophobic substituents generally improved the binding affinity by pointing into the same sub-binding pocket, whereas hydrophilic groups, like –CN in compound **1c**, preferred to point into the bulk water. Hydrophobic interactions are regarded as one of the key factors leading to improved potency among the **1** derivatives,[1] but the major overall contributor of the measured nanomolar inhibitory values for the scaffold was determined by our calculations to be strong hydrogen bonding interactions between the acylurea portion of the solute and the polar "saddle" residues in the active site.

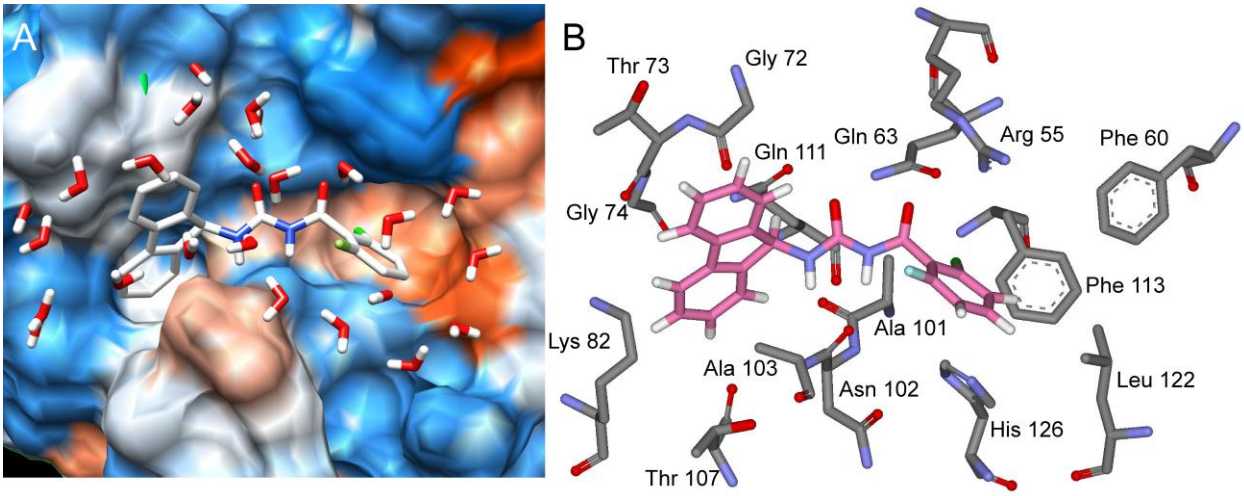

Figure 2. CypA active site and bound acylurea-inhibitor **1a** (R_1 = Cl and R_2 = F) with (A) nearby waters shown and a hydrophobic surface representation where blue is the most polar regions and orange-red is the most hydrophobic, and (B) key residues from the binding site.

In a recent study by Hamelberg and McCammon, molecular dynamic simulations were carried out for the *cis-trans* isomerization of the –Gly-Pro– ω angle of the Ace-His-Ala-Gly-Pro-Ile-Ala-Nme substrate in CypA.[6] Their simulations concluded that CypA better stabilizes the transition state, ω = 90°, as compared to the *cis* or *trans* isomers by forming long-lasting

hydrogen bonds with primarily two residues: Arg55 and Asn102. Gly was determined to form a hydrogen bond with the backbone NH group of Asn102 and Pro formed a hydrogen bond between its carbonyl oxygen and the guanidinium moiety of Arg55. In the current study, the same residues are essential in providing stabilizing interactions with compound **1**, which appears to mimic well the transition state conformation of the –Gly-Pro– substrate. For example, the average distances over the final 20 million MC/FEP configurations between the closest hydrogen on the Arg55 guanidinium moiety and the carbonyl oxygen closest to the 2,6-disubstituted phenyl ring were 2.8, 2.6, and 2.8 Å for the most favorable **1a**, **1f**, and **1h** compounds, respectively (Figure 2B). The hydrogen covalently bonded to nitrogen from Gln63 formed average hydrogen bond distances of 2.8, 3.0, and 3.0 Å with the carbonyl oxygen closest to the phenyl ring for **1a**, **1f**, and **1h**, respectively, and distances of 2.1, 1.9, and 2.0 Å with the carbonyl oxygen nearest the fluorene rings. The average distances between the carbonyl backbone oxygen of Asn102 and the hydrogen covalently bonded to the amide nearest the phenyl ring were 1.9, 2.3, and 1.8 Å for **1a**, **1f**, and **1h**, respectively, and 2.5, 2.1, and 2.3 Å for the amide hydrogen closest to the fluorene rings. A breakdown of the total Coulombic and van der Waals interaction energies between **1a** and the residues finds large values of −11.7 and −10.9 kcal/mol for Arg55 and Asn102, which is consistent with Hamelberg and McCammon's findings that those two residues are essential in stabilizing the transition state conformation.[6] The next best nonbonded solute-protein interaction energies were for Gln63 and Ala103 with values of −5.1 and −5.5 kcal/mol, respectively. However, for compound **1h** (R_1 = OH and R_2 = H) the energetic interactions with Arg55 and Asn102 were reduced to -10.1 and -6.9 kcal/mol, respectively, which is consistent with its reduced binding affinity as compared to the **1a** inhibitor (Table 1). In general, the most favorable acylurea-based derivatives maximize hydrogen bonding

with Arg55 and Asn102 and employ favorable hydrophobic interactions within the active site which may explain the origin of their experimentally-observed nanomolar inhibition potency.

Aryl 1-indanylketone-based compounds. A set of compounds based on an aryl 1-indanylketone scaffold (**2**) reported by Daum et al.[2] were also simulated by using the MC/FEP transformation sequence given in Figure 3. The computed $\Delta\Delta G_{bind}$ values in both CypA and CypB (Table 2) were found to yield excellent agreement with the experimental free-energy differences derived from the K_i protease-free PPIase assay at pH 7.8 and 283K.[2] The indanylketone-based compounds, **2a-2c**, have reduced μM inhibition K_i values for the cyclophilins when compared to the nM potency of the acylurea-based **1** compounds (Tables 1 and 2). The present calculations on **2a-2c** continue to lend support to the idea that the binding affinity is tied to the ability of the inhibitor to stabilize Arg55 and Asn102 in CypA and the analogous Arg63 and Asn110 residues in CypB. For example, the final 40 million MC/FEP configurations between the closest hydrogen on the Arg55 guanidinium moiety in CypA and oxygen of the nitro group nearest the **2a** indanyl ring found an average distance of 2.6 Å and a Coulombic and van der Waals interaction total energy of −16.3 kcal/mol between the ligand and

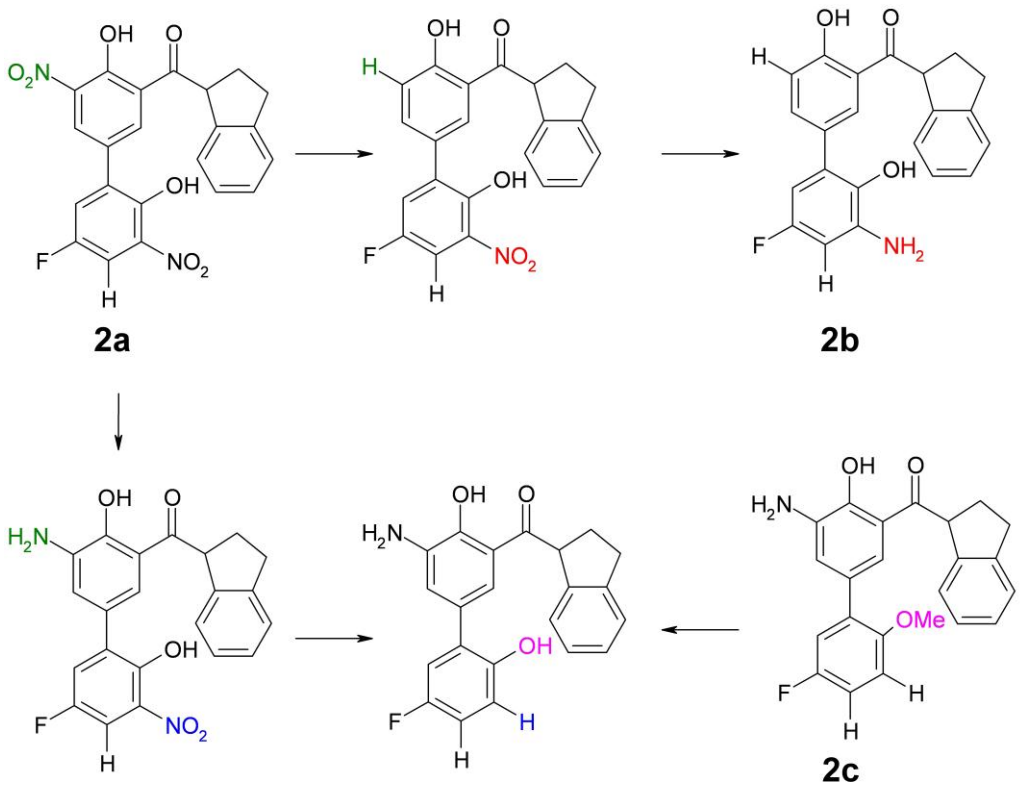

Figure 3. Transformation sequence used in the FEP simulations for the aryl 1-indanylketone-based compounds (**2**).

Table 2. MC/FEP Results for the Mutation of Aryl 1-indanylketone Inhibitors (**2**).

compd	$\Delta\Delta G_{bind}$ (calc)	$\Delta\Delta G_{bind}$ (exptl) [a]	K_i, (μM)[c]
		CypA	
2a	-0.61 ± 0.55	-0.67	0.52 ± 0.15
2b	-1.44 ± 0.69	-0.98	0.3 ± 0.1
2c	0.0	0.0	1.7 ± 0.5
		CypB	
2a	1.51 ± 0.64	> 1.38	> 100
2b	0.19 ± 0.58	0.19	12 ± 5
2c	0.0	0.0	8.6 ± 0.9

[a]Calculated from $\Delta\Delta G_{bind} = RT \ln [K_i(\mathbf{2}x)/K_i(\mathbf{2c})]$ at 283 K.

[b]Experimental K_i values from ref 2.

the residue (Figure 4). However, a significantly weakened nonbonded interaction energy of –4.6 kcal/mol between **2a** and Asn102 is consistent with the reduced μM potency observed when compared to the stronger interaction energies found for the **1a** nM inhibitor. Ala101, Gly72, and Lys82 in CypA also provided additional stabilizing nonbonded interactions with protein-solute energies of ca. –5.1 to –5.4 kcal/mol via hydrogen bonds; for example, an average distance of 1.9 Å was found between the backbone carbonyl oxygen of Ala101 and the **2a** hydroxyl group on the ring furthest from the indanyl ring.

Compound **2a** is particularly interesting because its K_i value is reported to be 0.52 ± 0.15 μM in CypA and >100 μM in CypB implying a >200-fold selectivity between the cyclophilins from *in vitro* and *in vivo* experiments despite a completely conversed active site.[2] The reasons behind the selectivity have been difficult to rationalize from an experimental perspective. Our calculations suggest that differences in the most favorable binding motifs for **2a** in CypA and CypB may be responsible for the observed selectivity. Figure 5 shows two binding modes for **2a** in the overlaid CypA and CypB active sites where the structure colored in gray is the preferred binding conformation in CypA and the structure in pink is favored in CypB (**2b** and **2c** are given in the Supporting Information Figure S2). It is clear from the figures that the major difference is the orientation of the indanyl ring: CypB prefers a binding motif where the indanyl ring is located in a hydrophobic sub-binding pocket, while CypA has the indanyl ring pointing up into a polar region with the adjacent carbonyl oxygen oriented towards His54 (although the nonbonded interactions between **2a** and His54 are weak as the total energy is –1.7 kcal/mol). Multiple FEP simulations were attempted from different starting geometries, but the reported structures were determined to be the most favorable as other configurations would exit the active site during the MC/FEP simulations or produce very poor energy evaluations. Autodock 4.2 calculations have

been carried out to validate the poses predicted by BOMB and good agreement was found. For example, **2a** was predicted to bind to CypA in conformations similar to that of Figures 4,5 and S2 and the free-energies of binding were predicted to be more negative than in CypB. Examples of the most relevant poses in CypA and CypB from the docking calculations are provided for comparison in the Supporting Information (Figures S3 and S4).

The weak binding of **2a** in CypB as compared to CypA is tied to poorer interactions between the ligand and the Arg63 and Asn110 residues. The final 40 million MC/FEP configurations between the closest hydrogen on the Arg63 guanidinium moiety in CypB to the oxygen of the carbonyl group nearest the **2a** indanyl ring found an average distance of 3.2 Å and a Coulombic and van der Waals interaction total energy of 0.0 kcal/mol between the ligand and the residue (Figure 4). The total nonbonded interaction energy between **2a** and Asn110 from CypB was -1.9 kcal/mol. The most favorable **2a**-CypB residue interaction was between Arg90 and the nitro group on the ring furthest away from the indanyl ring with a nonbonded interaction energy value of -10.7 kcal/mol. In addition, two waters formed average hydrogen bond distances of ca. 2.0 Å with the two hydroxyl groups present in **2a**, whereas waters were not required for ligand stabilization in CypA.

The aryl 1-indanylketones have been shown to behave as transition state inhibitors of Pin1, a PPIase of a different family, by mimicking the "twisted-amide" transition state of peptidyl-prolyl structures.[7] The current simulations suggest that **2a** also mimics the transition state in the active site of the cyclophilins and fine-tune their selectivity for CypA by weakening their nonbonded interactions with the catalytic Arg and Asn residues in CypB while simultaneously strengthening them in CypA. The computed functional differences in the residue

distances when bound to **2a** are consistent with NMR studies suggesting that the active site of CypB may exhibit structural differences as compared to CypA during transition state catalysis.[8]

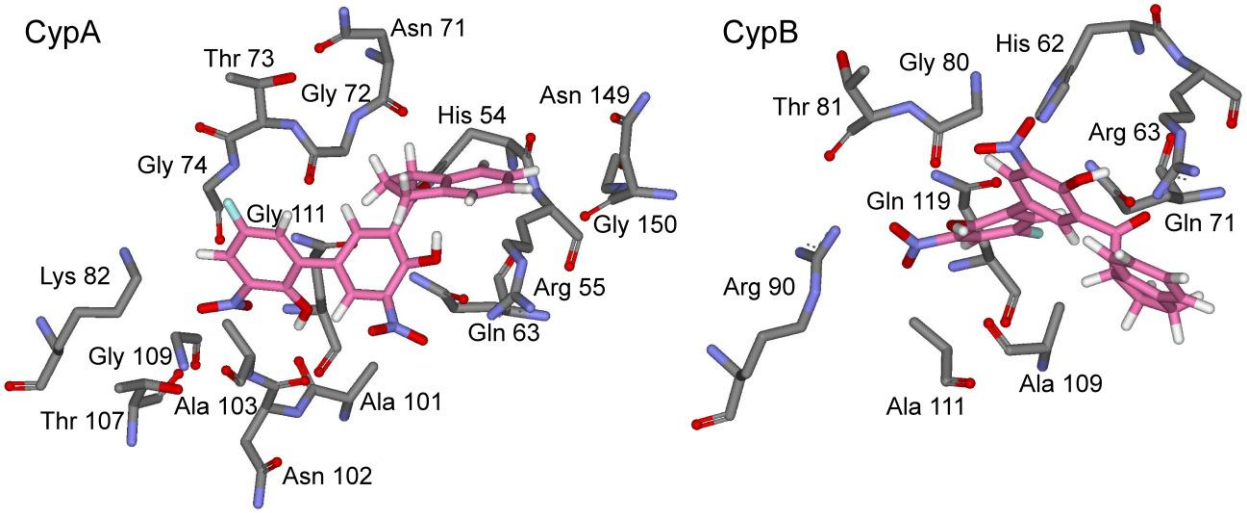

Figure 4. Aryl 1-indanylketone inhibitor **2a** bound to the active site of CypA (left) and CypB (right) with key residues shown. Nearby waters removed for clarity.

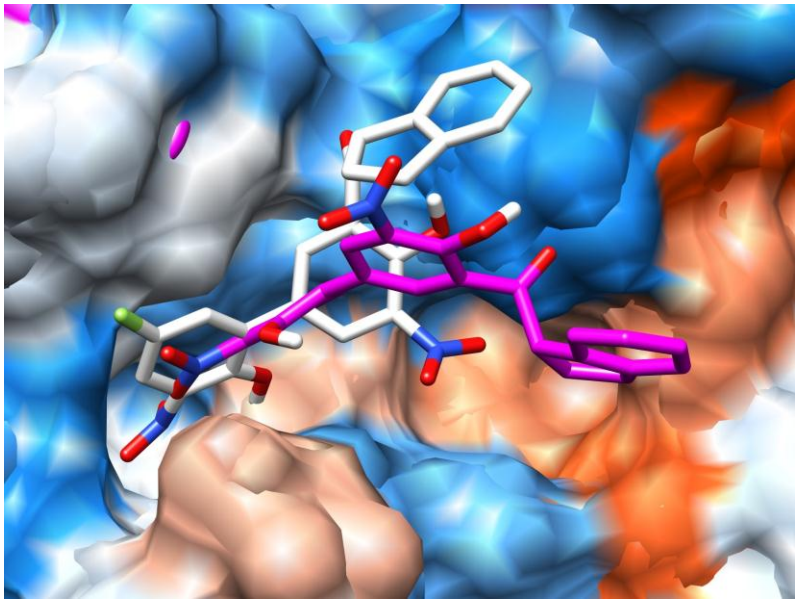

Figure 5. Overlaid CypA (gray) and CypB (pink) active sites with inhibitor **2a** bound at the active sites. Nearby waters removed for clarity.

Further variations in the aryl 1-indanylketone scaffold included the substitution of the biphenyl ring with a single phenyl moiety (**3** from Figure 1) that also yielded selectivity between CypA and CypB. For example, compound **3a** is ca. 10-fold more selective for CypA with a K_i value of 10 ± 2 μM compared to >100 μM in CypB (Table 3).[2] While not as impressive as the 200-fold selectivity of **2a**, a more detailed understanding could aid in the development of new inhibitors. MC/FEP mutations, as shown in Figure 6, were carried out for **3a** and the enantiomeric **3b** compounds and good agreement with the experimental $\Delta\Delta G_{bind}$ values was found (Table 3). Figure 7 shows comparable binding modes for **3a** in the overlaid CypA and CypB active sites with the indanyl ring pointing up into the polar active site saddle region in an orientation similar to that of **2a** in CypA. Autodock calculations predicted binding poses for **3a** in CypA and CypB similar to that of BOMB and the most favorable binding modes of **2a**, see Supporting Information Figures S6-A and S6-B.

The average distance of the final 40 million MC/FEP configurations between the closest hydrogen on the Arg55 guanidinium moiety in CypA and oxygen of the **3a** carbonyl group was 4.2 Å and a combined Coulombic and van der Waals nonbonded interaction energy of –4.6 kcal/mol was found. The Asn102 residue–**3a** ligand total nonbonded interaction energy was –0.1 kcal/mol. The reduced interactions of **3a** with the catalytic Arg55 and Asn102 residues compared to **2a** appears consistent with the reduction in K_i from 0.52 to 10 μM from **2a** and **3a** in CypA, respectively. Differences in the orientation of **3a** in the active site of CypB, see Figure 8, resulted in a total nonbonded interaction energy of –2.1 kcal/mol with Arg63 and -0.2 kcal/mol with Asn110, which agrees with the observed >100 μM inhibition. The considerable variation in the inhibition of CypA and CypB by the enantiomeric **3b** compounds was also well reproduced (Table 3). The discrepancy in binding affinity can be attributed to space requirements for the

methyl group within the active site that resulted in an unfavorable docking motif change for **(S)-3b** as compared to **(R)-3b**. Overlays of **(S)-3b** and **(R)-3b** in CypA and CypB are given in the Supporting Information Figure S5.

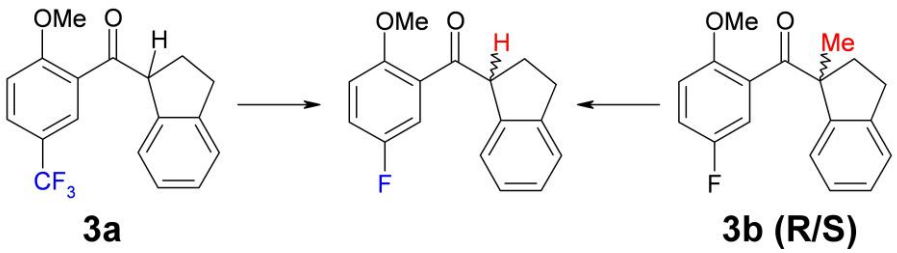

Figure 6. Transformation sequence used in the FEP simulations for the aryl 1-indanylketone-based compounds (**3**).

Table 3. MC/FEP Results for the Mutation of Aryl 1-indanylketone Inhibitors (**3**).

compd	$\Delta\Delta G_{bind}$ (calc)	$\Delta\Delta G_{bind}$ (exptl)[a]	K_i, (μM)[b]
		CypA	
3a	0.0	0.0	10 ± 2
(S)-3b	4.64 ± 0.24	> 1.29	> 100
(R)-3b	-0.88 ± 0.21	-0.16	7.5 ± 1.5
		CypB	
3a	0.0	0.0	> 100
(S)-3b	0.09 ± 0.21	-	> 100
(R)-3b	-0.34 ± 0.25	< -0.52	40 ± 10

[a]Calculated from $\Delta\Delta G_{bind}$ = RT ln [K_i(**3***x*)/K_i(**3a**)] at 283 K.

[b]Experimental K_i values from ref 2.

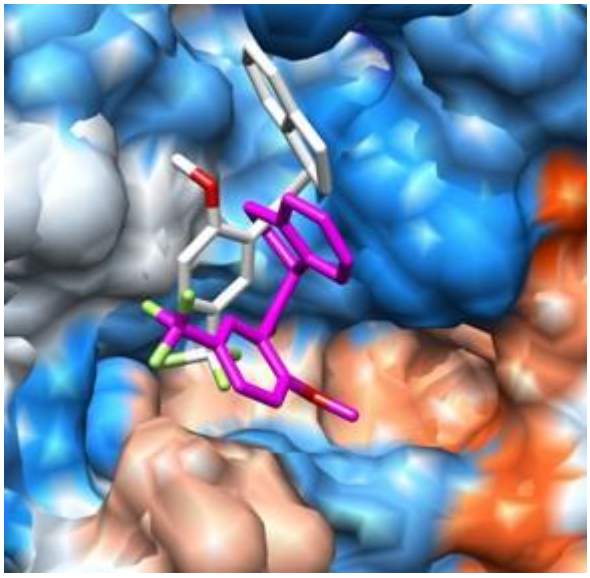

Figure 7. Overlaid CypA (gray) and CypB (pink) active sites with inhibitor **3a** bound at the active sites. Nearby waters removed for clarity.

MC/FEP calculations have been carried out on a varied set of nM to μM inhibitors of cyclophilins A and B based on acylurea and aryl 1-indanylketone small molecule scaffolds reported by Li[1] and Schiene-Fischer,[2] respectively, in order to elucidate the origin of their potency and specificity. The computed $\Delta\Delta G_{bind}$ values were in close agreement with experimental values derived from IC_{50} and K_i enzyme inhibition assay results. The present simulations find the nM inhibition of CypA from the acylurea-based derivatives, **1**, is primarily the result of favorable stabilization of residues Arg55 and Asn102 via nonbonded interactions. In addition, the planar fluorene rings and 2,6-disubstituted phenyl moiety of the **1** inhibitors inserted favorably into two adjacent hydrophobic sub-binding pockets; the inclusion of hydrophobic groups, e.g., Cl, on the phenyl ring was beneficial as it imparted positive hydrophobic interactions and displaced buried water molecules from the active site. However, any substitutions to the phenyl ring that resulted in the destabilization of the Coulombic or van

der Waals interactions between the inhibitor and catalytic Arg and Asn residues resulted in a loss of binding affinity. In addition, the excellent agreement between the computed and experimentally derived $\Delta\Delta G_{bind}$ for the μM aryl 1-indanylketones, **2** and **3**, inhibitors also supported the theory of the inhibitor binding affinity being tied to the stabilization of the conserved active site Arg and Asn residues in both CypA and CypB.

The **2a** aryl 1-indanylketone inhibitor is able to deliver a >200-fold selectivity between CypA and CypB and was predicted from our calculations to differentiate between the cyclophilins by using distinct binding motifs that exploit subtle differences in the active site arrangements. Previous NMR studies have also suggested that the active site of CypB may exhibit structural differences as compared to CypA during transition state catalysis[8] and the current simulations indicate that **2a** and **3a** take advantage of these subtle differences via different binding motifs that fine-tune their selectivity for CypA by exclusively weakening their nonbonded interactions with the catalytic Arg63 and Asn110 residues in CypB. A joint computational and experimental study is currently underway that explores small molecule hybrid structures of **1, 2** and **3**, and novel scaffolds that mimic the "twisted-amide" transition state of peptidyl-prolyl structures in the active site with the goal of obtaining selectivity between CypA and CypB with low-nanomolar inhibition potency.

Initially the compounds tested for Cyp inhibition are given in Figure 8. Compounds **4** and **5** were tested to address the following two items: 1) the Twisted ketones **2** and **3** from the Fischer group utilize a dihydroindane system with the proposal that this twist mimics the prolyl acyl and 2) the 2,6-dichlorobenzmide of compound **1b** has been suggested as mimicking this same prolyl acyl. Although the 2,6-dichlorophenyl keto dihydroindane system was initially desired, this compound was shown to be unstable under routine chemical manipulation ($NaHCO_3$

extractions, SiO_2 column chromatography, etc…) and serious doubt arose to the biological stability of these compounds. Consequently the indole **4** and 2-methyl indole **5** derivatives were synthesized by Dr. Patrick Flaherty and his research group at Duquesne University, and toxicity studies were carried out by Dr. Zandrea Ambrose and her research group at the University of Pittsburgh Medical School. Compound **6** has also been utilized as a starting point for the identification of any cyclophillin A inhibitory properties of **1** would increase starting points for non-prolyl based inhibitors.

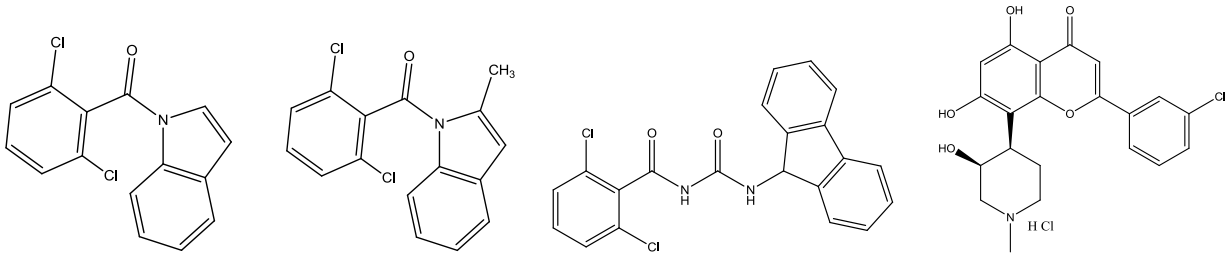

(**4**) PJ-B-5-68-3 (**5**) PTF-2-189 (**1b**) PTF-2-187 (**6**) Flavopiridol.HCl

Figure 8. New chemical structures for investigation of cyclophilin inhibition. 1b was also used to compare the results.

Cyclosporine A (CsA) was included as a control in the toxicity studies by Dr. Ambrose. Toxicity of each compound was tested in duplicate between 50 - 0.00064 uM in two cell lines. The cell lines used were HeLa cells and GHOST cells, the later being a modified version of human osteosarcoma (HOS) cells. A similar toxicity results in both cell lines for all drugs. PTF-2-187 was the least toxic and flavopiridol was the the most toxic. (Note: a lack of toxicity could mean that the compound is not significantly entering cells.) The toxicity data HeLa and GHOST cells were shown in Figures S17 & S18 of the Supporting information .

The ability of each compound was tested to inhibit WT HIV-1 infection at 2 concentrations in duplicate. The higher drug concentration was chosen that was the highest without causing significant toxicity (10uM for all compounds, except for flavopiridol which was

Table 4. MC/FEP Results for the Mutation of Indole-based Inhibitors (**4**).[a]

R_1	R_2	$\Delta\Delta G_{bind}$ (CypA) **4**	$\Delta\Delta G_{bind}$ (CypA) **5**	$\Delta\Delta G_{bind}$ (CypB) **4**	$\Delta\Delta G_{bind}$ (CypB) **5**
Cl	F	0.04	-0.24	0.00	0.45
F	Cl	0.17	0.33	0.68	0.74
Cl	Cl	0.00	0.00	0.00	0.00
F	F	-0.47	0.30	0.13	0.68
Cl	H	-0.79	0.80	0.70	0.63
H	Cl	-1.55	-1.06	-0.91	0.84
H	H	-2.45	-1.81	-0.04	1.03

[a]Positive $\Delta\Delta G_{bind}$ value (kcal/mol) means R_1=R_2=Cl was preferred and negative means new mutation is preferred.

set at 10nM). The lower concentration was 50-fold lower. As expected, the high concentration of CsA caused a decrease in infectivity of HIV-1 in both HeLa cells and GHOST cells, whereas the lower concentration of CsA only affected infectivity in GHOST cells. Only **4** (PJB-5-68-3) shows a modest decrease in infectivity at 10uM. A modest decrease in infectivity with flavopiridol in HeLa cells was not dose dependent, and that did not hold up in GHOST cells.

MC/FEP studies on the derivatives of **4** are showing more inhibitory activity for CypA and CypB than that of **5.** MC/FEP results for the mutation of indole-based inhibitors were shown in Table 4. Compound **4** with H, H shown to discriminate the selective inhibition between CypA and CypB.

Toxicity and FEP data shows that compound **4** was the surprising front runner for Cyp inhibition. The other compounds start with **4** and explore the following design strategies: omit the chloro atoms, convert the indole to an indolone to mimic the acyl urea, make non-benzofused derivatives, use proline mimics, make a ring expansion product, and attempt to fill the hydrophobic S2 pocket with a simple asymmetric compound. Finding selective inhibitors for

Cyps is an alternative strategy to treat HIV and HCV and, association of Cyps with HIV and HCV viral proteins is further investigated.

References

(1) Ni, S.; Yuan, Y.; Huang, J.; Mao, X.; Lv, M.; Zhu, J.; Shen, X.; Pei, J.; Lai, L.; Jiang, H.; Li, J. *J. Med. Chem.* **2009**, *52*, 5295-5298.

(2) Daum, S.; Schumann, M.; Mathea, S.; Aumller, T.; Balsley, M. A.; Constant, S. L.; Lacroix, B. F. d.; Kruska, F.; Braun, M.; Schiene-Fischer, C. *Biochemistry* **2009**, *48*, 6268-6277.

(3) (a) Michel, J.; Tirado-Rives, J.; Jorgensen, W. L. *J. Am. Chem. Soc.* **2009**, *131*, 15403-315411; (b) Gilson, M. K.; Given, J. A.; Bush, B. L.; McCammon, J. A. *Biophys. J.* **1997**, *72*, 1047-1069.

(4) Pettersen, E. F.; Goddard, T. D.; Huang, C. C.; Couch, G. S.; Greenblatt, D. M.; Meng, E. C.; Ferrin, T. E. *J. Comput. Chem.* **2004**, *13*, 1605-1612.

(5) Zeevaart, J. G.; Wang, L.; Thakur, V. V.; Leung, C. S.; Tirado-Rives, J.; Bailey, C. M.; Domaoal, R. A.; Anderson, K. S.; Jorgensen, W. L. *J. Am. Chem. Soc.* **2008**, *130*, 9492-9499.

(6) Hamelberg, D.; McCammon, J. A. *J. Am. Chem. Soc.* **2009**, *131*, 147-152.

(7) Daum, S.; Erdmann, F.; Fischer, G.; Féaux de Lacroix, B.; Hessamian-Alinejad, A.; Houben, S.; Frank, W.; Braun, M. *Angew. Chem. Int. Ed.* **2006**, *45*, 7454-7458.

(8) Neri, P.; Gemmecker, G.; Zydowsky, L. D.; Walsh, C. T.; Fesik, S. W. *FEBS Lett.* **1991**, *290*, 195-199.

Chapter IV. Development of OPLS-AA force field parameters for 68 unique ionic liquids

This study seeks to develop force field potentials for the atomistic simulation of both widely-used ionic liquid combinations and next-generation alternatives with smaller environmental impact. In this respect, OPLS-AA parameters have been created and validated for use in the simulation of 68 unique combinations of room temperature ionic liquids featuring [RMIM] (R = Me, Et, Bu, Hex, Oct), [RPyr], and [Chol] cations, along with [PF_6], [BF_4], [Sacc], [Ace], nitrate [NO_3], chloride [Cl], tetrachloroaluminate [$AlCl_4$], heptachlorodialuminate [Al_2Cl_7], and triflate [TfO] anions (see Chapter 1, Figure 3). Many of the ions presented in this work have already been featured in other molecular dynamics and Monte Carlo studies for a variety of force fields, e.g. CHARMM, AMBER, and OPLS-AA. Therefore it is important to stress that in addition to the parameterization of previously unpublished ionic liquids, e.g. [Chol], [Sacc], and [Ace], this study explored an unprecedented number of cation/anion combinations

*Reprinted in part from *J. Chem. Theory. Comput.* **2009**, 5(4), 1038-1050.

with two completely different charge and torsion sets for a detailed comparison of parameter transferability. The first charge/torsion set is potentially transferable to any alkyl side-chain length on the [RMIM] and [RPyr] cations (tested up to R = octyl) and the second set is specific to the ionic liquid cations: [EMIM], [BMIM], [MPyr], [EPyr], and [BPyr]. In addition, the current work validated the parameters for temperatures ranging from 5-90 °C against experimental densities for 11 unique ionic liquid combinations; most previous work focused on room temperature.

Monte Carlo (MC) simulations of the ionic liquid parameters gave predicted densities and heats of vaporization, ΔH_{vap}, in close agreement with experimentally observed values. The driving force behind the newly developed parameter set is to produce a computationally accurate representation of the reaction medium for use in mixed quantum and molecular mechanics (QM/MM) calculations.

Partial Charges. Ab initio calculations at the LMP2/cc-pVTZ(-f)//HF/6-31G(d) theory level were carried out on the isolated gas phase ions in order to facilitate the transferability of the charge model to multiple ionic liquid combinations. All anions were geometry optimized and Coulombic charges were assigned from the ESP fits (Table 1). For the cations, multiple low-energy geometry configurations exist stemming primarily from torsion rotations, i.e. the alkyl side-chains in the [RMIM] and [RPyr] ions and choline's internal N-C-C-O dihedral. This presented the challenge of developing a single set of charges per cation family that could accurately represent different alkyl lengths and orientations. ESP charges were initially computed for all available [RMIM] and [RPyr] energy-minimized stationary points, where R = Me, Et, and Bu. An average partial charge value for each atom in [RMIM] and [RPyr] was developed by appropriately weighting the contribution of each ground-state structure to the

overall conformational population. For example, the partial charges specific to [BMIM] (see values in Figure 1) were computed from a two-state model and the Boltzmann distribution based on *gauche* and *trans* side-chain optimized energies for cation. Charges specific to [EMIM], [MPyr], and [EPyr] are given in the Supporting Information. To assign a final charge set to [RMIM], all charges for [MMIM], [EMIM], and [BMIM] were appropriately weighted and averaged (see Table 2 and Figure 1). For the ring atoms, e.g. NA, CW, HW in [RMIM], departures in charge from symmetry were small in the R = Me, Et, and Bu ions, hence the atoms were given symmetrical values to facilitate transferability. Charges for the carbon and hydrogen atoms, CS and HS, present in the middle of the alkyl side-chains (-CH_2-) were taken directly from OPLS-AA alkane values[1] to allow the simulation of any [RMIM] desired chain length (tested up to octyl in the present work). In the simulations of [MMIM], the CM and HM atom types are used in both methyl groups attached to the 1 and 3 nitrogen positions of the imidazolium. A set of transferable charges for [RPyr] and a specific set for choline were computed in an identical fashion (Table 2).

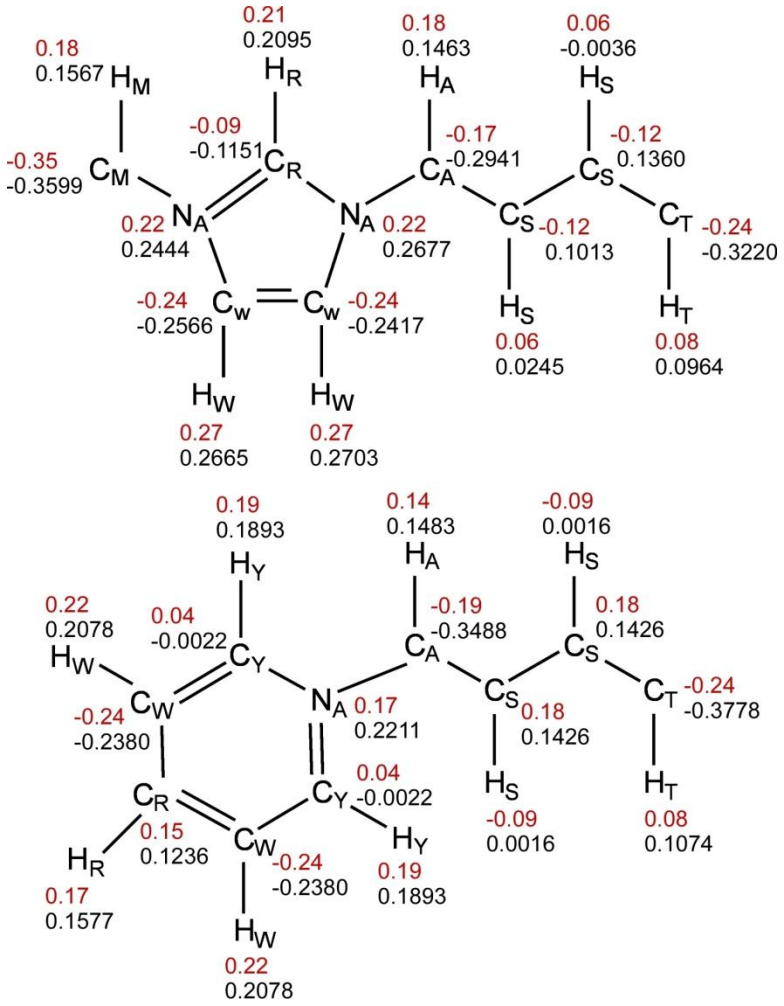

Figure 1. Partial charges assigned for atom types in [RMIM] and [RPyr] in red, and charges exclusively for use in [BMIM] and [BPyr] in black.

The use of averaged point charges was necessary for a fully transferable force field, however a direct comparison of the accuracy between these [RMIM] and [RPyr] charges versus point charges specific to [EMIM], [BMIM], [MPyr], [EPyr], and [BPyr] was evaluated in this study. Thirty-five ionic liquid combinations were computed using both charge sets, along with the appropriate torsion terms, to compare differences in predicted densities and heats of vaporization for a quantitative evaluation of the final charges presented in Table 2. Most Lennard-Jones (LJ) parameters were taken directly from the OPLS-AA force field, for example

parameters for [RMIM] and [RPyr] were based on imidazole[2] and pyridine[3], respectively. However, any LJ parameters not assigned from OPLS-AA are specified in Table 1.

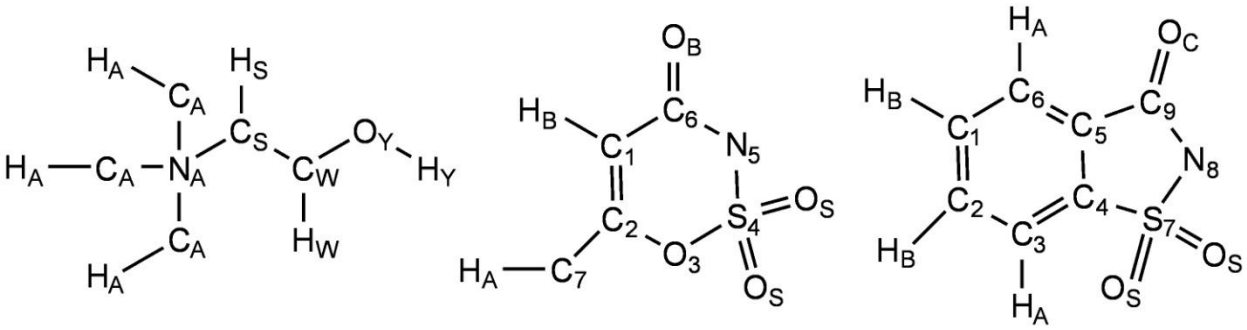

Figure 2. Atom types for choline [Chol], acesulfamate [Ace], and saccharinate [Sacc].

Table 1. Nonbonded Parameters for [Cl], [PF_6], [BF_4], [NO_3], [$AlCl_4$], [Al_2Cl_7], [TfO], Saccharinate [Sac], and Acesulfamate [Ace] Anions.[a]

Anion	Atom Type	q (e)	σ (Å)	ε (kcal mol^{-1})
[Cl][b]	Cl	-1.00	3.770	0.148
[BF_4][c]	B	0.8276	3.5814	0.095
	F	-0.4569	3.1181	0.060
[PF_6]	P	1.3400	3.740	0.200
	F	-0.3900	3.1181	0.061
[NO_3]	N	0.794	3.150	0.170
	O	-0.598	2.860	0.210
[$AlCl_4$][d]	Al	0.6452	4.050	0.100
	Cl	-0.4113	3.770	0.148
[Al_2Cl_7][d]	Al	0.5455	4.050	0.100
	ClM[e]	-0.1404	3.770	0.148
	Cl	-0.3251	3.770	0.148
[TfO]	S	1.1887	3.550	0.250
	O	-0.6556	2.960	0.210
	C	0.2692	3.500	0.066
	F	-0.1637	2.950	0.053
[Sac]	C1	-0.0519	3.550	0.070
	C2	-0.1882	3.550	0.070
	C3	-0.0235	3.550	0.070

	C4	-0.2759	3.550	0.070
	C5	0.1293	3.550	0.070
	C6	-0.1968	3.550	0.070
	C9	0.5502	3.750	0.105
	S7	1.2149	3.550	0.250
	N8	-0.6889	3.250	0.170
	OC	-0.5950	2.960	0.210
	OS	-0.6285	2.960	0.210
	HA	0.1132	2.420	0.030
	HB	0.0782	2.420	0.030
[Ace]	C1	-0.8536	3.550	0.070
	C2	0.6670	3.550	0.070
	C6	0.9507	3.750	0.105
	C7	-0.3083	3.500	0.066
	O3	-0.5087	2.900	0.140
	OB	-0.6573	2.960	0.210
	OS	-0.6158	2.960	0.170
	S4	1.3355	3.550	0.250
	N5	-0.8224	3.250	0.170
	HA	0.0666	2.500	0.030
	HB	0.2289	2.420	0.030

[a]All Lennard-Jones (LJ) nonbonded parameters are from the OPLS-AA force field unless otherwise stated. Atom types for [Sacc] and [Ace] are shown in Figure 2. [b]LJ parameter for Cl taken from ref 4. [c]LJ parameter for B taken from ref 5. [d]LJ parameters taken from refs 5,6. [e]Corresponds to Cl atom bridging the Al atoms.

Table 2. Nonbonded Parameters for 1-Alkyl-3-methylimidazolium [RMIM], N-alkylpyridinium [RPyr], and Choline [Chol] Cations.[a]

Cation	Atom Type	q (e)	σ (Å)	ε (kcal mol^{-1})
[RMIM]	CR	-0.09	3.55	0.070
	NA	0.22	3.25	0.170
	CW	-0.24	3.55	0.070
	CM	-0.35	3.50	0.066
	CA	-0.17	3.50	0.066
	CS	-0.12	3.50	0.066
	CT	-0.24	3.50	0.066
	HR	0.21	2.42	0.030
	HW	0.27	2.42	0.030
	HM	0.18	2.50	0.030
	HA	0.18	2.50	0.030
	HS	0.06	2.50	0.030
	HT	0.08	2.50	0.030
[RPyr]	CR	0.15	3.55	0.070
	CW	-0.24	3.55	0.070
	CY	0.04	3.55	0.070
	NA	0.17	3.25	0.170
	CM	-0.39	3.50	0.066
	CA	-0.19	3.50	0.066
	CS	0.18	3.50	0.066
	CT	-0.24	3.50	0.066
	HR	0.17	2.42	0.030
	HW	0.22	2.42	0.030
	HY	0.19	2.42	0.030
	HM	0.16	2.50	0.030
	HA	0.14	2.50	0.030
	HS	-0.09	2.50	0.030
	HT	0.08	2.50	0.030
[Chol]	NA	0.1640	3.250	0.170
	CA	-0.3847	3.500	0.066
	CS	-0.1111	3.500	0.066
	CW	0.2318	3.500	0.066
	OY	-0.6547	3.070	0.170
	HA	0.1934	2.500	0.030
	HS	0.1251	2.500	0.030
	HW	0.0398	2.500	0.030
	HY	0.4537	0.000	0.000

[a]Atom types for [RMIM], [RPyr], and [Chol] are given in Figures 1 and 2.

Intramolecular Potentials. The resultant geometries from the ab initio calculations were used to obtain the equilibrium bond and angle reference values, r_o and θ_o, for the simulations; the final values are given in the Supporting Information. To allow full flexibility for the cations, appropriate bond and angle force constants, and Fourier coefficients for ring atoms on [RMIM] and [RPyr] were taken directly from published OPLS-AA parameters.[2,3,7] In this work, new Fourier coefficients for the alkyl side-chains of [RMIM] and [RPyr] and an entire new set for the choline cation were developed to reproduce all possible rotations. Vibrational frequencies as is typical of the OPLS force field were not parameterized and will require further refinement of the force constants if greater accuracy is desired. The focus of the ionic liquid OPLS-AA parameter set is to accurately reproduce intermolecular interactions such as density and thermodynamic quantities such as the heats of vaporization.

Torsions. The procedure for establishing the missing Fourier coefficients involved direct adjustment of the OPLS-AA torsional parameters to reproduce the energy differences between conformational energy minima from ab initio calculations. For each dihedral angle, energy profiles were obtained by rotating the [RMIM] and [RPyr] alkyl side chains and all available [Chol] dihedrals in increments of 15 degrees for each ion with a constrained minimization carried out using the LMP2/cc-pVTZ(-f)//HF/6-31G(d) theory level. Only the dihedrals involved in the torsional potential energy surface were restrained; the remainder of the ion was fully flexible. Each [MMIM], [EMIM], [BMIM], [MPyr], [EPyr], [BPyr], and [Chol] cation was individually parameterized using their specific charge set with coefficients, V_1 to V_3, that gave the best overall fit for all rotatable bonds (Tables 3-5). The resultant Fourier coefficients were then refitted to give the best overall values for the general [RMIM] and [RPyr] cation families, taking into account the general atomic charge sets.

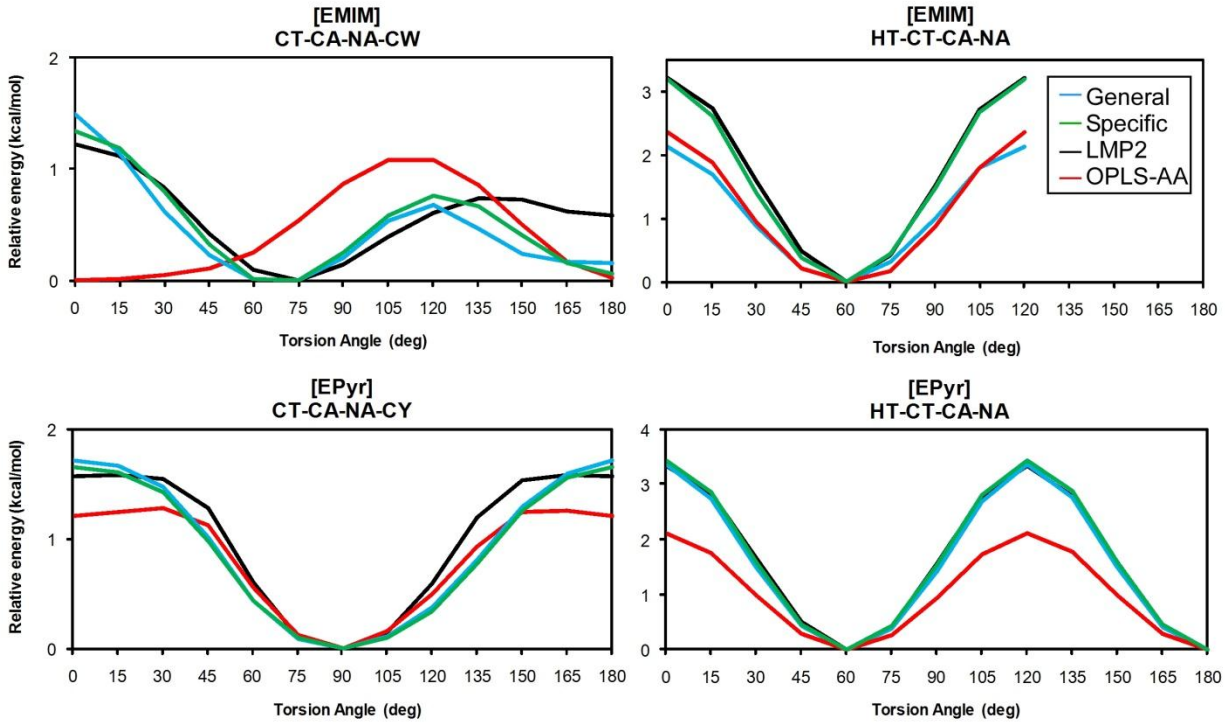

Figure 3. Torsion energy profiles for the rotation around dihedral angles for [EMIM] and [EPyr] cations. The transferable [RMIM] and [RPyr] parameters given in blue, parameters specific to [EMIM] and [EPyr] in green, LMP2/cc-pVTZ(-f)/HF/6-31G(d) in black, and the unaltered OPLS-AA force field in red.

As an example, the energy profiles for the CT-CA-NA-CW/Y and HT-CT-CA-NA rotations in [EMIM] and [EPyr] using the fully transferable parameters (in blue) and the parameters specific to the individual cations (in green) are given in Figure 3; LMP2/cc-pVTZ(-f)//HF/6-31G(d) energy values are presented in black along with the original OPLS-AA parameters in red. Positions of all the minima and maxima were shifted to achieve the lowest possible RMS energy error with respect to the quantum mechanical results. The specific charge/torsion parameter sets for the individual cations typically performed better than the generalized parameter set, e.g. the HT-CT-CA-NA rotation in [EMIM] (Figure 3). However, energy profiles for the dihedral rotations were considerably improved using both parameter sets when compared to the unaltered OPLS-AA potentials. The highly transferable [RMIM] and

[RPyr] general parameter set enabled most dihedral rotations to be appropriately modeled with good accuracy (multiple energy profiles for [RMIM] and [RPyr] given in the Supporting Information Figures S9-S16). For example, the energy barriers for dihedral rotations in the 1-propyl-3-methylimidazolium [PMIM] and N-1- propylpyridinium [PPyr] cations were well reproduced when using the general [RMIM] and [RPyr] parameter sets despite not being specifically taken into consideration during the parameterization process (Figures S10 and S13). In addition, the simulation of longer alkyl side-chains, such as hexyl and octyl, using the [RMIM] and [RPyr] general parameters also gave good agreement with experimental densities and heats of vaporization data, as discussed below.

Table 3. Torsional Fourier Coefficients (kcal/mol) for, 1-Alkyl-3-methylimidazolium [RMIM] and Specific to [EMIM] and [BMIM] Charge Sets.

Torsion	V_1	V_2	V_3	Cation
NA-CA-CT-HT	0.000	0.000	0.000	[RMIM]
	0.000	0.000	0.350	[EMIM]
CW-NA-CA-CT	-4.355	-4.575	-1.375	[RMIM]
	-0.599	-1.750	0.290	[EMIM]
CR-NA-CA-CT	-2.000	-0.275	-1.650	[RMIM]
	-0.555	0.479	0.200	[EMIM]
CW-NA-CA-HA	-2.700	-5.650	0.355	[RMIM]
	-0.755	-2.125	0.400	[EMIM]
	-1.400	-2.650	0.175	[BMIM]
CW-NA-CA-CS	-2.110	-5.000	0.345	[RMIM]
	-1.910	-1.500	0.290	[BMIM]
CR-NA-CA-CS	-0.159	0.095	-0.010	[RMIM]
	-1.659	-0.555	-0.375	[BMIM]
NA-CA-CS-CS	-0.788	0.800	0.400	[RMIM]
	-1.788	0.756	-0.288	[BMIM]
HA-CA-CS-HS	0.000	-0.150	0.518	[RMIM]
	0.000	0.000	0.318	[BMIM]

Table 4. Torsional Fourier Coefficients (kcal/mol) for, N-alkylpyridinium [RPyr] and Specific to [EPyr] and [BPyr] Charge Sets.

Torsion	V_1	V_2	V_3	Cation
CY-NA-CA-CT	0.000	0.010	0.000	[RPyr]
	0.000	0.150	0.000	[EPyr]
NA-CA-CT-HT	0.000	0.000	0.020	[RPyr]
	0.000	0.000	0.400	[EPyr]
HA-CA-CT-HT	0.000	0.000	0.518	[RPyr]
	0.000	0.000	0.332	[EPyr]
NA-CA-CS-HS	0.000	0.000	0.200	[RPyr]
	-0.700	-0.500	0.000	[BPyr]
HA-CA-CS-HS	0.000	0.000	0.418	[RPyr]
	-1.700	-1.710	0.655	[BPyr]
CY-NA-CA-CS	0.000	-0.050	-0.200	[RPyr]
	0.000	0.180	0.000	[BPyr]
NA-CA-CS-CS	-0.788	0.400	-0.288	[RPyr]
	-0.233	1.400	-0.290	[BPyr]

Table 5. Torsional Fourier Coefficients (kcal/mol) for Choline [Chol].

Torsion	V_1	V_2	V_3
CW-CS-NA-CA	0.100	0.550	0.650
CA-NA-CA-HA	0.000	0.000	0.825
CS-NA-CA-HA	0.000	0.000	0.940
HS-CS-NA-CA	0.000	1.000	0.700
OY-CW-CS-NA	-6.000	-5.000	3.200
OY-CW-CS-HS	-0.500	-2.500	0.250
HW-CW-CS-NA	-6.000	-7.000	0.750
HW-CW-CS-HS	6.000	-3.000	2.000
HY-OY-CW-CS	-0.356	-0.174	0.350
HY-OY-CW-HW	-3.000	1.000	-2.000
X-NA-X-X[a]	0.000	2.000	0.000

[a]Improper torsion.

Density. With satisfactory agreement achieved between the newly developed OPLS-AA parameters and the ab initio calculations for the ionic structures, subsequent MC simulations for 68 unique ionic liquid combinations were carried out. The systems were composed of 190 ion pairs at 25 °C and 1 atm. Each simulation required over 500 million MC configurations to properly equilibrate the periodic boxes using Ewald summations. The computed densities for the solvents are given in Tables 6, 7, and 8. The imidazolium-based ionic liquids provided the largest amount of experimental data to validate the newly developed force field (Figures 4 and 5). However, in many cases, different experimental measurements varied by as much as 5% per solvent (Table 6). Relative deviations from experimental density values were ca. 1-3% for most [RMIM] ionic liquid combinations using both the fully-transferable OPLS-AA force field and the parameters developed specifically for [EMIM] and [BMIM]. The limited amount of reported densities for the [RPyr][BF4] ionic liquids also compared well with the simulations (Table 7).

Chloroaluminate-based ionic liquids gave slightly larger deviations at ca. 4-5%. Exact agreement could not be expected since the ionic composition of the experimental and modeled systems is not identical. For example, Raman,[8] ^{27}Al NMR[9] and mass spectra[10] all indicate that when $AlCl_3$ comprises < 50% mol of the [EMIM][Cl] ionic liquid melt, $[AlCl_4]$ is the only chloroaluminate species present along with chloride ions that are not bound to aluminum. A ratio greater than 1:1 $AlCl_3$-to-EMIC gives $[AlCl_4]$ and $[Al_2Cl_7]$ as the principal anionic constituents of the melt from ^{27}Al NMR[11] and negative-ion FAB mass spectra.[12] Despite underestimating the densities, the simulations for [RMIM]$[AlCl_4]$ and [RMIM]$[Al_2Cl_7]$ reproduced the relative trend of decreasing density with increasing alkyl chain length. In addition, the computed heats of vaporization are strikingly similar to the experimental values for [BMIM]$[AlCl_4]$ and [HMIM]$[AlCl_4]$ (Table 6). The OPLS-AA chloroaluminate solvents have previously provided an

appropriate reaction medium environment for the Diels-Alder reaction using QM/MM methodology.[6]

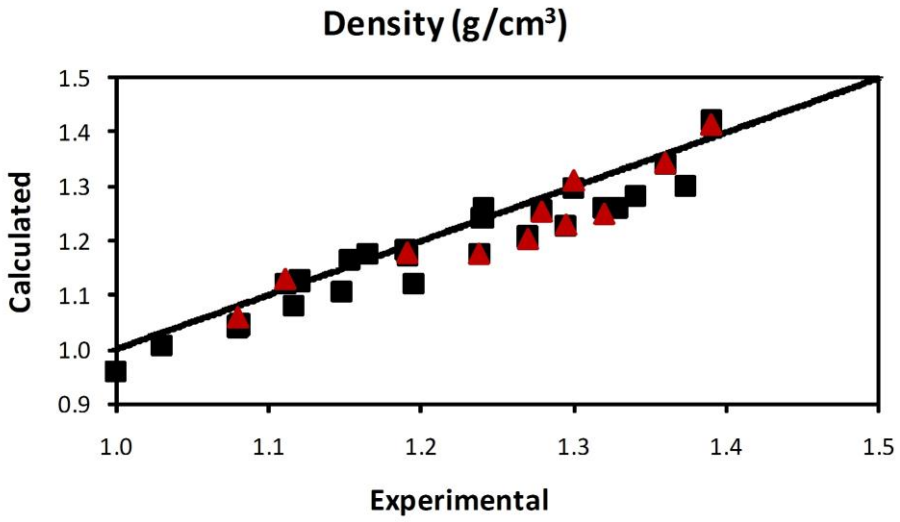

Figure 4. Computed OPLS-AA and experimental results for liquid densities for 1-alkyl-3-methylimidazolium [RMIM] based ionic liquids (black squares) at 25 °C and 1 atm. Computed values with OPLS-AA parameters specific to [EMIM] and [BMIM] given as red triangles.

The errors in the densities computed for choline-based ionic liquids were significantly larger (see Table 8) despite using the same parameterization procedure as the [RMIM] and [RPyr]-based ionic liquids. For example, simulation of [Chol][Sacc] gave a predicted density of 1.200 g/cm^3 compared to 1.383 g/cm^3 experimentally and [Chol][Ace] gave a calculated value of 1.206 g/cm^3 (exptl. 1.284 g/cm^3).[17] Improvements to the [Chol]-based ionic liquid parameters are difficult owing to the lack of experimental data available for refinement.

Table 6. Calculated and Experimental Liquid Densities (g/cm^3) and Heats of Vaporization (kcal/mol) at 25 °C for 1-Alkyl-3-methylimidazolium [RMIM] Based Ionic Liquids.[a]

Ionic Liquid	Density (Calc.)	Density (Exptl.)	Refs.	ΔH_{vap} (Calc.)	ΔH_{vap} (Exptl.)	Refs.
[MMIM][BF_4]	1.299	1.373	13	30.1		
[EMIM][BF_4]	1.254 (1.253)	1.279, 1.28	14,15	18.0 (24.0)		
[BMIM][BF_4]	1.171 (1.178)	1.19, 1.21, 1.26	14,16,17	27.8 (30.0)	*30.6*,[e] *48.6*[f]	18,19
[HMIM][BF_4]	1.105	1.1481, 1.1484, 1.177	13,20	35.8		
[OMIM][BF_4]	1.044	1.08, 1.0912, 1.105, 1.133	13,17,21, 22	41.9	38.7 ±0.7,[g] *29.2*[e]	26,18
[MMIM][PF_6]	1.512			33.1		
[EMIM][PF_6]	1.455 (1.455)	1.558[b]	23	21.4 (27.6)		
[BMIM][PF_6]	1.339 (1.342)	1.31, 1.36, 1.368, 1.37	13,17,24, 25	31.9 (31.9)	*37.0*,[e] *45.8*[f]	18,19
[HMIM][PF_6]	1.257	1.24, 1.278, 1.29, 1.292, 1.2935	16,20,24, 25	40.1	*33.4*[e]	18
[OMIM][PF_6]	1.181	1.19, 1.22, 1.237	17,24,25	47.3	40.4 ±1.0,[g] *34.5*[e]	26,18
[MMIM][Cl]	1.175	1.155	27	32.3		
[EMIM][Cl]	1.121 (1.130)	1.110	27	19.3 (25.5)		
[BMIM][Cl]	1.041 (1.060)	1.075, 1.08	24,27	29.1 (32.0)		
[HMIM][Cl]	1.007	1.03, 1.0338	24,28	37.5		
[OMIM][Cl]	0.959	1.00, 1.0104, 1.0124	24,28,29	44.6	*29.3*[e]	18
[MMIM][$AlCl_4$]	1.260	1.3289	30	31.1	*45.3*[e]	30
[EMIM][$AlCl_4$]	1.226 (1.229)	1.2947, 1.302	5,30	19.8 (26.3)	*43.6*[e]	30
[BMIM][$AlCl_4$]	1.175 (1.176)	1.238, 1.2381	5,30	41.9 (32.1)	*41.1*[e]	30
[HMIM][$AlCl_4$]	1.120	1.1952	30	38.3	*39.5*[e]	30
[MMIM][Al_2Cl_7]	1.282	1.341[c]	27,31	34.0		
[EMIM][Al_2Cl_7]	1.260 (1.249)	1.325[c]	27,31	22.3 (28.2)		
[BMIM][Al_2Cl_7]	1.206 (1.203)	1.272[c]	27,31	32.4 (33.6)		
[HMIM][Al_2Cl_7]	1.119			39.2		
[MMIM][NO_3]	1.305			31.8		
[EMIM][NO_3]	1.253 (1.258)			18.1 (25.8)	*39.1 ±1.3*[h]	32
[BMIM][NO_3]	1.163 (1.175)	1.15343	28	28.0 (31.9)	*38.8 ± 1.4*[h]	32

[HMIM][NO_3]	1.080	1.11658	[28]	34.9		
[MMIM][TfO]	1.489			32.5		
[EMIM][TfO]	1.420 (1.412)	1.37522, 1.38, 1.390	[16,33,34]	21.3 (26.7)		
[BMIM][TfO]	1.297 (1.310)	1.30, 1.30148, 1.3013[d]	[34,35]	31.1 (32.7)	*33.8*[f]	[19]
[HMIM][TfO]	1.241	1.24	[34]	40.6		
[OMIM][TfO]	1.125	1.12	[34,36]	46.5	36.1 ±0.7[g]	[26]

[a]Calculated density and ΔH_{vap} values given in parenthesis were computed using OPLS-AA charge/torsion parameters specific to [EMIM] and [BMIM]. ΔH_{vap} estimations from experimental data given in italics. R = M (methyl), E (ethyl), B (butyl), H (hexyl), and O (octyl). [b]23 °C; density computed from crystal structure cell parameters. [c][RMIM][Cl]-$AlCl_3$ 0.66 melt,[27] which should correspond to exclusively [RMIM][Al_2Cl_7].[31] [d]22.6 °C. [e]Experimental density and surface tension measurements in conjunction with Kabo's equation[18] was used to estimate ΔH_{vap}. [f]ΔH_{vap} estimated from Hildebrand's solubility parameter, δ, to solvent-controlled Diels-Alder reaction. [g]Temperature programmed desorption. [h]Experimental combustion calorimetry in conjunction with ab initio calculations (G3MP2) were used to estimate ΔH_{vap}.

Table 7. Calculated Liquid Densities (g/cm^3) and Heats of Vaporization (kcal/mol) at 25 °C for N-alkylpyridinium [RPyr] (R=Me, Et, Bu, Hex, Oct) Based Ionic Liquids.[a]

Ionic Liquid	Density	ΔH_{vap}	Ionic Liquid	Density	ΔH_{vap}
[MPyr][BF_4]	1.300 (1.302)	41.5 (41.0)	[MPyr][PF_6]	1.514 (1.520)	44.9 (44.3)
[EPyr][BF_4][b]	1.250 (1.256)	37.3 (29.8)	[EPyr][PF_6]	1.462 (1.459)	40.3 (33.5)
[BPyr][BF_4][c]	1.169 (1.176)	28.7 (41.1)	[BPyr][PF_6]	1.345 (1.347)	29.8 (39.0)
[HPyr][BF_4][d]	1.091	43.8	[HPyr][PF_6]	1.247	46.2
[OPyr][BF_4]	1.043	52.2	[OPyr][PF_6]	1.170	53.8
[MPyr][$AlCl_4$]	1.246 (1.253)	41.5 (41.3)	[MPyr][Al_2Cl_7]	1.271 (1.267)	44.1 (40.7)
[EPyr][$AlCl_4$]	1.221 (1.217)	37.8 (30.6)	[EPyr][Al_2Cl_7]	1.261 (1.241)	40.8 (28.9)
[BPyr][$AlCl_4$]	1.163 (1.161)	28.1 (36.3)	[BPyr][Al_2Cl_7]	1.181 (1.194)	29.7 (38.9)
[MPyr][NO_3]	1.312 (1.315)	41.6 (41.5)	[MPyr][TfO]	1.506 (1.504)	43.7 (42.5)
[EPyr][NO_3]	1.253 (1.263)	36.4 (29.5)	[EPyr][TfO]	1.421 (1.431)	38.4 (31.6)
[BPyr][NO_3]	1.161 (1.167)	25.2 (35.3)	[BPyr][TfO]	1.306 (1.318)	27.1 (37.3)
[MPyr][Cl]	1.181 (1.184)	44.9 (43.8)	[HPyr][Cl]	1.006	46.5
[EPyr][Cl]	1.122 (1.130)	39.3 (31.9)	[OPyr][Cl]	0.943	52.8
[BPyr][Cl]	1.041 (1.050)	28.3 (38.8)			

[a]Calculated density and ΔH_{vap} values given in parenthesis were computed using OPLS-AA charge/torsion parameters specific to [MPyr], [EPyr], and [BPyr]. [b]Exptl. density of 1.3020 g/cm^3.[37] [c]Exptl. density of 1.2144 and 1.22 g/cm^3.[15,22] [d]Exptl. density of 1.16 g/cm^3 at 20 °C.[38]

Table 8. Calculated Liquid Densities (g/cm^3) and Heats of Vaporization (kcal/mol) at 25 °C for Choline [Chol] Based Ionic Liquids.

Ionic Liquid	Density	ΔH_{vap}	Ionic Liquid	Density	ΔH_{vap}
[Chol][Cl][a]	1.040	78.9	[Chol][$AlCl_4$]	1.192	75.3
[Chol][Ace][b]	1.206	70.9	[Chol][Al_2Cl_7]	1.195	77.5
[Chol][Sacc][c]	1.200	79.2	[Chol][NO_3]	1.159	76.9
[Chol][BF_4]	1.165	75.7	[Chol][TfO]	1.326	76.0
[Chol][PF_6]	1.375	77.8			

[a]Exptl. density from crystal structure at 85 °C is 1.12 g/cm^3.[39] [b]Exptl. density is 1.284 g/cm^3.[40] [c]Exptl. density is 1.383 g/cm^3.[40]

Densities were also computed for 11 ionic liquid combinations over temperatures ranging from 5 to 90 °C and compared with experimentally observed values (Table 9). Various chain lengths were tested for [RMIM] from R = Et to Oct with multiple anions, [BF_4], [PF_6], [$AlCl_4$], and [TfO]. The relative deviations from experiment were ca. 1-3% with the exception of [EMIM][$AlCl_4$], which gave deviations of ca. 4-5%, similar to the simulations at 25 °C. The general trend of a decreasing density as temperature increases was reproduced for all ionic liquids tested (Figure 5). Good agreement was also found between the fully transferable parameters and the charge/torsion set specific to [EMIM] and [BMIM] (Table 9).

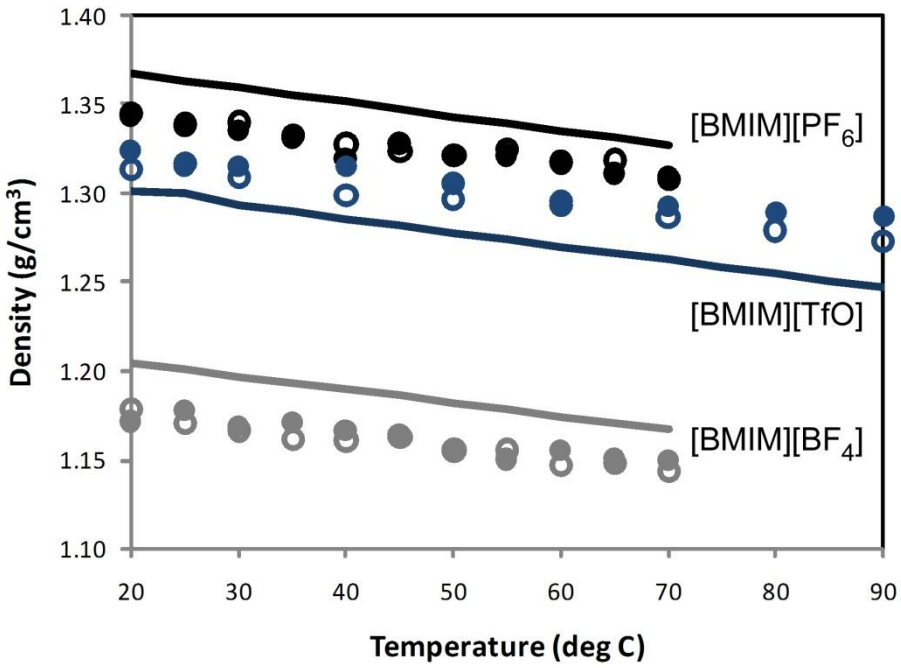

Figure 5. Calculated and experimental liquid densities versus temperature for 1-butyl-3-methylimidazolium [BMIM] based ionic liquids with [BF_4] in black, [TfO] in blue, and [PF_6] in gray. (O = general OPLS-AA [RMIM] parameter set, ● = specific OPLS-AA [BMIM] parameter set, and solid lines = experimental values)

Table 9. Calculated and Experimental Liquid Densities (g/cm^3) Versus Temperature for 1-Alkyl-3-methylimidazolium [RMIM] and N-alkylpyridinium [RPyr] (R=Me, Et, Bu, Hex, Oct) Based Ionic Liquids.[a]

Ionic Liquid	Temp. (°C)	Density (Calc.)	Density (Exptl.)	Refs.
[EMIM][BF_4]	20	1.255 (1.260)	1.283	15
	25	1.253 (1.254)	1.279	15
	30	1.255 (1.251)	1.275	15
	35	1.246 (1.251)	1.271	15
	40	1.247 (1.246)	1.266	15
[EMIM][TfO]	5	1.431 (1.428)	1.40052	33
	15	1.431 (1.420)	1.39204	33
	25	1.425 (1.422)	1.38360	33
	35	1.414 (1.411)	1.37522	33
	45	1.412 (1.414)	1.36690	33
	55	1.401 (1.404)	1.35863	33
	65	1.397 (1.391)	1.35043	33
	75	1.393 (1.385)	1.34230	33
[EMIM][$AlCl_4$]	10	1.240 (1.244)	1.3060	30
	15	1.238 (1.239)	1.3020	30
	20	1.234 (1.228)	1.2979	30
	25	1.229 (1.229)	1.2947	30
	30	1.222 (1.224)	1.2908	30
	35	1.221 (1.216)	1.2870	30
	40	1.217 (1.216)	1.2833	30
	45	1.214 (1.214)	1.2798	30
	50	1.209 (1.206)	1.2759	30
	55	1.207 (1.200)	1.2725	30
	60	1.203 (1.201)	1.2689	30
	65	1.200 (1.195)	1.2651	30
[BMIM][BF_4]	20	1.179 (1.172)	1.2049, 1.2038	41
	25	1.171 (1.178)	1.2011, 1.2000	41
	30	1.167 (1.169)	1.1974, 1.1962	41
	35	1.161 (1.171)	1.1938, 1.1924	41
	40	1.161 (1.167)	1.1901, 1.1889	41

	45	1.168 (1.165)	1.1865, 1.1854	[41]
	50	1.155 (1.155)	1.1827, 1.1813	[41]
	55	1.167 (1.174)	1.1790, 1.1779	[41]
	60	1.147 (1.155)	1.1753, 1.1741	[41]
	65	1.162 (1.151)	1.1717, 1.1705	[41]
	70	1.143 (1.150)	1.1680, 1.1669	[41]
[BMIM][PF_6]	20	1.345 (1.343)	1.3698, 1.3681	[41]
	25	1.339 (1.338)	1.3657, 1.3641	[41]
	30	1.340 (1.335)	1.3616, 1.3600	[41]
	35	1.333 (1.331)	1.3574, 1.3557	[41]
	40	1.328 (1.319)	1.3533, 1.3518	[41]
	45	1.324 (1.328)	1.3492, 1.3475	[41]
	50	1.322 (1.321)	1.3451, 1.3435	[41]
	55	1.325 (1.321)	1.3410, 1.3394	[41]
	60	1.318 (1.318)	1.3369, 1.3352	[41]
	65	1.319 (1.311)	1.3327, 1.3311	[41]
	70	1.308 (1.309)	1.3286, 1.3270	[41]
[BMIM][TfO]	20	1.314 (1.324)	1.3013	[41]
	25	1.317 (1.315)	1.30, 1.30148	[34,35]
	30	1.309 (1.315)	1.2934	[41]
	40	1.299 (1.315)	1.2856	[41]
	50	1.296 (1.305)	1.277	[41]
	60	1.293 (1.296)	1.2699	[41]
	70	1.286 (1.293)	1.2623	[41]
	80	1.279 (1.289)	1.2545	[41]
	90	1.273 (1.288)	1.2469	[41]
[HMIM][BF_4]	25	1.102	1.14532	[42]
	35	1.094	1.13851	[42]
	45	1.097	1.13167	[42]
	55	1.088	1.12489	[42]
	65	1.080	1.11816	[42]
	75	1.077	1.11147	[42]
	85	1.070	1.10484	[42]
[HMIM][PF_6]	5	1.267	1.3101	[43]
	10	1.265	1.3060	[43]
	15	1.266	1.3019	[43]

	20	1.262	1.2979	[43]
	25	1.255	1.2937, 1.29341	[42,43]
	30	1.253	1.2896	[43]
	35	1.256	1.2854, 1.28578	[42,43]
	40	1.249	1.2813	[43]
	45	1.250	1.2772, 1.27792	[42,43]
	55	1.244	1.26988	[42]
	65	1.237	1.26213	[42]
	75	1.232	1.25436	[42]
	85	1.229	1.24681	[42]
[OMIM][BF_4]	25	1.034	1.0912	[22]
	30	1.037	1.0887	[22]
	40	1.039	1.0823	[22]
	50	1.028	1.0747	[22]
	60	1.027	1.0685	[22]
	70	1.025	1.0618	[22]
[OMIM][PF_6]	25	1.178	1.2245	[22]
	30	1.163	1.2207	[22]
	40	1.161	1.2141	[22]
	50	1.159	1.2069	[22]
	60	1.156	1.1999	[22]
	70	1.149	1.1922	[22]
[BPyr][BF_4]	25	1.175 (1.177)	1.2144	[22]
	30	1.175 (1.177)	1.2118	[22]
	40	1.165 (1.172)	1.2053	[22]
	50	1.162 (1.164)	1.1988	[22]
	60	1.155 (1.163)	1.1922	[22]
	70	1.148 (1.156)	1.1856	[22]

[a]Calculated density values given in parenthesis were computed using OPLS-AA charge/torsion parameters specific to [EMIM], [BMIM], [HMIM], [OMIM], and [BPyr], respectively.

Heats of Vaporization. Ionic liquids are generally characterized by vaporization enthalpies that are almost 1 order of magnitude higher than for molecular liquids due to strong electrostatic interactions between the ions.[44] The importance of properly reproducing the heats of vaporization, ΔH_{vap}, in addition to densities for ionic liquids cannot be minimized as they both serve as key properties representative of molecular size and the average intermolecular interactions.[45] Heats of vaporization are readily computed from the simulation results using equation 1.

$$\Delta H_{vap} = \Delta H_{gas} - \Delta H_{liquid} = E_{total}(\text{gas}) - E_{total}(\text{liquid}) + RT \quad (1)$$

Experimental evidence suggests that ionic liquids go into the vapor phase in ion pairs.[26] Hence, the E_{total}(gas) term was computed from the average intra- and intermolecular energy for the ion pair in the gas phase from each ionic liquid combination. E_{total}(liquid) is the total potential energy of the liquid consisting of both the average intramolecular energy, E_{intra}(liquid) and the average intermolecular energy, E_{inter}(liquid), from the ionic liquid. The RT term is used in place of a PV-work term in the enthalpy. The heats of vaporization obtained from the MC simulations for the ionic liquids are presented in Tables 6, 7, and 8, and for [RMIM] in Figure 6.

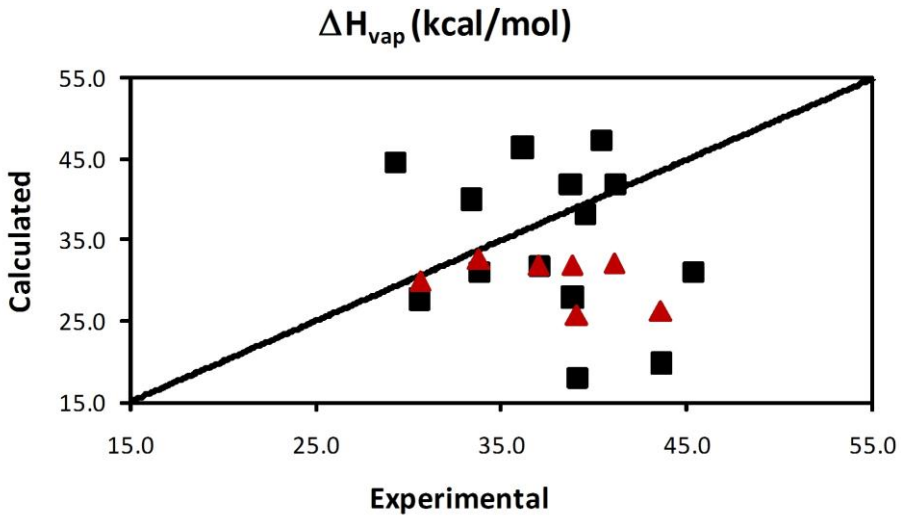

Figure 6. Computed OPLS-AA and experimental results for heats of vaporization for 1-alkyl-3-methylimidazolium [RMIM] based ionic liquids (black squares) at 25 °C and 1 atm. Computed values with OPLS-AA parameters specific to [EMIM] and [BMIM] given as red triangles.

Comparison between the computed and experimental heats of vaporization, ΔH_{vap}, values is particularly difficult owing to the large reported deviations between different experimental-based techniques. For example, earlier ΔH_{vap} estimates derived from correlations of Hildebrand's solubility parameter, δ, to solvent-controlled chemical reactions[19] and viscosity data[46] have been found to significantly overestimate experimentally measured ΔH_{vap} values.[44] Accordingly, the new ionic liquid parameters were not adjusted to improve agreement with reported experimental data. Instead, the parameters were fit to reproduce ab initio calculations and directly compared to available experimental values. The MC simulations gave favorable correlations with direct measurements of the ionic liquids using a temperature programmed desorption technique[26] and with more accurate ΔH_{vap} estimates derived from density and surface tensions measurements coupled to Zaitsau et. al's empirical equation.[30] For example, ΔH_{vap} values of 41.9 and 38.3

kcal/mol were computed for the chloroaluminate ionic liquids [BMIM][$AlCl_4$] and [HMIM][$AlCl_4$], respectively, using the general [RMIM] parameter set which were found to be in close agreement with the experimentally estimated values of 41.1 and 39.5 kcal/mol.[60] Calculations of [OMIM] based ionic liquids with [BF_4] and [PF_6] counteranions gave ΔH_{vap} values of 41.8 and 47.0 kcal/mol, respectively, in reasonable agreement with experimentally measured values of 38.7 ± 0.7 and 40.4 ± 1.0 kcal/mol.[26] The computed ΔH_{vap} values of 27.8 and 31.9 kcal/mol for [BMIM][BF_4] and [BMIM][PF_6], respectively, are in good agreement with recent experimental estimates of 30.6 and 37.0 kcal/mol;[18] the simulations confirm earlier estimates of 48.6 and 45.8 kcal/mol[19] from correlations of Hildebrand's solubility parameter to be overestimated.[44] Further comparisons of calculated versus experimental ΔH_{vap} values for [RMIM] based ionic liquids are given in Table 6.

A general trend found in the calculation of the ΔH_{vap} was a smaller predicted value in the [EMIM] cation based ionic liquids relative to other [RMIM] values. For example, [RMIM][NO_3] ΔH_{vap} values of 31.8, 18.1, and 28.0 kcal/mol were computed using the general OPLS-AA parameter set for [MMIM], [EMIM], and [BMIM], respectively. Experimental combustion calorimetry in conjunction with ab initio calculations (G3MP2) estimate ΔH_{vap} as 39.1 ± 1.3 and 38.8 ± 1.4 kcal/mol for [EMIM] and [BMIM] in the [NO_3] based ionic liquids.[32] The computed heats of vaporization are particularly sensitive to the charge sets used, as the specific OPLS-AA charge set reduced the deviation between the ionic liquids and brought the results closer to the estimates with computed values of 25.8 and 31.9 kcal/mol for [EMIM][NO_3] and [BMIM][NO_3]. The general parameters maybe more susceptible to deviations for [EMIM] due to the use of the same atom types CT and HT to model the end carbon and hydrogens as the longer alkyl side-chains, such as butyl and hexyl. Earlier parameterization efforts used an atom type specific to

[EMIM] to cap the alkyl chain.[4] The use of a polarizable force field may also improve agreement.[47] However, the large differences in the computed ΔH_{vap} values when using the transferable and cation specific OPLS-AA parameters were not seen for the predicted densities (Figure 4) which were generally insensitive to the charge/torsion set used.

ESP charges specific to [EMIM], [MPyr], and [EPyr]; Equilibrium bond and angle reference values, r_o and θ_o, and force constants, k, for the simulations; Additional torsion Fourier coefficients for the cations; Additional torsion energy profiles for the cations; box sizes for all ionic liquids simulated are given in Supporting information of this Thesis.

The development and testing of the OPLS-AA force field for use in the simulation of 68 unique ionic liquids has been described. Charges, equilibrium geometries, and torsional Fourier coefficients were derived to reproduce gas-phase structures and conformational energetics from LMP2/cc-pVDZ(-f)//HF/6-31G(d) quantum mechanical calculations. Multiple alkyl chain lengths were considered in the fitting process and the quality of the fits for the transferable force field yielded energy profiles for bond rotations comparable to that of ab initio calculations. In addition, the highly transferable parameters for [RMIM] and [RPyr] were compared to potentials developed specifically for individual ionic liquid cations and good agreement in liquid densities values was found between both sets. Relative deviations from experimental density values were ca. 1-3%, however chloroaluminate-based ionic liquids had slightly larger deviations at ca. 4-5%. The errors in the densities computed for choline-based ionic liquids were significantly larger, but are difficult to improve owing to the lack of available experimental data for refinement. Agreement between the computed ΔH_{vap} and experimental estimates are generally good, however absolute errors in the vaporization enthalpies are more difficult to assess due to inconsistencies between reported experimental values. In addition, the computed heats of

vaporization were found to be more sensitive to the charge set used. The importance of testing the cation and anion parameters in a large number of ionic liquid combinations is highlighted in this work by the liquid simulation of an unprecedented number of ionic liquids, with 35 of the 68 solvents recomputed using specific cation parameters for a detailed comparison of the new parameters set's transferability between different alkyl chain lengths and anion combinations.

MC simulations play a major role in understanding of the chemistry of ionic liquids. These molecular simulations can be used predict thermodynamic and transport properties of ionic liquids. Property predictions will be important tools to know the nature of the conditions under extremely high temperatures and pressures, where experiments are difficult to perform. Ionic liquids are a medium for variety of organic reactions. Molecular simulations can also be performed on solubility of CO_2 in ionic liquids, dissolution of cellulose with ionic liquids, dispersion of petroleum asphaltenes using ionic liquids, ionic liquids in solar energy conversion, and batteries with ionic liquids as electrolytes. Accurate new force fields with polarization effects for different anion and cation classes are required. Development and validation of new force fields is tedious process, but this should be carried to perform molecular simulations in order to design new ionic liquids.

References

(1) Jorgensen, W. L.; Maxwell, D. S.; Tirado-Rives, J. *J. Am. Chem. Soc.* **1996,** *118*, 11225-11236.

(2) McDonald, N. A.; Jorgensen, W. L. *J. Phys. Chem. B* **1998,** *102*, 8049-8059.

(3) Jorgensen, W. L.; McDonald, N. A. *J. Mol. Struct. (THEOCHEM)* **1998,** *424*, 145-155.

(4) Canongia Lopes, J. N.; Deschamps, J.; Padua, A. H. *J. Phys. Chem. B* **2004,** *108*, 2038-2047.

(5) de Andrade, J.; Böes, E. S.; Stassen, H. *J. Phys. Chem. B* **2002,** *106*, 13344-13351.

(6) Acevedo, O.; Jorgensen, W. L.; Evanseck, J. D. *J. Chem. Theory Comput.* **2007,** *3*, 132-138.

(7) Canongia Lopes, J. N.; Padua, A. A. H. *J. Phys. Chem. B* **2006,** *110*, 19586-19592.

(8) Gale, R. J.; Gilbert, B. P.; Osteryoung, R. A. *Inorg. Chem.* **1978,** *17*, 2728-2729.

(9) Wilkes, J. S.; Frye, J. S.; Reynolds, G. F. *Inorg. Chem.* **1983,** *22*, 3870-3872.

(10) (a) Ackermann, B. L.; Tsarbopoulos, A.; Allison, J. *Anal. Chem.* **1985,** *57*, 1766-1768; (b) Wicelinski, S. P.; Gale, R. J.; Pamidimukkala, K. M.; Laine, R. A. *Anal. Chem.* **1988,** *60*, 2228-2232.

(11) Gray, J. L.; Maciel, G. E. *J. Am. Chem. Soc.* **1981,** *103*, 7147-7151.

(12) Franzen, G.; Gilbert, B. P.; Pelzer, G.; Depauw, E. *Org. Mass Spectrom.* **1986,** *21*, 443-444.

(13) Ohlin, C. A.; Dyson, P. J.; Laurenczy, G. *Chem. Commun.* **2004**, 1070-1071.

(14) Nishida, T.; Tashiro, Y.; Yamamoto, M. *J. Fluorine Chem.* **2003,** *120*, 135-141.

(15) Noda, A.; Hayamizu, K.; Watanabe, M. *J. Phys. Chem. B* **2001,** *105*, 4603-4610.

(16) Zhang, S.; Sun, N.; He, X.; Lu, X.; Zhang, X. *J. Phys. Chem. Ref. Data* **2006,** *35*, 1475-1517.

(17) Branco, L. C.; Rosa, J. N.; Ramos, J. J. M.; Afonso, C. A. M. *Chem. Eur. J.* **2002,** *8*, 3671-3677.

(18) Zaitsau, D. H.; Kabo, G. J.; Strechan, A. A.; Paulechka, Y. U.; Tschersich, A.; Verevkin, S. P.; Heintz, A. *J. Phys. Chem. A* **2006,** *110*, 7303-7306.

(19) Swiderski, K.; McLean, A.; Gordon, C. M.; Vaughan, D. H. *Chem. Commun.* **2004**, 2178-2179.

(20) (a) Letcher, T. M.; Reddy, P. *J. Chem. Thermodyn.* **2005,** *37*, 415-421; (b) Letcher, T. M.; Reddy, P. *Fluid Phase Equil.* **2004,** *219*, 107-112.

(21) Arce, A.; Rodil, E.; Soto, A. *J. Solution Chem.* **2006,** *35*, 63-78.

(22) Gu, Z.; Brennecke, J. F. *J. Chem. Eng. Data* **2002,** *47*, 339-345.

(23) Matsumotoa, K.; Hagiwara, R. *J. Fluorine Chem.* **2007,** *128*, 317-331.

(24) Huddleston, J. G.; Visser, A. E.; Reichert, W. M.; Willauer, H. D.; Broker, G. A.; Rogers, R. D. *Green Chem.* **2001,** *3*, 156-164.

(25) Dzyuba, S. V.; Bartsch, R. A. *ChemPhysChem* **2002,** *3*, 161-166.

(26) Armstrong, J. P.; Hurst, C.; Jones, R. G.; Licence, P.; Lovelock, K. R. J.; Satterley, C. J.; Villar-Garcia, I. J. *Phys. Chem. Chem. Phys.* **2007,** *9*, 982-990.

(27) Fannin Jr., A. A.; Floreani, D. A.; King, L. A.; Landers, J. S.; Piersma, B. J.; Stech, D. J.; Vaughn, R. L.; Wilkes, J. S.; Williams, J. L. *J. Phys. Chem.* **1984,** *88*, 2614-2621.

(28) Seddon, K. R.; Stark, A. S.; Torres, M.-J., In *In Clean Solvents: Alternative Media for Chemical Reactions and Processing*, Abraham, M.; Moens, L., Eds. ACS Symposium Series 819, American Chemical Society: Washington DC, 2002; Vol. 3, pp 4–49.

(29) Letcher, T. M.; Deenadayalu, N. *J. Chem. Thermodyn.* **2003,** *35*, 67-76.

(30) Tong, J.; Liu, Q.-S.; Xu, W.-G.; Fang, D.-W.; Yang, J.-Z. *J. Phys. Chem. B* **2008,** *112*, 4381-4386.

(31) Fannin Jr., A. A.; King, L. A.; Leveisky, J. A.; Wilkes, J. S. *J. Phys. Chem.* **1984,** *88*, 2609-2614.

(32) Emel'yanenko, V. N.; Verevkin, S. P.; Heintz, A.; Schick, C. *J. Phys. Chem. B* **2008,** *112*, 8095-8098.

(33) Rodriguez, H.; Brennecke, J. F. *J. Chem. Eng. Data* **2006,** *51*, 2145-2155.

(34) Ye, C.; Shreeve, J. n. M. *J. Phys. Chem. A* **2007,** *111*, 1456-1461.

(35) (a) Olivier-Bourbigou, H.; Magna, L. *J. Mol. Catal. A: Chem.* **2002,** *182*; (b) Fredlake, C. P.; Crosthwaite, J. M.; Hert, D. G.; Aki, S. N. V. K.; Brennecke, J. F. *J. Chem. Eng. Data* **2004,** *49*, 954-964; (c) Tokuda, H.; Hayamizu, K.; Ishii, K.; Susan, M. A. B. H.; Watanabe, M. *J. Phys. Chem. B* **2004,** *108*, 16593-16600.

(36) Papaiconomou, N.; Yakelis, N.; Salminen, J.; Bergman, R.; Prausnitz, J. M. *J. Chem. Eng. Data* **2006,** *51*, 1389-1393.

(37) Valderrama, J. O.; Sanga, W. W.; Lazzus, J. A. *Ind. Eng. Chem. Res.* **2008,** *47*, 1318-1330.

(38) Merck ionic liquid database, http://ildb.merck.de/ionicliquids/en/startpage.html.

(39) Shanley, P.; Collin, R. L. *Acta. Cryst.* **1961,** *14*, 79-80.

(40) Nockemann, P.; Thijs, B.; Driesen, K.; Janssen, C. R.; Van Hecke, K.; Van Meervelt, L.; Kossmann, S.; Kirchner, B.; Binnemans, K. *J. Phys. Chem. B* **2007,** *111*, 5254-5263.

(41) Jacquemin, J.; Ge, R.; Nancarrow, P.; Rooney, D. W.; Costa Gomes, M. F.; Pádua, A. A. H.; Hardacre, C. *J. Chem. Eng. Data* **2008,** *53*, 716-726.

(42) Muhammad, A.; Mutalib, M. I. A.; Wilfred, C. D.; Murugesan, T.; Shafeeq, A. *J. Chem. Thermodynamics* **2008,** *40*, 1433-1438.

(43) Pereiro, A. B.; Tojo, E.; Rodríguez, A.; Canosa, J.; Tojo, J. *J. Chem. Thermodynamics* **2006,** *38*, 651-661.

(44) Weingaertner, H. *Angew. Chem. Int. Ed.* **2008,** *47*, 654-670.

(45) Jorgensen, W. L.; Tirado-Rives, J. *Proc. Nat. Acad. Sci. USA* **2005,** *102*, 6665-6670.

(46) Lee, S. H.; Lee, S. B. *Chem. Commun.* **2005**, 3469-3471.

(47) Yan, T.; Burnham, C. J.; Del Pópolo, M. G.; Voth, G. A. *J. Phys. Chem. B* **2004,** *108*, 11877-11881.

Chapter V. Enhancement of chemical reactivity from ionic liquids is primarily a transition state effect

As an initial test of the newly developed ionic liquid parameters, mixed quantum and molecular mechanical (QM/MM) calculations were carried out on the Kemp elimination of benzisoxazole with piperidine in [BMIM][PF_6] (Figure 1), and β-elimination of 1,1,1-tribromo-2,2-bis(phenyl-substituted)ethane with piperidine and pyrrolidine as bases in [BMIM][BF_4], [BMIM][PF_6] (Figure 2). The solutes were treated with the PDDG/PM3 semiempirical QM method.[1] PDDG/PM3 has given excellent results in our recent QM/MM studies of the Kemp elimination of 5-nitro-benzisoxazole via catalytic antibody 4B2[2] and the condensed-phase Kemp decarboxylation of benzisoxazole-3-carboxylic acid.[3] Potentials of mean force (PMF) calculations coupled to Metropolis Monte Carlo (MC) statistical mechanics were used to build a free-energy profile for the ring opening at 25 °C and 1 atm.

*Sambasivarao, S.V.; Acevedo, O. (To be submitted)

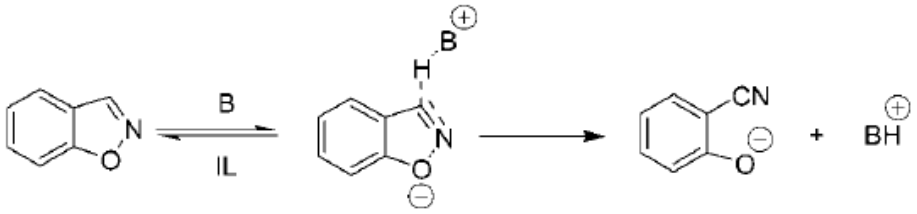

Figure 1. Schematic representation of Kemp elimination; benzisoxazole (1), o-cyanophenolate (2), piperidine (B), [BMIM][PF_6] (IL).

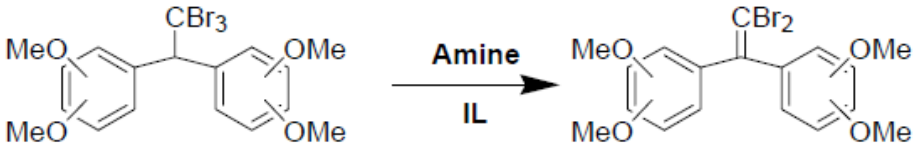

Figure 2. β-elimination of 1,1,1-tribromo-2,2-bis(phenyl-substituted)ethane into corresponding ethene; piperidine and pyrrolidine (Amine), [BMIM][PF_6] and [BMIM][BF_4] (IL).

A reacting distance, R_{NH} - R_{CH}, was used for the proton transfer between the nitrogen on piperidine and the hydrogen on the isoxazole ring (Figure 3); R_{NH} + R_{CH} was kept constant at 2.85 Å. The fixed distance of 2.85 Å was determined to be appropriate from our recent study of the reaction.[2] A second perturbation was necessary, R_{NO}, which entailed the opening of the isoxazole ring via an increasing N-O distance. Combining the R_{NH} - R_{CH} PMF which runs along one reaction coordinate with the R_{NO} PMF in a second direction produced a two-dimensional (2D) PMF. The result is a free-energy map that can be used to identify minima and the transition state present in the reaction. The breaking of the N-O bond was split into ca. 24 windows with an increment of 0.04 Å. Each PMF calculation required 5 million configurations of equilibration followed by 10 million configurations of averaging.

For the hydrogen transfer, a novel method was developed in our recent study of the ring-opening of 5-nitro-benzisoxazole, where it was found that free-energy changes for individual windows can be fit almost perfectly by a 5th order polynomial.[2] Using only 7 windows out of the usual 50 and analytically integrating the values yielded a sextic polynomial for the overall proton-transfer PMF that is essentially identical to running the full simulation. The new methodology provided a 7-fold improvement in speed over traditional PMF methods for the enzymatic calculations and the largest deviation found between the approximate and the detailed calculation was 1 kcal/mol. The 5th order polynomial quadrature method was used to compute the free energy of activation for the Kemp elimination in a periodic box of 378 [BMIM][PF_6] ionic liquid ions in the NPT ensemble. Ewald sums were used to handle the long-range electrostatics and electrostatic contributions to the solute-solvent energy were calculated using CM3 charges,[4] with a scale factor of 1.14.

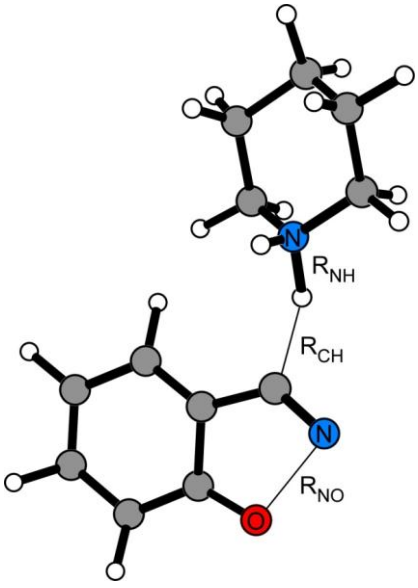

Figure 3. Reaction coordinates, $R_{NH} - R_{CH}$ and R_{NO}, used to locate stationary points from free-energy maps obtained via PMF simulations for the Kemp elimination of benzisoxazole using piperidine. Illustrated structure corresponds to the transition state computed from QM/MM calculations.

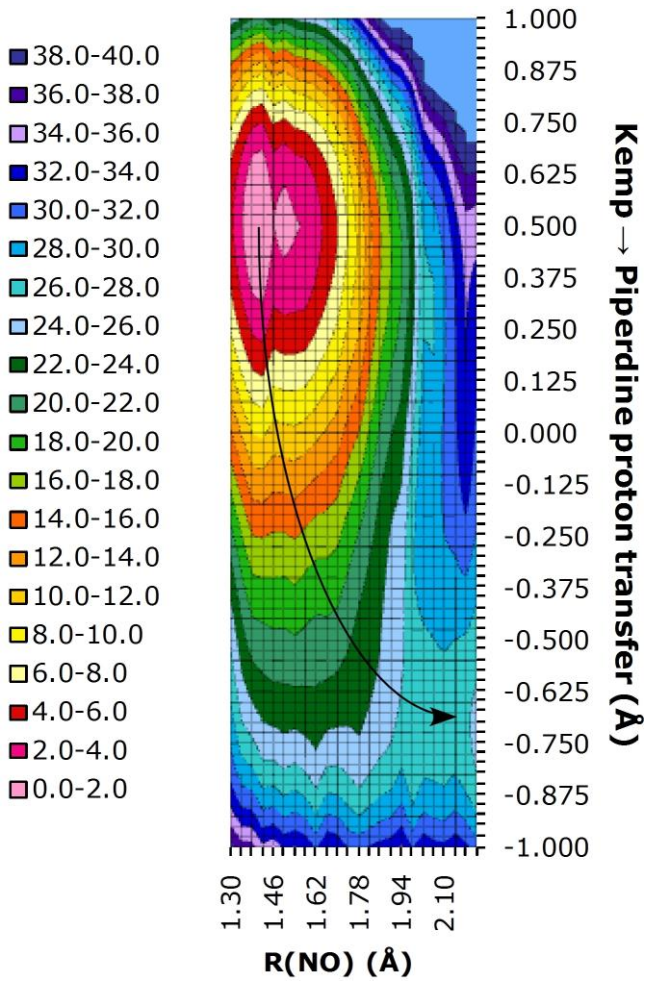

Figure 4. Two-dimensional potentials of mean force (free energy map, kcal/mol) for the Kemp elimination reaction of benzisoxazole via piperidine in [BMIM][PF_6]. Free energy values truncated to 40 kcal/mol for clarity. The arrow follows the reaction path toward product.

The free-energy surface for the Kemp elimination of benzisoxazole via piperidine is shown in Figure 4. The reaction follows a concerted mechanism where the R_{NO} distance of the isoxazole ring in the transition structure is 2.06 Å while the R_{NH} and R_{CH} distances are 1.10 and 1.75 Å, respectively. Computed changes in free energy yielded a $\Delta G^{\ddagger}$ value of 25.2 kcal/mol after a cratic entropy correction of 1.89 kcal/mol.[5] The level of uncertainty is less than ± 1 kcal/mol based on fluctuations in the averages for the individual free-energy perturbation (FEP)

windows. The experimental $\Delta G^{\ddagger}$ for the reaction under the same conditions is 22.6 ± 0.5 kcal/mol.[6] The calculations reproduce the activation values well, particularly when considering the computed and experimental uncertainties and the additional overestimation of ca. 1 kcal/mol for the Kemp elimination from the 5th order polynomial methodology.[2] The good agreement suggests that the ionic liquid microenvironment is being appropriately modeled by the new parameters.

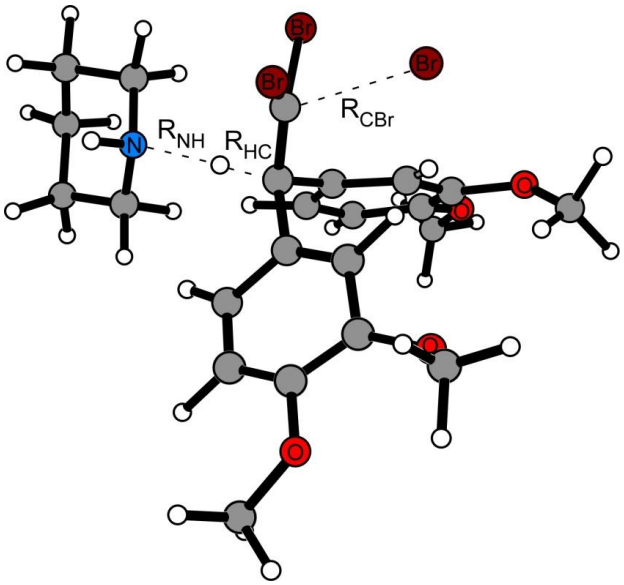

Figure 5. Reaction coordinates, $R_{NH} - R_{CH}$ and R_{CBr}, used to locate stationary points from free-energy maps obtained via PMF simulations for the β-elimination of 1,1,1-tribromo-2,2-bis(phenyl-substituted)ethane using piperidine in [BMIM][BF_4]. Illustrated structure corresponds to the transition state computed from QM/MM calculations.

Above similar methodology and reaction conditions were applied to build a free energy surface for the β-elimination of 1,1,1-tribromo-2,2-bis(phenyl-substituted)ethane using piperidine and pyrrolidine as bases in [BMIM][BF_4], [BMIM][PF_6], CH_3OH. A reacting distance, R_{NH} - R_{CH}, was used for the proton transfer between the nitrogen on piperidine and the

β-hydrogen on the 1,1,1-tribromo-2,2-bis(phenyl-substituted)ethane shown in Figure 5. R_{NH} + R_{CH} was kept constant at 2.85 Å. A second perturbation R_{CBr}, which entailed bond breaking of C-Br at an increasing C-Br distance. Combining the R_{NH} - R_{CH} PMF which runs along one reaction coordinate with the R_{CBr} PMF in a second direction produced a two-dimensional (2D) PMF. The breaking of the C-Br bond was split into ca. 89 windows with an increment of 0.025 Å.

Each PMF calculation required 95 million configurations of equilibration followed by 10 million configurations of averaging in ionic liquids and 5 million configurations of equilibration followed by 10 million configurations of averaging in CH_3OH. The 5^{th} order polynomial quadrature method was used to compute the free energy of activation for the β-elimination in a periodic box of 374 [BMIM][BF_4], 376 [BMIM][PF_6] ionic liquid ions in the NPT ensemble. After the cratic entropic correction of 1.89 kcal/mol, computed activation energies $\Delta G^{\ddagger}$ and geometries for the β-elimination reaction are given Tables 1 and 2.

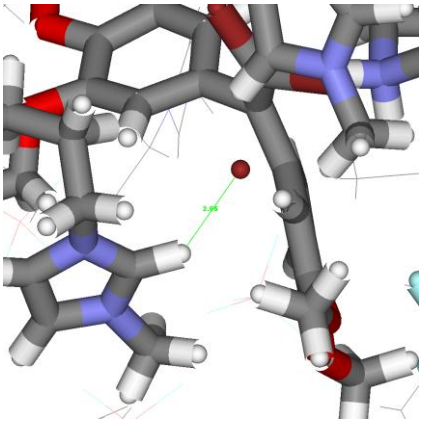

Figure 6: Hydrogen bond donation to bromine departure during transition state in the β-elimination of 1,1,1-tribromo-2,2-bis(phenyl-substituted)ethane using piperidine in [BMIM][BF_4]

Table 1. Activation energies of β-elimination of 1,1,1-tribromo-2,2-bis(phenyl-substituted)ethane.

Ionic liquid	$\Delta G^{\ddagger}_{E1}$ kcal/mol	$\Delta G^{\ddagger}_{E2}$ kcal/mol	$\Delta G^{\ddagger}_{Exptl}$[7] Kcal/mol
	Base:	Piperidine	
[BMIM][BF_4]	38.27	36.46	24.16
[BMIM][PF_6]	37.83	34.78	23.87
CH_3OH		38.39	
	Base:	Pyrrolidine	
[BMIM][BF_4]	43.82	39.82	22.74
[BMIM][PF_6]	39.64	34.46	
CH_3OH		36.49	

Table 2. Geometries of CBr of β-elimination of 1,1,1-tribromo-2,2-bis(phenyl-substituted)ethane

Ionic liquid	CBr(E1) Å	CBr(E2) Å
	Base:	Piperidine
[BMIM][BF_4]	2.775	2.775
[BMIM][PF_6]	2.800	2.800
CH_3OH		2.425
	Base:	Pyrrolidine
[BMIM][BF_4]	2.850	3.075
[BMIM][PF_6]	2.925	3.200
CH_3OH		2.325

The free-energy surface for β-elimination of 1,1,1-tribromo-2,2-bis(phenyl-substituted)ethane via piperidine is shown in Figure 7 of the Supporting Imformation. The activation energies are overestimated by 10 -15 kcal/mol. The overestimation happened in all the cases. The β-elimination occurs through either concerted E2 and/or stepwise E1cB (see Chapter 1, Figure 4, eq 1-3) mechanisms. Three curves have been shown in Figure 7. Blue curve

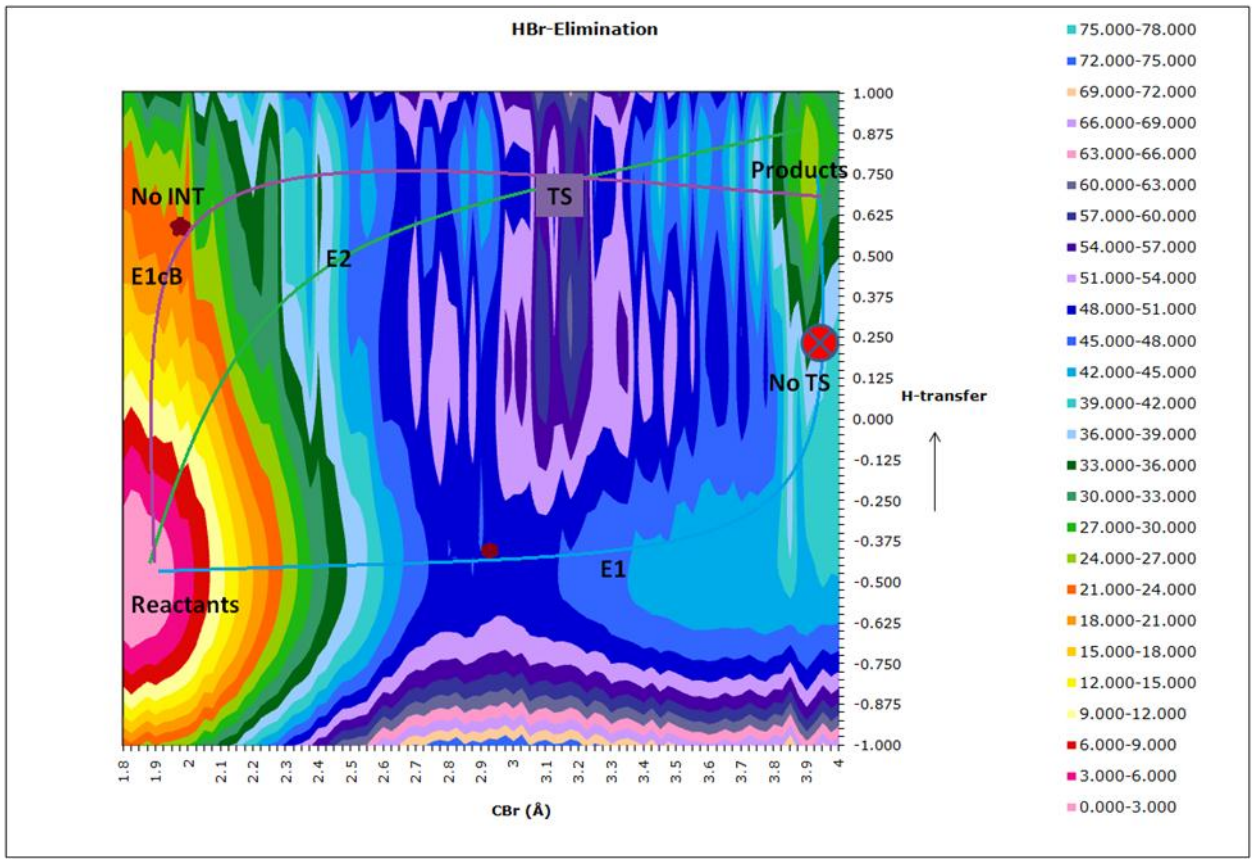

Figure 7. Two-dimensional potentials of mean force (free energy map after 5M configurations of equilibration and 10M configurations of averaging, kcal/mol) for the β-elimination of 1,1,1-tribromo-2,2-bis(phenyl-substituted)ethane into corresponding ethene using piperidine in [BMIM][BF_4].

indicates the mechanism occurs through E1, but there is no transition state appeared after formation of carbocation. This route is not consistent with the $E2_{ip}$ mechanism, where a large activation barrier should be present after a ionization of substituted ethane. If elimination occurs through E1cB, an intermediate should be there with large activation barrier in the first step. A lack of an activation barrier, and no formation of intermediates indicates β-elimination should not occur through a E1cB mechanism. The green curve shows the elimination occurs through E2 mechanism. In this concerted mechanism, the hydrogen transfers from C of ethane to N of

piperidine, and the C-Br bond is breaking simultaneously. The transition state shows the hydrogen is transferred fully towards to N of amine. It means elimination may have some E1cB character even with a lack of an intermediate. The currents simulations are consistent with a β-elimination that occurs through E2 mechanism with E1cB character. E2 mechanism assisted by bromine departure with imidazolium cation through donation of hydrogen bond can be seen in Figure 6. The transition state is stabilized by electrostatic interactions and л-л interactions.

QM/MM simulations for the Kemp elimination of benzisoxazole using piperidine as the base in [BMIM][PF_6] yielded good agreement with the experimental free energy of activation, i.e. $\Delta G^{\ddagger}$(calc.) = 25.2 ± 1 kcal/mol compared to $\Delta G^{\ddagger}$(exptl.) = 22.6 ± 0.5 kcal/mol.[6] Kemp elimination occurs through concerted E2 mechanism. However, the β-elimination of 1,1,1-tribromo-2,2-bis(phenyl-substituted)ethane using piperidine, pyrrolidine as the bases in [BMIM][BF_4], [BMIM][PF_6], CH_3OH, the activation energies are overestimated. The elimination appears to favor the E2 mechanism, but shows E1cB character in ionic liquids. In CH_3OH, the β-elimination occurs through E2 mechanism.

References

(1) Repasky, M. P.; Chandrasekhar, J.; Jorgensen, W. L. *J. Comput. Chem.* **2002,** *23*, 1601-1622.

(2) Acevedo, O. *J. Phys. Chem. B* **2009**, *113*, 15372-15381.

(3) Acevedo, O.; Jorgensen, W. L. *J. Am. Chem. Soc.* **2005,** *127*, 8829-8834.

(4) Thompson, J. D.; Cramer, C. J.; Truhlar, D. G. *J. Comp. Chem.* **2003,** *24*, 1291-1304.

(5) Hermans, J.; Wang, L. *J. Am. Chem. Soc.* **1997,** *119*, 2707-2714.

(6) D'Anna, F.; La Marca, S.; Noto, R. *J. Org. Chem.* **2008,** *73*, 3397-3403.

(7) D'Anna, F.; Frenna, V.; Pace, V.; Noto, R. *Tetrahedron,* **2006,** *62*,1690-1698.

Supporting Information

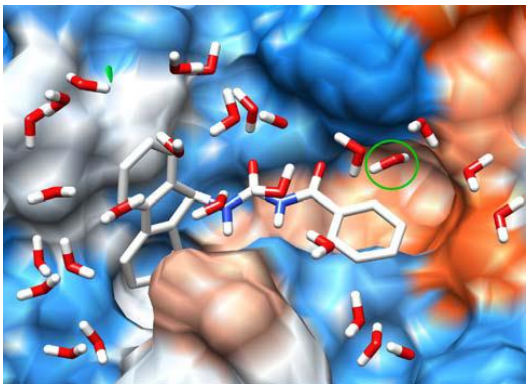

Figure S1. CypA active site with acylurea-based compound **1j** (R1=R2=H) and nearby waters shown bound in a hydrophobic surface representation where blue is the most polar regions and orange-red is the most hydrophobic. The water circled in green is located deep in the hydrophobic sub-binding pocket.

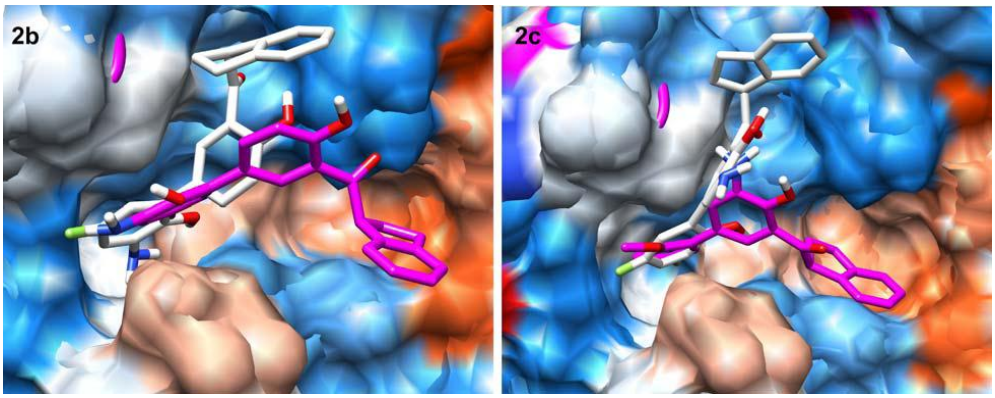

Figure S2. Overlaid CypA (gray) and CypB (pink) active sites with inihibitors **2b** (left) and **2c** (right) bound at the active sites. Nearby waters removed for clarity.

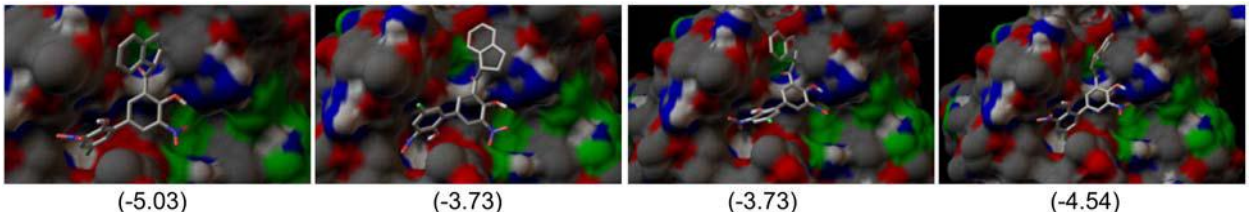

Figure S3. Autodock 4.2 docking calculations illustrated with the best possible binding modes of **2a** in CypA. Estimated free-energy of binding (kcal/mol) given in parentheses.

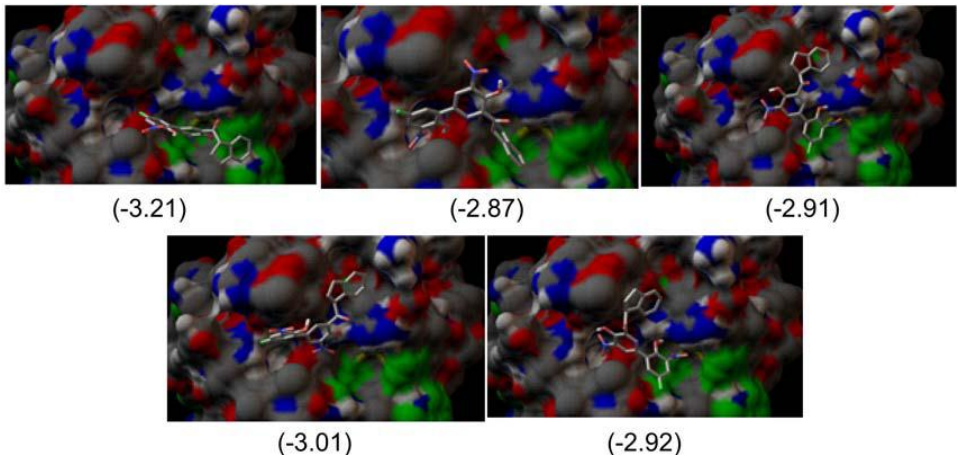

Figure S4. Autodock 4.2 docking calculations illustrated with the best possible binding modes of **2a** in CypB. Estimated free-energy of binding (kcal/mol) given in parentheses.

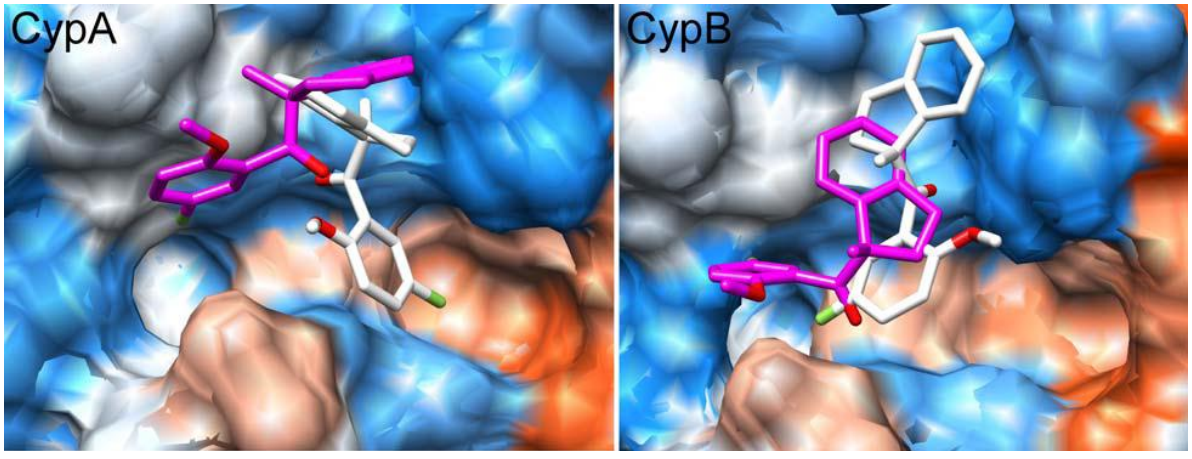

Figure S5. Overlaid **(R)-3b** (gray) and **(S)-3b** (pink) inihibitors in the CypA (left) and CypB (right) active sites. Nearby waters removed for clarity.

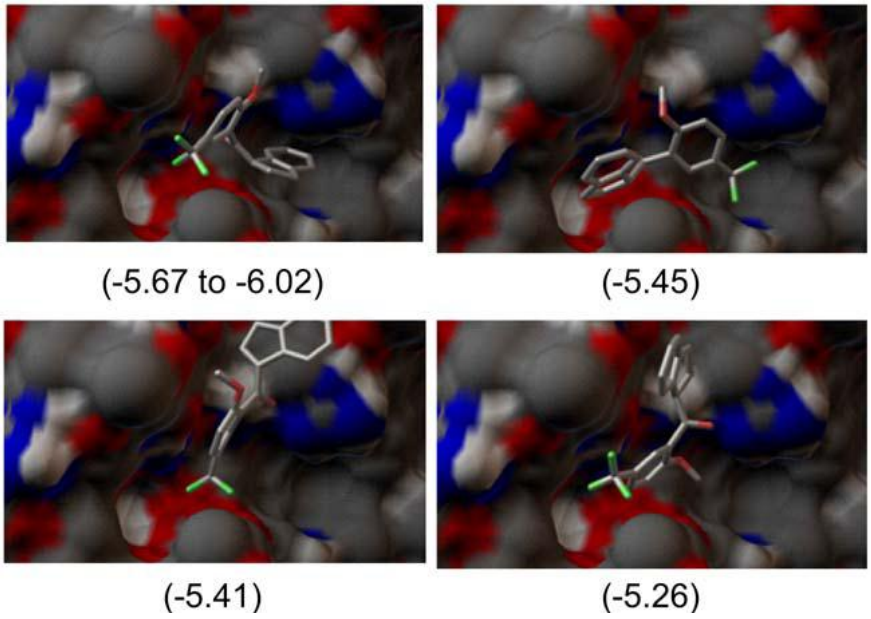

Figure S6-A. Autodock 4.2 docking calculations illustrated with the best possible binding modes of **3a** in CypA. Estimated free-energy of binding (kcal/mol) given in parentheses.

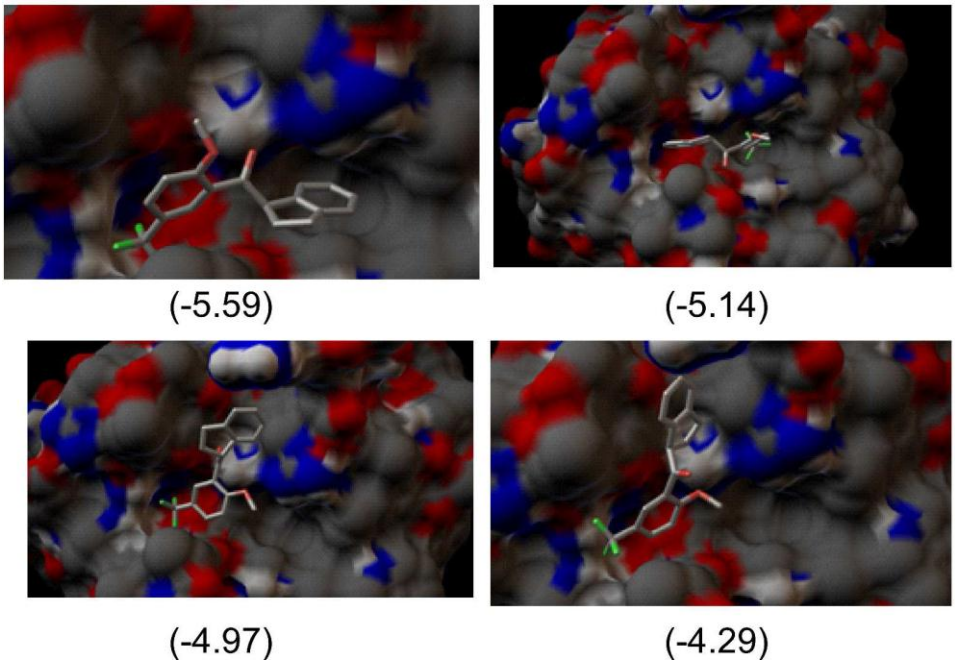

Figure S6-B. Autodock 4.2 docking calculations illustrated with the best possible binding modes of **3a** in CypB. Estimated free-energy of binding (kcal/mol) given in parentheses.

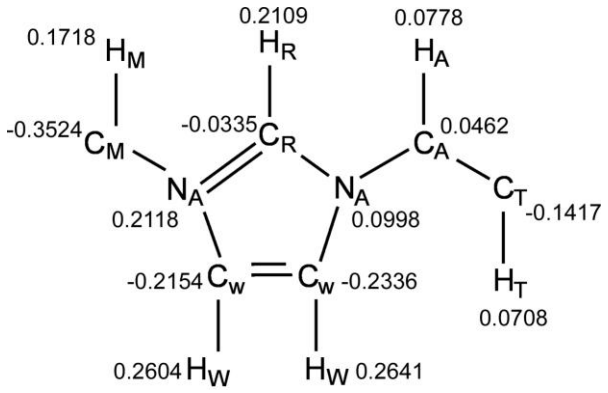

Figure S7. Partial charges assigned for atom types exclusively for use in [EMIM].

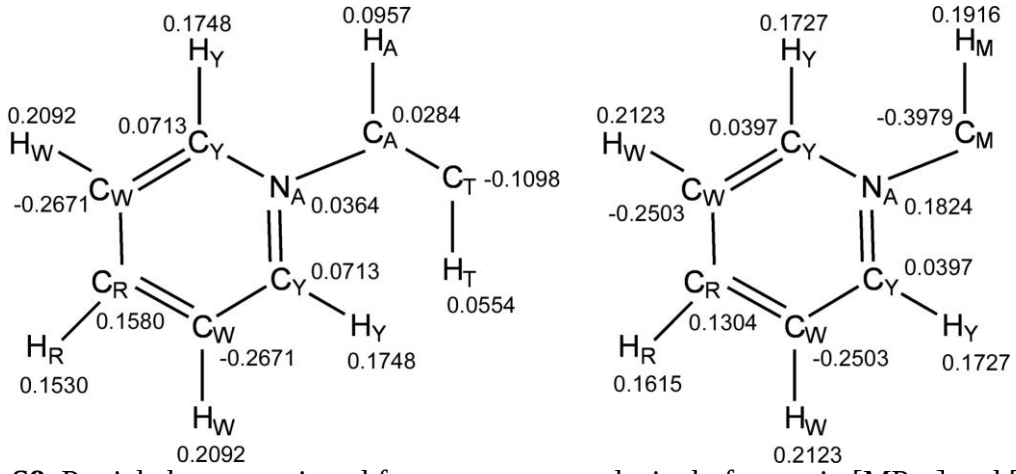

Figure S8. Partial charges assigned for atom types exclusively for use in [MPyr] and [EPyr].

Table S1. Bond and angle force constants, k_r (kcal mol^{-1} Å^{-2}) and k_θ (kcal mol^{-1} rad^{-2}), and equilibrium distances and angles, r_o (Å) and θ_o (degrees), for [RMIM].[a]

Bonds	k_r	r_o	angles	k_θ	θ_o
CR-NA	477.00	1.315	HM-CM-HM	33.00	109.80
HM-CM	340.00	1.080	HM-CM-NA	37.50	109.20
CM-NA	337.00	1.465	CM-NA-CR	70.00	126.40
CR-HR	367.00	1.069	CM-NA-CW	70.00	125.60
CW-NA	427.00	1.378	NA-CR-HR	35.00	125.10
CW-CW	520.00	1.336	NA-CR-NA	70.00	109.80
CW-HW	367.00	1.068	CR-NA-CW	70.00	107.90
NA-CA	337.00	1.476	NA-CW-CW	70.00	107.10
CA-HA	340.00	1.080	NA-CW-HW	35.00	122.00
CA-CT	268.00	1.521	HW-CW-CW	35.00	130.90
CA-CS	268.00	1.526	CW-NA-CA	70.00	125.30
CS-HS	340.00	1.087	CR-NA-CA	70.00	126.80
CS-CS	268.00	1.531	NA-CA-HA	37.50	107.50
CS-CT	268.00	1.528	NA-CA-CS	58.35	113.00
CT-HT	340.00	1.084	HA-CA-CT	37.50	111.20
			HA-CA-CS	37.50	111.10
			HA-CA-HA	33.00	108.90
			CA-CT-HT	37.50	110.70
			CA-CS-HS	37.50	108.60
			CA-CS-CT	58.35	113.10
			CA-CS-CS	58.35	113.30
			HS-CS-CT	37.50	109.70
			HS-CS-CS	37.50	109.60
			HS-CS-HS	33.00	106.70
			CS-CS-CT	58.35	112.30
			CS-CS-CS	58.35	112.30
			CS-CT-HT	37.50	111.10
			HT-CT-HT	33.00	107.90
			NA-CA-CT	58.35	112.60

[a]Force constants from OPLS-AA force field. Equilibrium bond and angle geometries computed here at the HF/6-31G(d) level of theory.

Table S2. Bond and angle force constants, k_r (kcal mol^{-1} Å^{-2}) and k_θ (kcal mol^{-1} rad^{-2}), and equilibrium distances and angles, r_o (Å) and θ_o (degrees), for [RPyr].[a]

Bonds	k_r	r_o	angles	k_θ	θ_o
CR-HR	367.00	1.074	HR-CR-CW	35.00	120.30
CR-CW	469.00	1.387	CW-CR-CW	63.00	119.40
CW-HW	367.00	1.072	CR-CW-HW	35.00	121.50
CW-CY	469.00	1.372	CR-CW-CY	63.00	118.80
CY-HY	367.00	1.072	HW-CW-CY	35.00	119.60
CY-NA	483.00	1.337	CW-CY-HY	35.00	122.40
NA-CM	337.00	1.481	CW-CY-NA	70.00	121.20
CM-HM	340.00	1.079	HY-CY-NA	35.00	116.50
NA-CA	337.00	1.493	CY-NA-CY	70.00	120.70
CA-HA	340.00	1.080	CY-NA-CA	70.00	119.70
CA-CT	268.00	1.522	NA-CA-HA	37.50	106.70
CA-CS	268.00	1.528	NA-CA-CS	58.35	112.20
CS-HS	340.00	1.087	HA-CA-CS	37.50	112.20
CS-CS	268.00	1.532	HA-CA-HA	33.00	107.80
CS-CT	268.00	1.529	CA-CS-HS	37.50	108.60
CT-HT	340.00	1.084	CA-CS-CS	58.35	113.10
			HS-CS-CS	37.50	109.80
			CA-CS-CT	58.35	112.80
			HS-CS-CT	37.50	109.70
			HS-CS-HS	33.00	106.60
			CS-CT-HT	37.50	111.10
			CS-CS-CS	58.35	112.20
			CS-CS-CT	58.35	112.20
			CY-NA-CM	70.00	119.70
			NA-CM-HM	37.50	109.00
			HM-CM-HM	33.00	109.90
			NA-CA-CT	58.35	112.10
			HA-CA-CT	37.50	111.60
			CA-CT-HT	37.50	110.60
			HT-CT-HT	33.00	108.00

[a]Force constants from OPLS-AA force field. Equilibrium bond and angle geometries computed here at the HF/6-31G(d) level of theory.

Table S3. Bond and angle force constants, k_r (kcal mol^{-1} Å^{-2}) and k_θ (kcal mol^{-1} rad^{-2}), and equilibrium distances and angles, r_o (Å) and θ_o (degrees), for choline [Chol].[a]

bonds	k_r	r_o	angles	k_θ	θ_o
HA-CA	340.00	1.0990	HA-CA-HA	35.00	110.01
CA-NA	490.00	1.4980	HA-CA-NA	35.00	108.90
NA-CS	490.00	1.5160	CA-NA-CS	51.80	110.20
CS-HS	340.00	1.0805	NA-CS-HS	35.00	106.40
CS-CW	317.00	1.5210	NA-CS-CW	70.00	116.60
CW-HW	340.00	1.0850	CS-CW-HW	35.00	108.30
CW-OY	450.00	1.3950	CS-CW-OY	80.00	109.60
OY-HY	553.00	0.9490	HS-CS-CW	35.00	109.30
			HW-CW-OY	35.00	111.60
			CW-OY-HY	35.00	110.90
			CA-NA-CA	55.00	108.73
			HS-CS-HS	35.00	108.60
			HW-CW-HW	35.00	107.40

[a]Force constants from OPLS-AA force field. Equilibrium bond and angle geometries computed here at the HF/6-31G(d) level of theory.

Table S4. Torsional fourier coefficients for 1-alkyl-3-methylimidazolium [RMIM], kcal/mol.

Torsion	V_1	V_2	V_3	Torsion	V_1	V_2	V_3
HM-CM-NA-CR	0.000	0.000	0.000	CA-CS-CS-HS	0.000	0.000	0.366
HM-CM-NA-CW	0.000	0.000	0.124	CA-CS-CS-CT	1.300	-0.050	0.200
CM-NA-CR-HR	0.000	4.651	0.000	HS-CS-CS-HS	0.000	0.000	0.318
CM-NA-CR-NA	0.000	4.651	0.000	HA-CA-CT-HT	0.000	0.000	0.318
CM-NA-CW-CW	0.000	3.000	0.000	CA-CS-CT-HT	0.000	0.000	0.366
CM-NA-CW-HW	0.000	3.000	0.000	NA-CA-CS-CT	-0.688	0.650	0.900
NA-CR-NA-CA	0.000	4.651	0.000	HA-CA-CS-CT	0.000	0.000	0.366
NA-CW-CW-HW	0.000	10.750	0.000	HS-CS-CT-HT	0.000	0.000	0.318
NA-CW-CW-NA	0.000	10.750	0.000	HS-CS-CS-CT	0.000	0.000	0.366
HR-CR-NA-CW	0.000	4.651	0.000	CA-CS-CS-CS	1.300	-0.050	0.200
CR-NA-CW-HW	0.000	3.000	0.000	CS-CS-CS-CS	1.300	-0.050	0.200
CR-NA-CW-CW	0.000	3.000	0.000	CS-CS-CS-CT	1.300	-0.050	0.200
HR-CR-NA-CA	0.000	4.651	0.000	CS-CS-CS-HS	0.000	0.000	0.366
HW-CW-NA-CA	0.000	3.000	0.000	CS-CS-CT-HT	0.000	0.000	0.366
CW-CW-NA-CA	0.000	3.000	0.000	HW-CW-CW-HW	0.000	10.750	0.000
CR-NA-CA-HA	0.000	0.000	0.000	X -NA-X -X[a]	0.000	2.000	0.000
NA-CA-CS-HS	0.000	0.000	0.000	X -CW-X -X[a]	0.000	2.200	0.000
HA-CA-CS-CS	0.000	0.000	0.366	X -CR-X -X[a]	0.000	2.200	0.000
CW-NA-CR-NA	0.000	4.651	0.000				

[a]Improper torsion.

Table S5. Torsional fourier coefficients for N-alkylpyridinium [RPyr], kcal/mol.

Torsion	V_1	V_2	V_3	Torsion	V_1	V_2	V_3
HR-CR-CW-HW	0.000	7.250	0.000	HS-CS-CS-HS	0.000	0.000	0.318
HR-CR-CW-CY	0.000	7.250	0.000	CA-CS-CS-CS	1.300	-0.050	0.200
CR-CW-CY-HY	0.000	7.250	0.000	CS-CS-CS-CS	1.300	-0.050	0.200
CR-CW-CY-NA	0.000	7.250	0.000	CA-CS-CS-CT	1.300	-0.050	0.200
HW-CW-CY-HY	0.000	7.250	0.000	CS-CS-CS-CT	1.300	-0.050	0.200
HW-CW-CY-NA	0.000	7.250	0.000	HS-CS-CS-CT	0.000	0.000	0.318
HW-CW-CR-CW	0.000	7.250	0.000	CS-CS-CT-HT	0.000	0.000	0.366
CW-CY-NA-CY	0.000	0.300	0.000	HS-CS-CS-CS	0.000	0.000	0.366
CW-CR-CW-CY	0.000	7.250	0.000	HA-CA-CS-CS	0.000	0.000	0.366
CW-CY-NA-CA	0.000	0.300	0.000	CW-CY-NA-CM	0.000	3.000	0.000
HY-CY-NA-CA	0.000	0.300	0.000	HY-CY-NA-CM	0.000	3.000	0.000
CY-NA-CA-HA	0.000	0.000	0.000	CY-NA-CM-HM	0.000	3.500	0.000
NA-CA-CS-CT	-0.700	0.000	-0.250	HY-CY-NA-CY	0.000	3.000	0.000
HA-CA-CS-CT	0.000	0.000	0.366	X-X-NA-X[a]	0.000	0.200	0.000
CA-CS-CT-HT	0.000	0.000	0.366	X-CY-NA-X[a]	0.000	2.199	0.000
HS-CS-CT-HT	0.000	0.000	0.318	X-CW-X-X[a]	0.000	2.199	0.000
CA-CS-CS-HS	0.000	0.000	0.366	X-CR-X-X[a]	0.000	2.199	0.000

[a]Improper torsion.

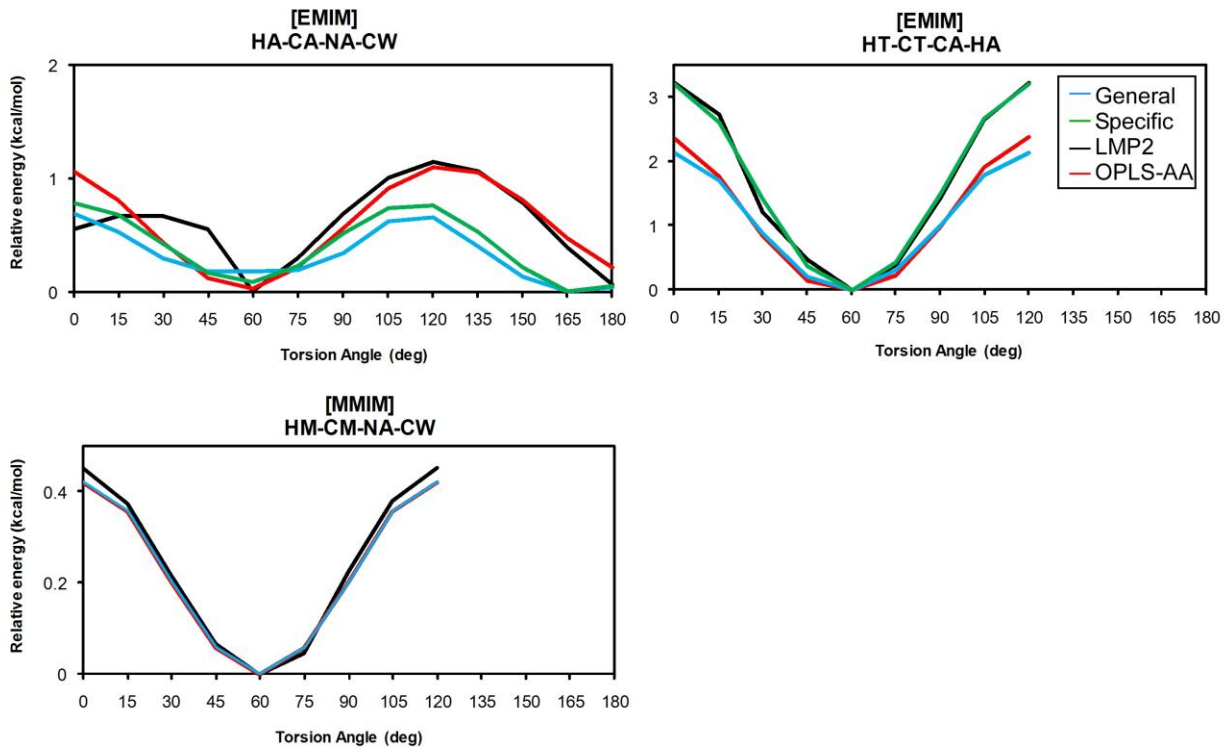

Figure S9. Torsion energy profiles for the rotation around dihedral angles for 1-ethyl-3-methylimidazolium [EMIM] and 1-methyl-3-methylimidazolium [MMIM] cation. The transferable [RMIM] parameters given in blue, parameters specific to [EMIM] in green LMP2/cc-pVTZ(-f)/HF/6-31G(d) in black, and the original OPLS-AA force field in red.

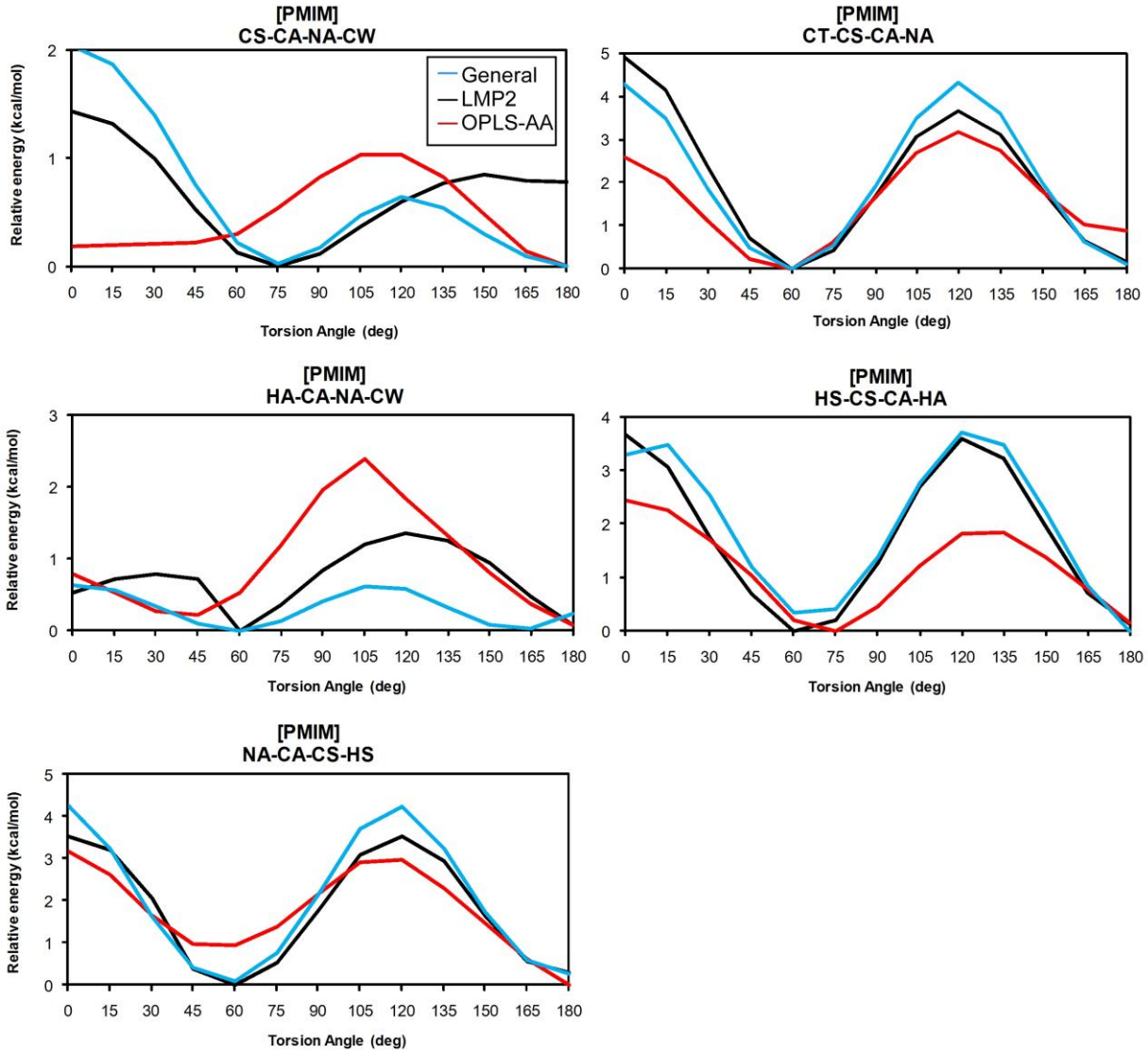

Figure S10. Torsion energy profiles for the rotation around dihedral angles for 1-propyl-3-methylimidazolium [PMIM] cation. The transferable [RMIM] parameters given in blue, LMP2/cc-pVTZ(-f)/HF/6-31G(d) in black, and the original OPLS-AA force field in red.

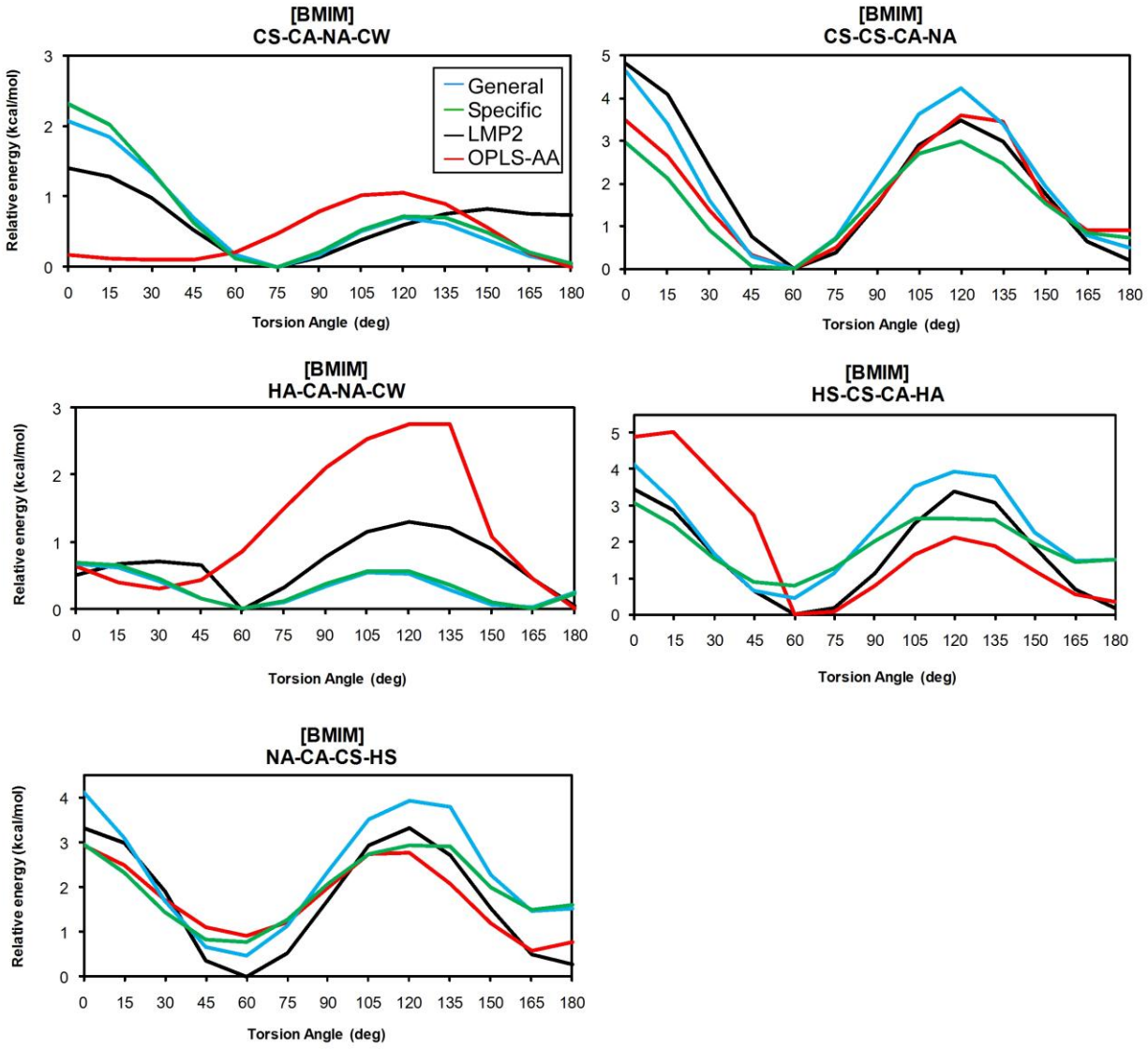

Figure S11. Torsion energy profiles for the rotation around dihedral angles for 1-butyl-3-methylimidazolium [BMIM] cation. The transferable [RMIM] parameters given in blue, parameters specific to [BMIM] in green LMP2/cc-pVTZ(-f)/HF/6-31G(d) in black, and the original OPLS-AA force field in red.

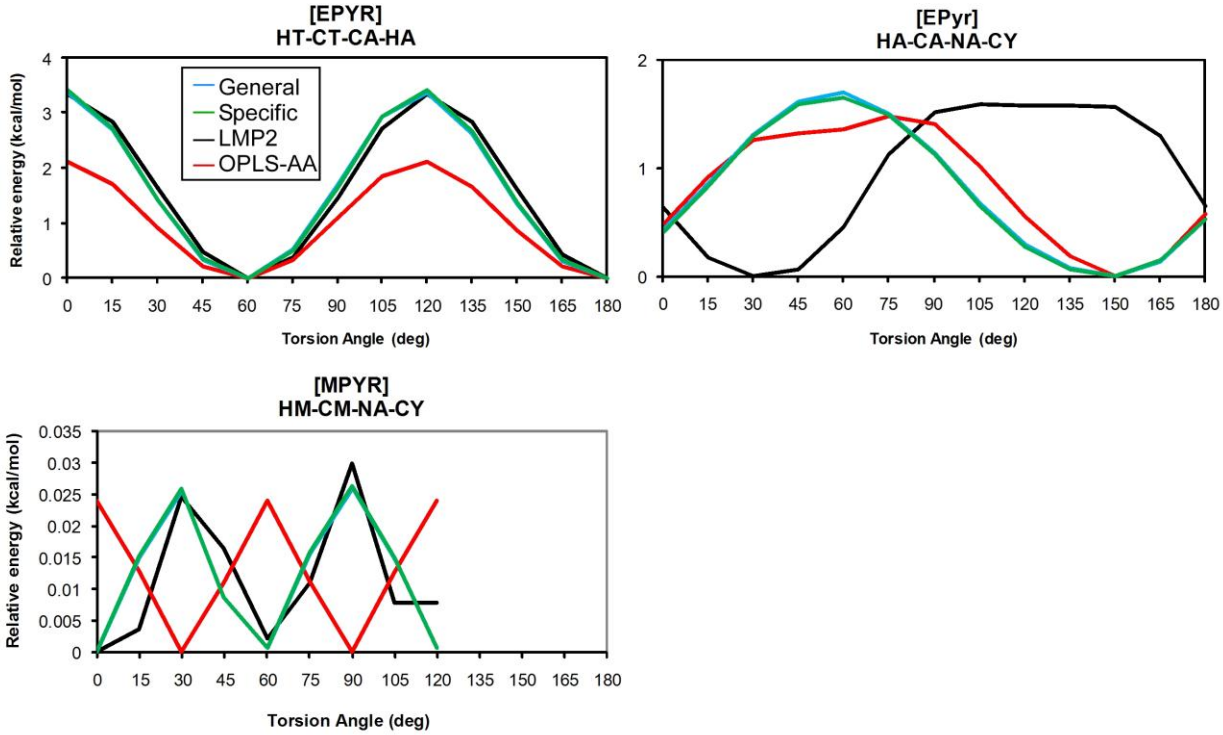

Figure S12. Torsion energy profiles for the rotation around dihedral angles for N-1-ethylpyridinium [EPyr] and N-1- methylpyridinium [MPyr] cations. The transferable [RPyr] parameters given in blue, parameters specific to [EPyr] and [MPyr] in green, LMP2/cc-pVTZ(-f)/HF/6-31G(d) in black, and the original OPLS-AA force field in red.

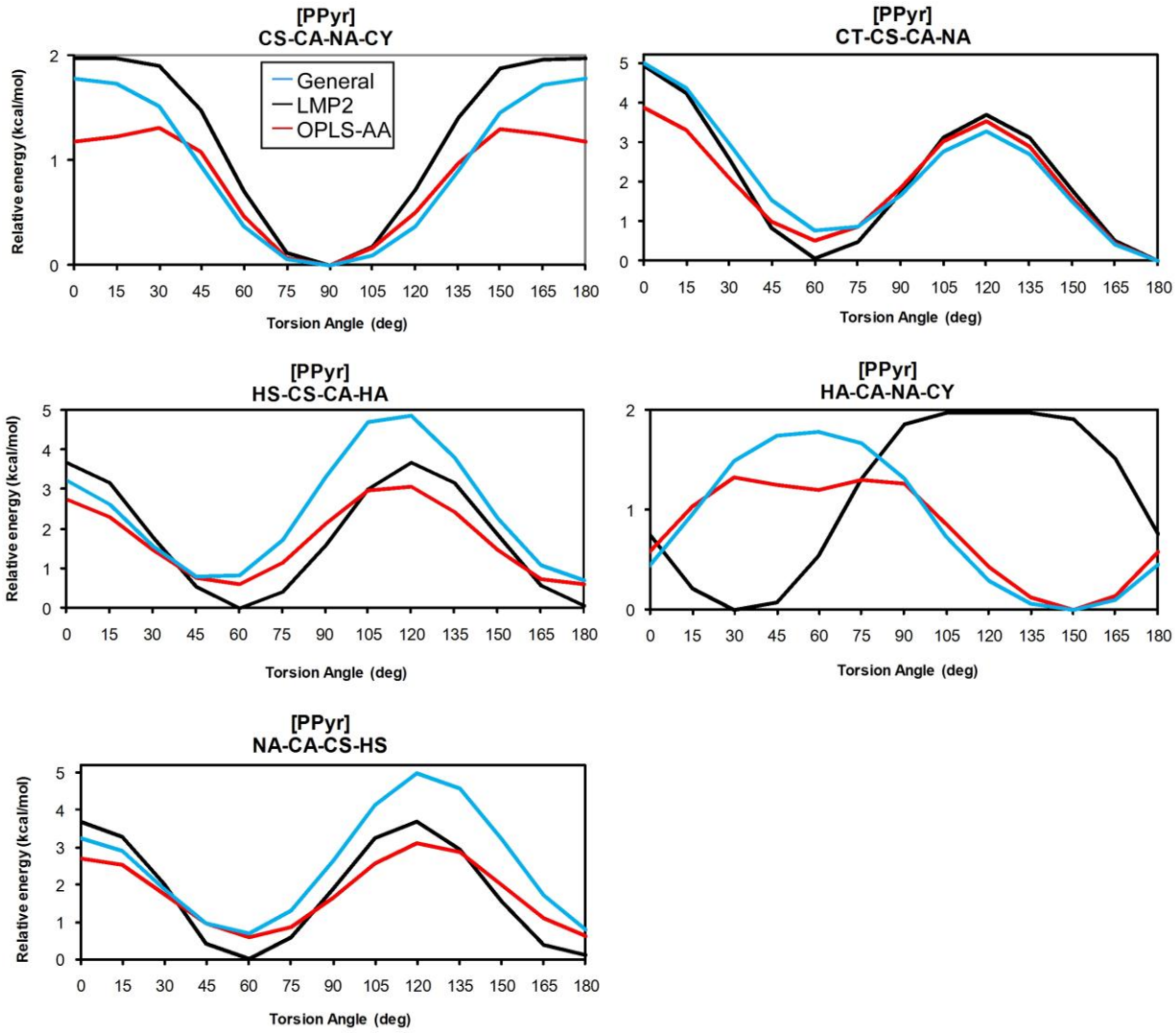

Figure S13. Torsion energy profiles for the rotation around dihedral angles for N-1-propylpyridinium [PPyr] cation. The transferable [RPyr] parameters given in blue, LMP2/cc-pVTZ(-f)/HF/6-31G(d) in black, and the original OPLS-AA force field in red.

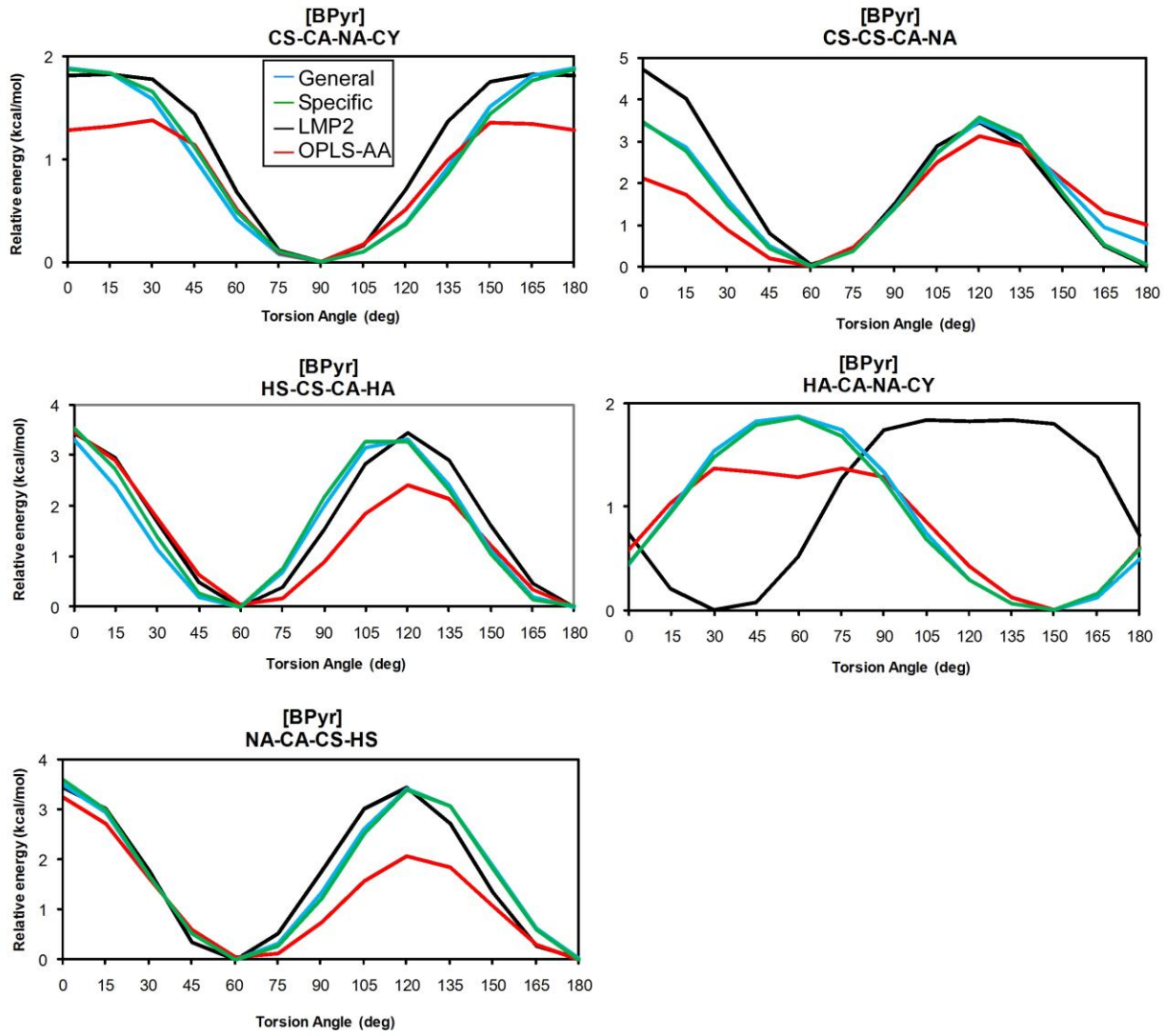

Figure S14. Torsion energy profiles for the rotation around dihedral angles for N-1-butylpyridinium [BPyr] cation. The transferable [RPyr] parameters given in blue, parameters specific to [BPyr] in green, LMP2/cc-pVTZ(-f)/HF/6-31G(d) in black, and the original OPLS-AA force field in red.

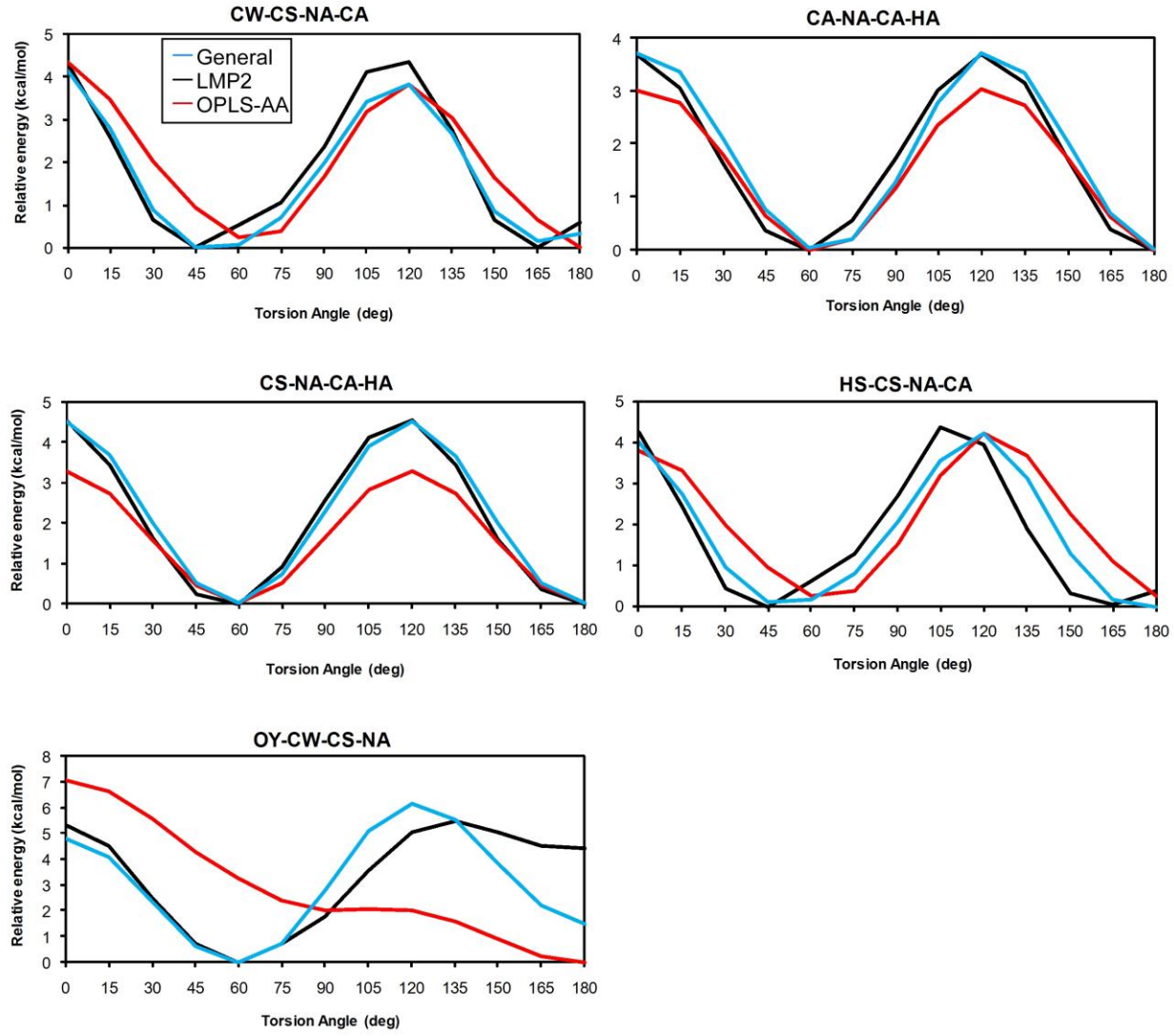

Figure S15. Torsion energy profiles for the rotation around dihedral angles for choline [Chol] cation. The [Chol] parameters given in blue, LMP2/cc-pVTZ(-f)/HF/6-31G(d) in black, and the original OPLS-AA force field in red.

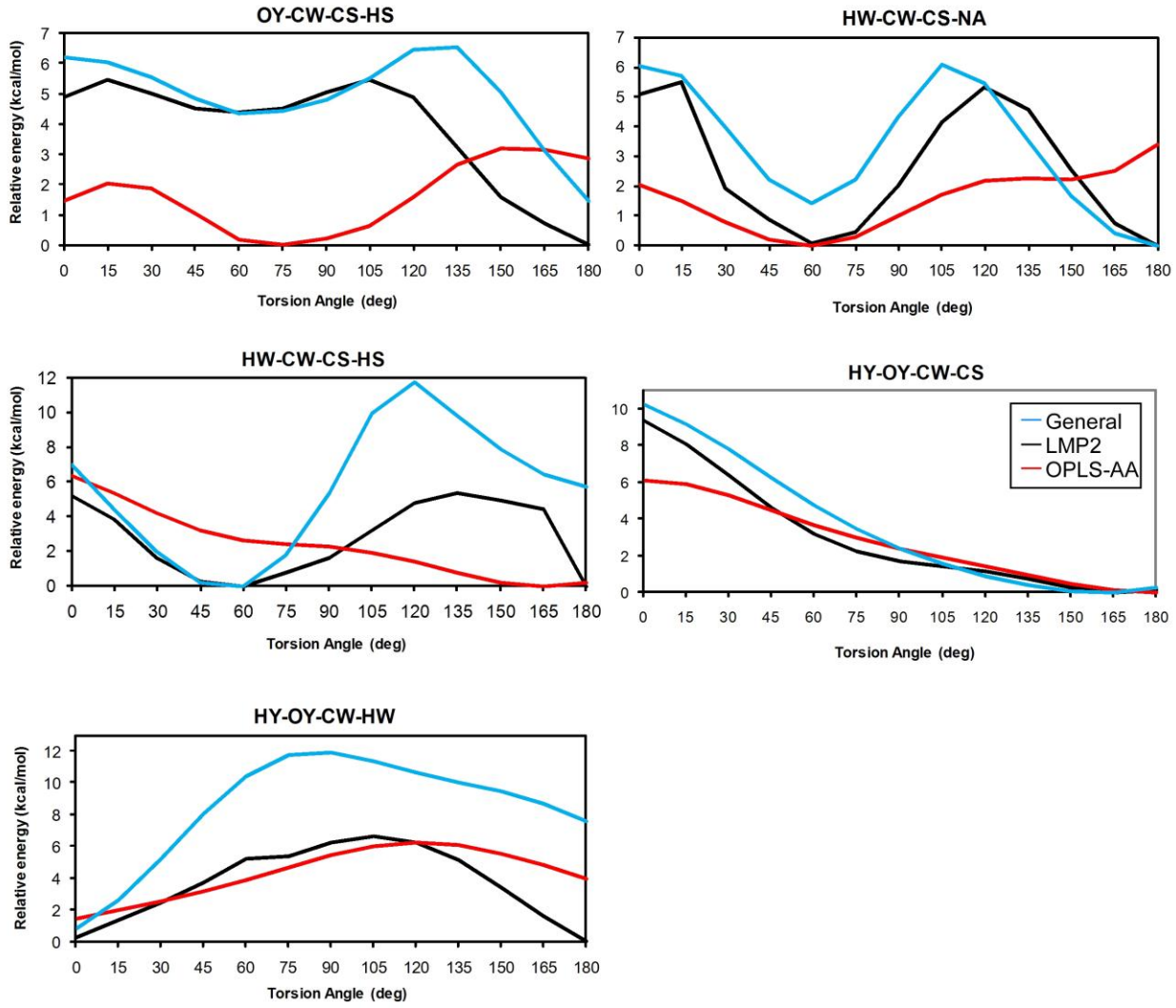

Figure S16. Additional torsion energy profiles for the rotation around dihedral angles for choline [Chol] cation. The [Chol] parameters given in blue, LMP2/cc-pVTZ(-f)/HF/6-31G(d) in black, and the original OPLS-AA force field in red.

Table S6. Box Sizes (Å) for Equilibrated Ionic Liquids. Systems were periodic and tetragonal with $c/a = 1.5$.

Ionic Liquid	*a*	Ionic Liquid	*a*	Ionic Liquid	*a*
[MMIM][BF_4]	31.0	[MMIM][PF_6]	32.3	[MMIM][Cl]	28.7
[EMIM][BF_4]	32.2	[EMIM][PF_6]	33.4	[EMIM][Cl]	30.2
[BMIM][BF_4]	34.3	[BMIM][PF_6]	35.5	[BMIM][Cl]	32.8
[HMIM][BF_4]	36.5	[HMIM][PF_6]	37.4	[HMIM][Cl]	34.8
[OMIM][BF_4]	38.4	[OMIM][PF_6]	39.4	[OMIM][Cl]	37.0
[MMIM][NO_3]	29.5	[MMIM][TfO]	32.6	[MMIM][$AlCl_4$]	35.5
[EMIM][NO_3]	30.7	[EMIM][TfO]	33.7	[EMIM][$AlCl_4$]	36.3
[BMIM][NO_3]	33.1	[BMIM][TfO]	36.0	[BMIM][$AlCl_4$]	38.1
[HMIM][NO_3]	35.5	[HMIM][TfO]	37.7	[HMIM][$AlCl_4$]	39.7
		[OMIM][TfO]	40.1		
[MMIM][Al_2Cl_7]	40.4	[MPyr][BF_4]	30.8	[MPyr][PF_6]	32.2
[EMIM][Al_2Cl_7]	41.1	[EPyr][BF_4]	31.9	[EPyr][PF_6]	33.0
[BMIM][Al_2Cl_7]	42.5	[BPyr][BF_4]	34.2	[BPyr][PF_6]	35.2
[HMIM][Al_2Cl_7]	44.5	[HPyr][BF_4]	36.4	[HPyr][PF_6]	37.4
		[OPyr][BF_4]	38.3	[OPyr][PF_6]	39.2
[MPyr][Cl]	28.4	[MPyr][NO_3]	29.3	[MPyr][TfO]	32.4
[EPyr][Cl]	29.9	[EPyr][NO_3]	30.6	[EPyr][TfO]	33.6
[BPyr][Cl]	32.6	[BPyr][NO_3]	33.0	[BPyr][TfO]	35.8
[HPyr][Cl]	34.7				
[OPyr][Cl]	37.0				
[MPyr][$AlCl_4$]	35.4	[MPyr][Al_2Cl_7]	40.3	[Chol][BF_4]	32.5
[EPyr][$AlCl_4$]	36.3	[EPyr][Al_2Cl_7]	40.8	[Chol][PF_6]	33.6
[BPyr][$AlCl_4$]	38.0	[BPyr][Al_2Cl_7]	42.6	[Chol][Cl]	30.4
[Chol][$AlCl_4$]	36.3	[Chol][TfO]	34.2		
[Chol][Al_2Cl_7]	41.5	[Chol][Sacc]	36.9		
[Chol][NO_3]	31.1	[Chol][Ace]	35.8		

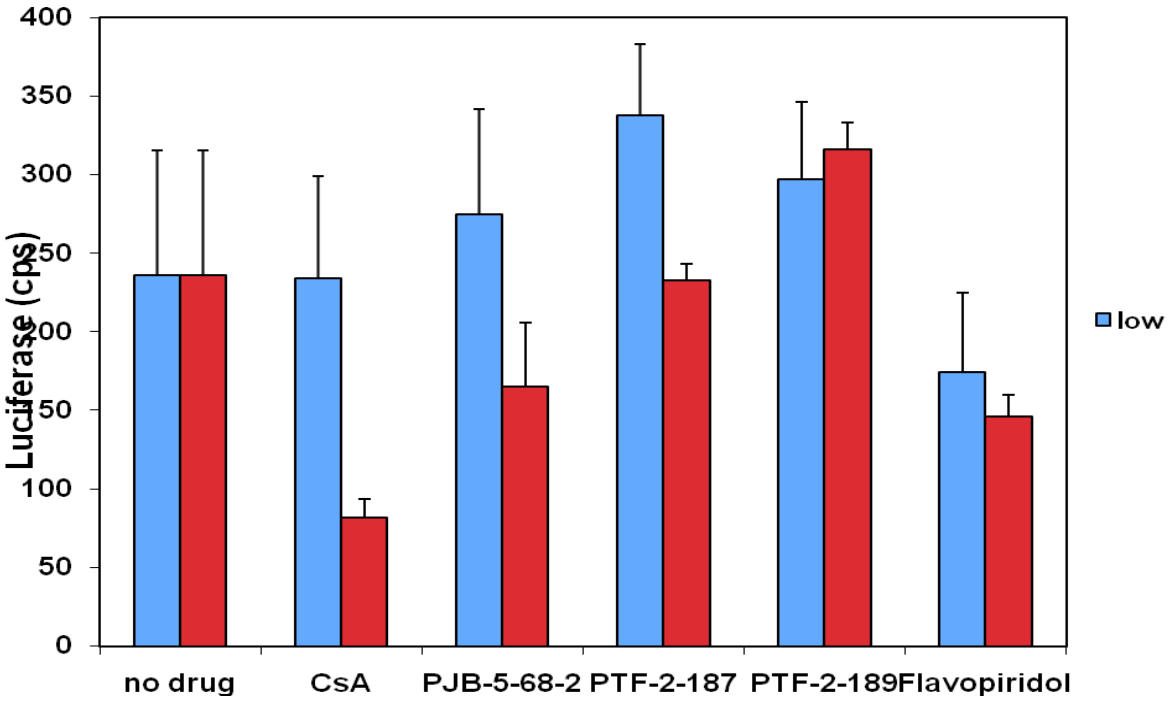

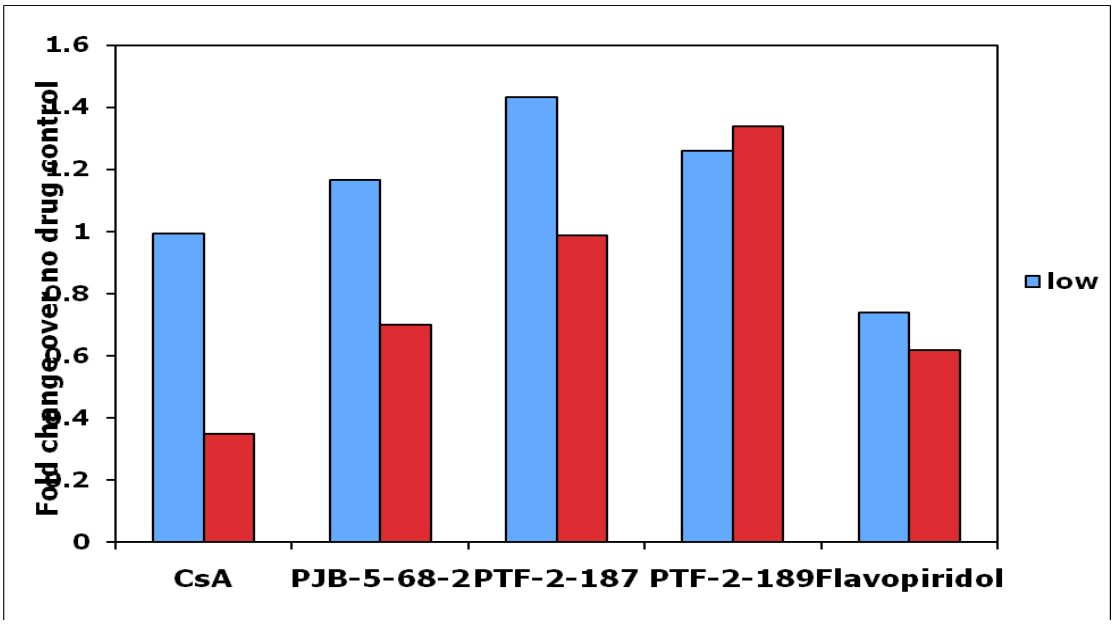

Figure S17: Toxicity data on Hela cell lines

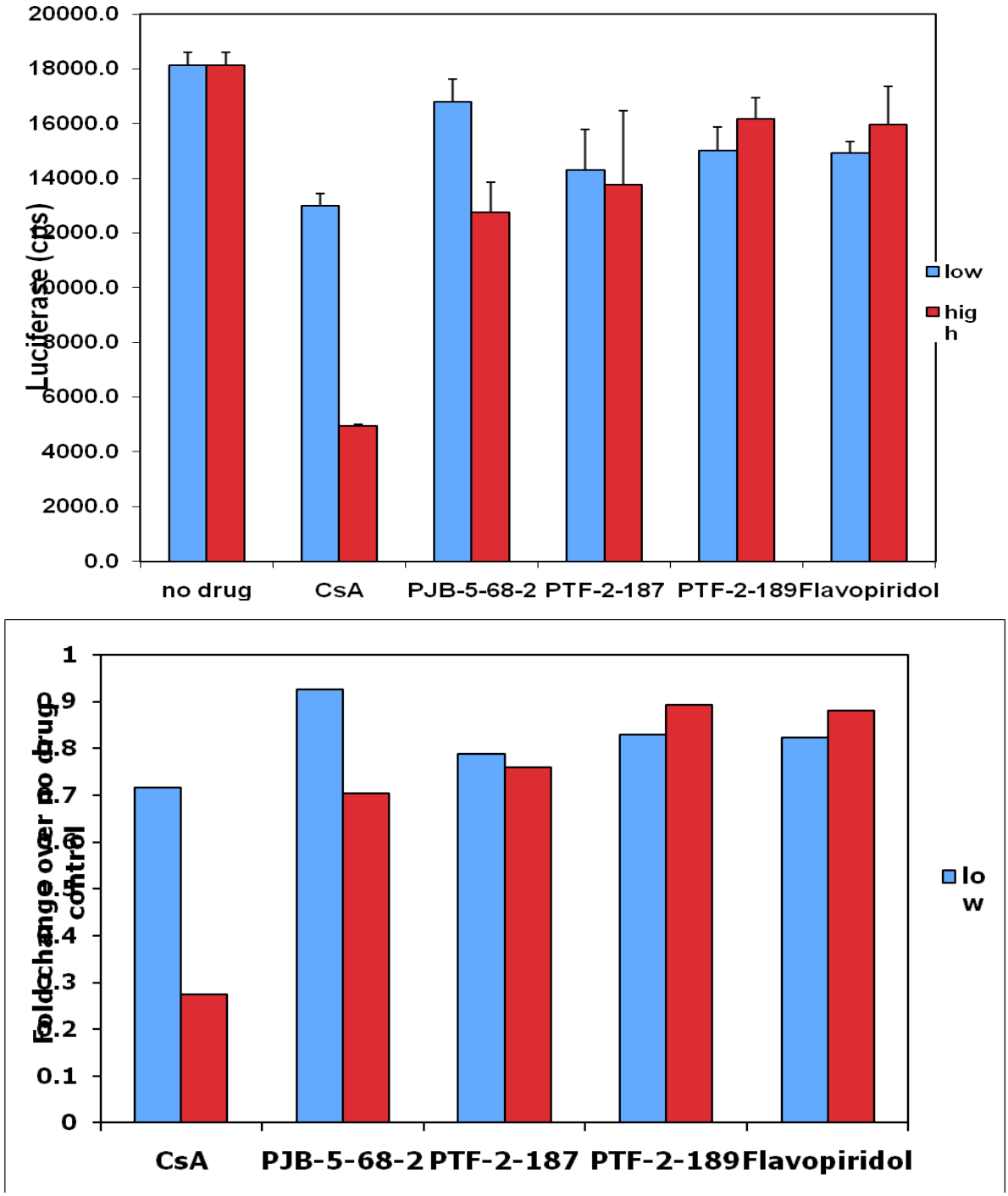

Figure S18: Toxicity data on GHOST cell lines.